Ocean Modelling 181 (2023) 102149

Contents lists available at ScienceDirect

Ocean Modelling

journal homepage: www.elsevier.com/locate/ocemod

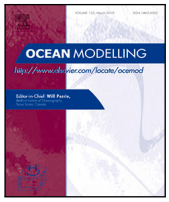

# The impact of climate change on the storm surges of the Mediterranean Sea: Coastal sea level responses to deep depression atmospheric systems

Christos V. Makris [a,*], Konstantia Tolika [b], Vasilis N. Baltikas [a], Kondylia Velikou [b], Yannis N. Krestenitis [a]

[a] Laboratory of Maritime Engineering and Maritime Works, School of Civil Engineering, Aristotle University of Thessaloniki, GR-54124, Thessaloniki, Greece
[b] Department of Meteorology and Climatology, School of Geology, Aristotle University of Thessaloniki, GR-54124, Thessaloniki, Greece

## ARTICLE INFO

*Keywords:*
Storm surge
Deep depression
Coastal zone
Climate change
Mediterranean Sea
Sea surface height
Inverse barometer effect
Representative Concentration Pathway
Med-CORDEX

## ABSTRACT

This study aims to systematically assess the impacts of projected climate change on episodic events of sea level elevation in coastal areas of the Mediterranean, induced by severe weather conditions identified as deep depressions. We try to add new insight in the long-term, climatic timescale, identification of affected parts of the Mediterranean coastal zone correlated to low atmospheric pressure systems, indicative of the Mediterranean basin during the 21st century. To achieve this goal, an integrated quantitative assessment is proposed by combining projections from available and established, green-house gasses emission/concentration scenarios (based on Representative Concentration Pathways; RCP 4.5 and 8.5) with advanced numerical modelling and statistical post-processing for the definition of cyclonic weather impacts on characteristic coastal zone hotspots. To this end, climate projections and outputs from three Regional Climate Models (RCMs) of the Med-CORDEX initiative at the Mediterranean basin scale are used and extensively evaluated against re-analysis data. These atmospheric datasets feed a robust storm surge model (MeCSS) for the simulation of barotropic hydrodynamics (sea level elevation and currents) thoroughly validated against *in situ* sea level observations by tide-gauges. Our results corroborate a projected storminess attenuation for the end of the 21st century, yet local differentiations in storm surge maxima around the Mediterranean coastal zone are pinpointed. Moreover, a slight reduction of average storm-induced Mean Sea Level (MSL; component attributed solely to the meteorological residual of sea level elevation) is also apparent towards the end of the 21st century. Extreme storm surge magnitudes range between 0.35 and 0.50 m in the Mediterranean with higher values along parts of its northern coasts (Venice lagoon, Gulf of Lions, northern Adriatic and Aegean Seas, *etc.*) and the Gulf of Gabes in its southern part. Overall, the spatial distributions of surge maxima are estimated to remain similar to those of the past throughout the entire Mediterranean coastal zone. Differentiations between the two scenarios (RCP4.5-8.5) used are obvious, not so much related to the spatiotemporal distribution of storm surge maxima, which shows a very stable pattern, but more in terms of their magnitudes. Indicatively, a decrease of surge maxima from -30% to -2% can be observed towards the end of the 21st century, especially for RCP8.5-driven MeCSS simulations. This is a spatially averaged estimation, yet for some specific coastal sites in Croatia, Spain Italy, and France, such as Rovinj, Bakar, Toulon, Trieste, Ajaccio, Genova, Marseilles, Naples, Venice, Cagliari, Ancona, Ibixa, and Barcelona, the storm surge maxima might increase from 1% to 22% under different RCM/RCP combinations towards the end of the 21st century. Our analysis leads to the quantification of deep depression systems' effect on the coastal sea level elevation due to storm surges towards 2100. The strongest correlations of deep depression events to high sea levels are observed in several parts along the northern Mediterranean coasts (Gulfs of Valencia and Lions, Ligurian and northern Adriatic Seas). They are followed by mid-latitude areas around Corsica, Sardinia, the mid-zonal Italian Peninsula and the Adriatic, and the northern Aegean Sea. The influence of deep depressions on storm surges is lower for Sicily, South Italy, Peloponnese, Crete, the southern Aegean archipelago, and Alboran Sea. The only exceptions in the generally unaffected southern Mediterranean littorals are the Gulfs of Gabes and Alexandretta. These apply to the 20th century; however, they seem to repeat for the 21st century estimations, with even more pronounced differentiations between the southern and the northern parts. A projected northward shift of the main deep depression centres over the Mediterranean towards the end of the 21st century, is likely the reason for the latter. The climate change signal (difference of Future–Reference Period) of the deep cyclones' effect on the episodic increases of coastal sea level seems

* Corresponding author.
*E-mail address:* cmakris@civil.auth.gr (C.V. Makris).

https://doi.org/10.1016/j.ocemod.2022.102149
Received 8 April 2022; Received in revised form 11 October 2022; Accepted 9 November 2022
Available online 14 November 2022

to have a very clear pattern of slight attenuation in certain regions, i.e., Sardinia, Corsica, the Ligurian and Adriatic Seas, and the entire Italian peninsula for all RCM-fed implementations towards the end of the 21st century. Conditionally, this is the case for the Gulf of Valencia, the north-western African coasts, the Alboran, Ionian, Aegean, and Libyan Sea coasts, under specific combinations of RCM/RCP forcings. On the other hand, a possible increase of the Mediterranean deep depressions' influence on the coastal storm surges might be the case for the Gulf of Lions, the Ionian, Aegean and Levantine Sea basins, covering the north-central and north-eastern coasts of Africa. In general, a positive influence of deep depressions to storm surge maxima would probably refer to areas of mid-to-high storm surge maxima (*e.g.*, Aegean, Ionian, Gulf of Lions or Valencia or Gabes, *etc.*), but not the highest throughout the basin (*e.g.*, Venice lagoon, Ligurian, Adriatic, *etc.*). In the latter coastal regions, however, intense local wind forcing mechanisms (*i.e.*, Scirocco) are bound to play an essential role in the formation of high storm surges. The produced results can be used in focused studies for integrated hydrologic/hydrodynamic modelling under projected climate change conditions in the 21st century.

## 1. Introduction

The Mediterranean Sea is a regional aquatic body that has been identified as a "hotspot" in terms of possible climatic impacts (Nicholls and Hoozemans, 1996; Cramer et al., 2018). The latter have based on several projected climate change scenarios (*e.g.*, Special Report on Emissions Scenarios; SRES scenarios B1, A1B and A2) for the 21st century (Giorgi, 2006; Nicholls, 2006; Lionello et al., 2006a, 2014; Li et al., 2011; Anagnostopoulou et al., 2014; Adloff et al., 2015). The Mediterranean coastal zone is particularly vulnerable to the climatic variability influencing sea level variations (Von Storch and Woth, 2008; Cid et al., 2016; Satta et al., 2017). To incorporate the regional scale effects and local peculiarities of weather patterns over the basin, during the last 20 years, researchers have simulated the storm surges in the Mediterranean, focusing on sea level elevation and hydrodynamics, with the use of regional scale, barotropic circulation models in long-term projection mode, based on the output of respective climatic studies (*e.g.*, Giorgi and Lionello, 2008; Li et al., 2011; Carillo et al., 2012; Jordà et al., 2012; Gualdi et al., 2013; Calafat et al., 2014; Lionello et al., 2014; Adloff et al., 2018).

### 1.1. Research theme

The immediate environmental impacts of extreme storm surge events can be identified as coastal flooding, beach erosion, degradation of coastal vegetation and agriculture, saltwater intrusion in coastal aquifers, lagoons, and other bodies of freshwater resources (Nicholls, 2010). Storm surges can lead to the destruction of coastal infrastructure (ports, protection works, roads and railways, and industry), built environment and property (residential, touristic, and commercial), loss of fauna and human lives with immense societal and economic effects (Ciavola et al., 2011; Hallegatte et al., 2013; Fang et al., 2014; Wahl et al., 2017; Hochman et al., 2021; Lionello et al., 2021).

Boyes and Elliott (2019) recently demonstrated the significant issues of coastal management against the storm surge hazard, in terms of first responders to the problem, on a European scale. They pinpointed several low-land coastal areas of the Mediterranean littoral zone that are threatened by the combination of high tides and storm surges, and related inundation. These include, *e.g.*, the northern Adriatic, the Venice lagoon, the Gulf of Gabes, the northern Aegean, the western Peloponnese in the Ionian Sea, and many Greek islands, as well as almost all the deltaic areas of Egypt, France, Greece, Italy, and Spain (*e.g.*, Nile, Po, Rhone, Ebro, Vardar/Axios rivers, *etc.*). Enríquez et al. (2020) have further stressed the need to pay attention to the spatial analysis of storm surge occurrence introducing the spatial footprint notion along coastline stretches. Withal, the peculiarities of the complex topography and highly varying bathymetry in the Mediterranean basin have also been identified as a crucial factor for surge-induced coastal risk, *e.g.*, due to local hydrodynamic circulation driven by specific aeolian patterns, *i.e.*, lengthy fetch Scirocco winds in the Adriatic, wind canalization in the northern Aegean, *viz.*, persistent Etesian winds in the highly exposed central Aegean archipelago, and Mediterranean extratropical cyclones, *etc.* (Lionello et al., 2006b; Sánchez-Arcilla et al., 2008; Ullmann and Moron, 2008; Marcos et al., 2011; Lionello et al., 2012; Šepić et al., 2012; Calafat et al., 2014; Conte and Lionello, 2013; Androulidakis et al., 2015; Cid et al., 2016; Makris et al., 2016; Lionello et al., 2019, 2021; Mel et al., 2022).

Most of the studies, based on future simulations with barotropic (tide-) surge models under SRES (A2, A1B and B1) approaches, have estimated a general decrease in the frequency and intensity of extreme surge events and attenuation of marine storminess over the entire Mediterranean basin towards the end of the 21st century (after 2050) with a possible increase of extremes locally only for the early quarter of the 21st century (Gomis et al., 2008; Marcos et al., 2009; Jordà et al., 2012; Tsimplis and Shaw, 2010; Lionello et al., 2012; Conte and Lionello, 2013; Androulidakis et al., 2015; Makris et al., 2016; *etc.*). However, the projected rising Mean Sea Level (MSL) globally and the local isostatic changes (land subsidence) combined with low pressure systems (affecting by the inverse barometer effect and intense onshore winds blowing in shallow waters), and high tides may still induce individual, enhanced, episodic events of storm surge (Calafat et al., 2022). The latter are likely to inflict catastrophic impacts on many areas of the Mediterranean, *i.e.*, the northern Aegean Sea, the eastern Ionian coasts, the entire Adriatic coastline (with emphasis on the northern part of it), the Gulf of Gabes, the Alboran Sea, the Gulfs of Valencia and Lion, the eastern coastal areas of the Ligurian Sea, The Nile Delta, the north-eastern Levantine Sea, and the Gulf of Alexandretta (Sánchez-Arcilla et al., 2008; Snoussi et al., 2008; Ullmann and Moron, 2008; Mosso et al., 2009; Krestenitis et al., 2011; Cid et al., 2014; Conte and Lionello, 2013; Androulidakis et al., 2015; Makris et al., 2016; *etc.*).

All the aforementioned studies discuss in either a concise or a more elaborate manner the model validation approaches and predictive model skill issues that may arise due to erroneous treatment of boundary conditions, low resolution of simulations, ambiguity of bathymetric data, uncertainty in MSL (owing to eustatic changes and steric effects) estimation under climate change conditions, and parametric assumptions of physical processes. Thus herein, we follow the same reasonable approach of comparing model simulation output of sea level elevation against field observations by tide gauges for a historical "Control Run" period in terms of main statistical measures (maxima, statistically significant indexes, percentiles, probabilities of exceedance, *etc.*) for the simulated/field datasets of sea level (*e.g.*, Marcos et al., 2009; McInnes et al., 2009; Jordà et al., 2012; Conte and Lionello, 2013, Androulidakis et al., 2015; Makris et al., 2016; *etc.*). Nevertheless, the achieved good skill metrics does not ensure a good model performance for the 21st century climatic projections in terms of timing and magnitude prediction, as the storm surge models' skill mainly rely on projected atmospheric forcing input.

Given the above, the comprehensive analyses of synoptic-scale meteorology and climatology over the Mediterranean basin are numerous (Trigo et al., 1999; Maheras et al., 2001; Trigo et al., 2002a; Lionello et al., 2002; Nissen et al., 2010; Garcies and Homar, 2011; Campins et al., 2011; Sanchez-Gomez and Somot, 2018; Velikou et al., 2019; Tolika et al., 2021) and their relation to the occurrence of storm

surges has been investigated extensively in recent literature (Krestenitis et al., 2011; Conte and Lionello, 2013; Androulidakis et al., 2015; Šepić et al., 2015; Makris et al., 2015, 2016, 2018, 2020a; Vousdoukas et al., 2016; Lionello et al., 2019, 2021; Tolika et al., 2021; *etc.*). It is found that coastal inundation events are usually caused by enfeebled extra-tropical cyclones following the South-European extension of the North Atlantic storm tracks or by secondary triggered cyclones in the north-western Mediterranean basin (cyclogenetic centre of the Gulf of Lions). The North-African cyclogenesis centre can also produce deep depressions pronounced in the east-central Mediterranean probably affected by climate change signals mid-latitude storm tracks and their Mediterranean branches towards the Adriatic, Ionian, and Aegean Seas (Alpert et al., 1990; Trigo et al., 1999; Maheras et al., 2001; Flaounas et al., 2018; Lionello et al., 2016; Reale and Lionello, 2013). The main centres of cyclogenesis around and over the Mediterranean Sea are the Genoa aera, the Saharan cyclonic regions (mainly during spring), the Iberian Peninsula thermal lows, the Aegean Sea (during winter and spring), the eastern Black Sea region (enhanced during summer), the leeward regions of the Alps and Atlas Mountains, the Cyprus cyclone source, and the Middle Eastern centre over Syria (as an extension of the Indian Monsoon low) (Maheras et al., 2001; Makris et al., 2016). Several characteristic atmospheric low-pressure systems exist over the basin, in the form of extratropical cyclones induced by deep depressions, occasionally termed as Medicanes (Radinovic, 1987; Cavicchia et al., 2014; Cid et al., 2016; Fortelli et al., 2021; Toomey et al., 2022; Flaounas et al., 2021), such as the recent "Ianos" event (Lagouvardos et al., 2021; Androulidakis et al., 2022). Such severe storm conditions may cause extended damages on the Mediterranean coasts driven by sea level elevation due to the combinatory action of storm surges, high tides, and rough seas (long and high waves with large energetic content) (Martzikos et al., 2021). Past research about related climate change projections for the 21st century, based on SRES scenarios, reveal significant alterations in the occurrence of cyclones and coastal sea level response, particularly during winter (Lionello et al., 2008; Marcos et al., 2011; Jordà et al., 2012). More recently, Međugorac et al. (2021) found a small probability of significant change in the frequency, intensity, annual cycle, and spatial structure of the local wind status inducing storm surges in the Adriatic under the Med-CORDEX climate projections, independently of the RCM, boundary conditions, RCP scenarios, or future time interval considered. Moreover, Reale et al. (2022) presented an analysis of Mediterranean cyclone characteristics in projected future climatic conditions based on Med-CORDEX ensemble of coupled RCSMs under RCP8.5, estimating the spatial patterns and cyclone activity in the Mediterranean during the 21st century. In general, the RCSMs showed a decrease in the number and an overall enfeeblement of cyclones moving across the Mediterranean towards 2100. The authors corroborated the observed CMIP5 projections for the area, where an obvious increase in the central Mediterranean is estimated compared to a decrease in its south-eastern part. A pronounced inter-model discrepancy of RCSM outputs refers to the cyclone adjusted deepening rate, seasonal cycle occurrence and associated wind patterns over some areas of the basin (Ionian Sea and Iberian Peninsula).

### 1.2. Study objectives

In all the above, emphasis was put on the analysis of synoptic-scale climatic weather patterns and tidal-surge sea level anomalies; astronomical tides can be more or less predicted within a deterministic framework in the long run, whereas surges and waves and their extremes are estimated to evolve in a stochastic mode during the 21st century driven by projected climate change and have thus been treated probabilistically (Wahl et al., 2012; Wahl and Chambers, 2016; Vousdoukas et al., 2018). Yet, what seems to be fairly missing from literature is a long-term and basin-scale systematic analysis of deep depressions (intense low barometric systems) and their correlation to storm surges at the entire Mediterranean basin's coastal zone (*e.g.*, Lionello et al., 2019). This motivates the present analysis to focus on coastal sea level variations of mid- to short-term timescale events but within a climatic (30-years) timeframe. Therefore, we engage filtering operations on the used tide-gauge data in order to remove long-term (higher than a month) effects of sea level variability prompted by basin-scale oscillations, planetary or edge waves, steric effects, and eustatic changes of the Mediterranean water masses. Accordingly, herein, the storm surge (on the coast) is defined as the phenomenon that causes temporary (short- to mid-term) deviations (*e.g.*, setup) of the Sea Surface Height (SSH) from MSL with simultaneous barotropic currents pushing seawater onshore. These events usually last from a few hours to a few days, having a large spatial extent, and they are induced by severe, synoptic timescale, weather conditions, combining the action of wind and Sea Level Pressure (SLP) on the free surface of seawater in local or regional scales (Međugorac et al., 2018). Identifying the frequency and intensity of extratropical cyclones' occurrence in climatic timescales (≥30 years) is relevant to its correlation with coastal impacts and quantification of coastal hazards (surges, wave run-up, and floods). Hence, in the present paper we try to recognize the evolution of cyclonic patterns and characteristics under possible future climatic conditions. Their influence on the coastal sea level response is then determined to assist the mapping of vulnerable littoral areas against possible inundation hazard, specifically for the low-lying coastal plains.

Therefore, the general objective of the paper is to systematically assess the impacts of projected climate change on episodic events of sea level elevation in coastal areas of the Mediterranean, induced by severe weather conditions identified as deep depressions. Thus, our aim is to add new insight in the climatic-scale identification of vulnerable parts of the coastal zones correlated to peculiar atmospheric patterns indicative of the Mediterranean basin during the 21st century. An integrated quantitative assessment is proposed to achieve these goals by combining projections from available established climate change scenarios (based on Representative Concentration Pathways; RCPs) with advanced numerical modelling and statistical post-processing for the definition of cyclonic weather impacts on exposed coastal zone hotspots. To this end, climate projections and outputs from several Global Climate Models (GCMs) generating outputs of Regional Climate Models (RCMs) at the Mediterranean basin scale are used and extensively evaluated. The latter atmospheric datasets fed a validated, robust, storm surge model for the simulation of barotropic hydrodynamics (sea level elevation and currents).

The proposed methodology incorporates and enhances older numerical simulations of the storm-driven hydrodynamic circulation in the entire Mediterranean basin with special focus on the meteorologically induced sea level variations on the coastal zone, based on MeCSS model (initially set up and presented by De Vries et al., 1995; further implemented by Krestenitis et al., 2011; established by Androulidakis et al., 2015; and enhanced with nested simulations by Makris et al., 2015, 2016, 2018, 2020a). Moreover, the produced results of the present study have already been used in a focused site-specific study, integrated within a local-scale hydrologic/hydrodynamic modelling approach under projected climate change conditions in the 21st century (Makris et al., 2020b; Skoulikaris et al., 2021). The application involved coastal flooding estimations of the Nestos River delta in the northern Aegean Sea, Greece (east-central Mediterranean).

In the following we refer to: the methodology and data selection and analysis (Section 2); the processing and thorough validation of a unified set of atmospheric data (based on IPCC's emission scenarios) against re-analysis sets (Section 3); the extended evaluation of hydrodynamic modelling simulations for storm surges against *in situ* sea level observations by tide-gauges (Section 4); the estimation of regional projections' climatic weather patterns from the Med-CORDEX database *in tandem* with storm surge projections in the Mediterranean for the 21st century leading to quantification of deep depression systems' effect on the coastal sea level elevation (Section 5); the discussion and conclusive remarks of the study (Section 6).

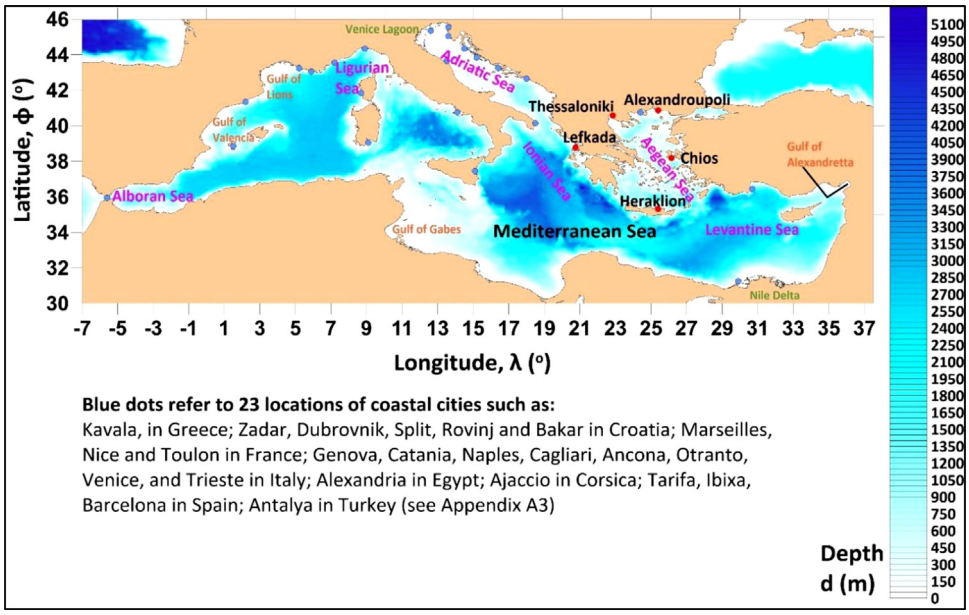


**Fig. 1.** Study area map of the Mediterranean Sea bathymetry, d (m), representing MeCSS model domain. Characteristic Gulfs and sub-basins are also marked with orange and purple colour. Red dots refer to the five Greek tide-gauge stations (Alexandroupoli, Chios, Heraklion, Lefkada, Thessaloniki) used for MeCSS model validation against field observations of sea level.

## 2. Methodology

### 2.1. Study domain

The study region refers to the Mediterranean basin for both analyses of the climatic and the storm-driven hydrodynamic processes, especially focusing on the sea level response over the entire Mediterranean coastal zone related to storm surge impacts on vulnerable, low-land, littoral areas. For this purpose, the modelling component of hydrodynamic circulation for storm surges is implemented by a 1/10° × 1/10° horizontal resolution. The entire study area *in tandem* with the used tide-gauge stations for validation are shown in Fig. 1. The General Bathymetric Chart of the Oceans (GEBCO; http://www.gebco.net/) was used to build the storm surge model bathymetries with bilinear interpolation into the models' ortho-regular computational grid with a resolution down to a spatial discretization step of almost $dx = 10$ km. The atmospheric forcing, namely the winds at 10 m elevation from MSL and the SLP fields, are provided in daily format within the spatial window of Fig. 1.

The Mediterranean Sea's quite unique character results both from its complex morphology and the specific socio-economic conditions (highly urbanized littorals) of coastal countries in southern Europe, northern Africa, and the southwestern (Anatolian) part of Asian continent. Therefore, it is a practically enclosed aquatic basin in terms of storm surges (and waves), confined by the southern European continental land, Asia Minor and the western part of the Middle East, and North Africa, connected to the Atlantic Ocean and the Black Sea through the very narrow Straits of Gibraltar and Bosporus, respectively. The Mediterranean basin includes several microtidal marginal seas (sub-basins) and has its own peculiar, very active, regional thermohaline and weather-driven circulation patterns, the first induced by deep and intermediate dense water formation and convection in the Gulf of Lions, the Adriatic, the South Aegean, and the North-East Levantine (Adloff et al., 2015), and the latter by a specific regional cyclogenetic regime and local aeolian patterns. The Mediterranean basin is surrounded by a variable coastline and complex continental orography, which causes several channelling regional winds (*e.g.*, Mistral, Tramontane, Bora, Etesian, Sirocco, *etc.*). This defines certain peculiarities in simulating local climatic conditions considering a spread out and strong land–sea contrast, land–atmosphere feedback, and intense air–sea coupling; *viz.* the existence of many mid- to large-size islands and smaller insular formations (*e.g.*, in Aegean archipelago) may limit or enhance low-level air flow, defining local wind patterns, *etc.* (Makris et al., 2016).

### 2.2. Climatic data

The climatic data, used as forcing to the hydrodynamic model implementation, were retrieved from the Med-CORDEX database (www.medcordex.eu), a regional contribution to the COordinated Regional Climate Downscaling Experiment (CORDEX) initiative, dedicated to the broader region of the Mediterranean basin (Ruti et al., 2016). Med-CORDEX is supported by HyMeX (https://www.hymex.org/) and MedCLIVAR (http://www.medclivar.eu/) international programs and follows up previous and existing initiatives by the Mediterranean climate research community. Med-CORDEX takes advantage of high-resolution RCM runs (with spatial discretization down to 10 km) and of new fully coupled Regional Climate System Models (RCSMs), integrating various components of the regional climate (Sevault et al., 2014; Reale et al., 2022). Med-CORDEX constitutes a freely available framework of regional atmospheric, land surface, river and oceanic climate models and coupled RCSMs, aiming at the reliability enhancement of past and future regional climate information and processes in the Mediterranean (Somot et al., 2018).

The grid resolution of the Med-CORDEX sub-domain is set to 0.44° × 0.44° for the RCMs using a rotated pole system, where the model operates over an equatorial domain with a quasi-uniform resolution of approximately 45 km. Being a continuous effort, the Med-CORDEX database includes simulation outputs of different spatial resolutions (*e.g.*, down to 10 km); yet at the time of the presented research and modelling implementation the only full climatic datasets for several combinations of GCMs, RCMs and RCPs were the aforementioned Med-44 domain components. Original Med-44 data were further processed, in order to match the requirements of the study's simulations by means of the Climate Data Operators (CDO) toolset (https://code.mpimet.mpg.de/projects/cdo/), in order to match the requirements of the study's simulations and validation against the CERA-20C dataset (Laloyaux et al., 2016; see Section 2.6). First, the data coordinates were transformed from the original rotated-pole coordinate system to an ortho-regular longitude–latitude one. Subsequently, they were cropped

and interpolated to the extents and resolution of the simulations' desired domains. The available and post-processed (interpolated) datasets cover a Reference (1971–2000) and a Future (2071–2100) Period of climate projections. The atmospheric parameters used as forcing of the hydrodynamic ocean model consist of wind (velocity and direction) and atmospheric pressure fields by three high-resolution RCMs, developed and implemented by three institutions in the framework of the Med-CORDEX initiative (Ruti et al., 2016), namely:

(1) CMCC (https://www.cmcc.it/models/cmcc-med), model COSMO-Climate Limited-area Modelling CMCC-CCLM4-8-19 v.1 (https://www.pik-potsdam.de/research/climate-resilience/models/cclm).
(2) CNRM (https://www.umr-cnrm.fr/spip.php?article1094&lang=en), using ALADIN (Aire Limitée Adaptation dynamique Développement InterNational) limited area bi-spectral model CNRM-ALADIN52 v.1 (http://www.umr-cnrm.fr/gmgec-old/site_engl/aladin/aladin_en.html; Bubnová et al., 1995; Radnóti et al., 1995) of ARPEGE model (http://www.umr-cnrm.fr/) using also ERA40 re-analysis to study regional climate processes, air–sea flux over the Mediterranean at the regional scale, test of physical parameterizations, regional climate change scenarios, and comparison of regional climate methods (Spiridonov et al., 2005; Somot et al., 2008)
(3) GUF (http://www.goethe-university-frankfurt.de/75364063/), using GUF-CCLM-NEMO4-8-18 v.1., *i.e.*, a coupled atmospheric-ocean circulation ensemble model collaboration of CCLM with NEMO (Nucleus for European Modelling of the Ocean, www.nemo-ocean.eu/; Madec et al., 2017).

The main features and attributes (GCM driving field, ensemble member, experiments, numbers of grid points and vertical levels, horizontal resolution, grid type, domain extent, etc.) of the three RCMs by CMCC, CNRM, and GUF institutions are presented analytically in Table 1. Historical climate data for the available and post-processed (interpolated) dataset that covers the Reference Period (1971–2000) by all the RCMs are validated against ECMWF re-analysis fields (see Section 2.6 for analytical presentation of them and Section 3 for the extensive evaluation). Anthropogenic greenhouse gas (GHG) emissions are mainly driven by human population size, economic activities and policies, lifestyles, energy uses, land use patterns, technology developments and climate policies. The RCPs make projections based on the aforementioned factors and describe four different 21st century pathways of GHG atmospheric concentrations, air pollutant emissions and land use in IPCC-AR5 (Moss et al., 2010). The RCPs include a stringent mitigation scenario (RCP2.6), two intermediate scenarios (RCP4.5 and RCP6.0) and one scenario with very high GHG emissions (RCP8.5). They are consistent with the wide range of scenarios in the literature, which indicate strong, consistent, almost linear relationships between cumulative $CO_2$ emissions and projected global temperature change to the year 2100 in all RCPs and the wider set of proposed mitigation. RCP scenarios include timeseries of emissions and concentrations of full-suite GHGs, aerosols and chemically active gases, as well as land use/cover (Moss et al., 2008). Two out of the four RCPs presented in the IPCC-AR5 are used herein:

• RCP4.5 is an intermediate stabilization pathway in which radiative forcing is stabilized at approximately 4.5 W/m$^2$ and 6.0 W/m$^2$ after 2100 (assuming constant concentrations after 2150). It describes a possible climate future that depends on "modest" estimations about greenhouse gases concentrations in coming years.

• RCP8.5 considers radiative forcing that reaches >8.5 W/m$^2$ by 2100 and continues to rise for some amount of time (assuming constant emissions after 2100 and constant concentrations after 2250). It poses a "worst case scenario" among the four RCPs.

RCP4.5 can be characterized as a medium stabilization pathway with an estimated increase of temperature, by comparison of the future period (2081–2100) to the pre-industrial period (1850–1900) of 2.4 °C (range 1.7–3.2 °C). On the other hand, aiming on estimating the future storm surges under the most "pessimistic" scenario we also choose RCP8.5, in which the increase of the global mean temperature is estimated to rise to 4.3 °C (range 3.2–5.4 °C) according to Moss et al. (2010) and Van Vuuren et al. (2011). Moreover, for an easy association with the previous SRES scenarios, RPC4.5 is mainly similar to B2 (low emissions scenario) and RCP8.5 with SRES A1F1 (high emissions scenario).

### 2.3. Storm surge model

The numerical modelling of maritime hydrodynamics comprises regional scale simulations of the entire Mediterranean basin in terms of meteorologically induced SSH and barotropic currents on the coastal zone. Computations were done with the Mediterranean Climatic Storm Surge (MeCSS) model (Krestenitis et al., 2011, 2014; Androulidakis et al., 2015; Makris et al., 2015). MeCSS is a long-term (climatic mode) running version of the operational High-Resolution Storm Surge (HiReSS) model set up in the Mediterranean basin (Krestenitis et al., 2015, 2017; Makris et al., 2019, 2021). HiReSS/MeCSS is a 2-D horizontal, barotropic, hydrodynamic circulation model that solves the depth-averaged shallow water equations for the high-resolution simulation of storm surges and related flows in large-scale, enclosed, or semi-enclosed water bodies (De Vries et al., 1995; Krestenitis et al., 2011, 2014, 2015).

MeCSS simulates the meteorologically induced sea level variations and depth-averaged currents by considering large-scale shear forces on the air–seawater interface and the inverse barometer effect. Thus, it takes into account the atmospheric forcing, *i.e.*, zonal and meridional wind fields at 10 m from MSL and SLP fields, the geostrophic effects of the Coriolis force, the influence of astronomical tides on the open boundaries (based on harmonic tidal elevation), bottom friction on the seabed, and "internal friction" forces due to horizontal vortices based on the eddy viscosity concept and the Smagorinsky model approach (Makris et al., 2015, 2021). MeCSS computations are executed on an ortho-regular staggered Cartesian grid of the Arakawa-C type, and the chosen numerical scheme of integration is an explicit first order Forward-Time-Cantered-Space (FTCS) algorithm of the Finite Difference Method (FDM) with small time step $dt \approx 30$ s to keep a sufficiently low Courant number, producing output in a 3-hourly time interval over the entire Mediterranean computational domain and on the coastal zone cells. A contingency file for restart of computations and uninterrupted continuity of simulations is produced systematically, in case of numerical blow-ups or power failure, as simulations are quite demanding in terms of computational resources and time.

It has been widely implemented in the Mediterranean and other, similar scale, water bodies during the past decade for both climatic type long-term simulations and short-term operational forecasts of storm surges with ranging resolutions for the entire Mediterranean basin, *e.g.*, 1/10° × 1/10° down to a ~5 km horizontal grid and even 1.6 km in shallower water coastal areas, *viz.* Thermaikos Gulf and Thesaloniki Bay or Nestos Delta littoral zone in northern Greece (Androulidakis et al., 2015; Krestenitis et al., 2014, 2017; Makris et al., 2016; Skoulikaris et al., 2021). It has been successfully calibrated and validated in the past to produce reliable estimates of sea level elevation during shallow and deep barometric systems giving acceptable to quite good estimations of negative and positive surges, respectively, in nearshore areas (Makris et al., 2018, 2019, 2021; Skoulikaris et al., 2021). Herein, we examine the long-term, inter-annual patterns of daily-scale peak values of SSH induced by severe events of "meteorological tides", for which the storm surge impacts on the coast may last from several hours up to a few days, depending on the inundation levels and extents (Makris et al., 2020b; Skoulikaris et al., 2021; Tolika et al., 2021).

**Table 1**
Main features and attributes of the three RCMs by CMCC, CNRM, and GUF institutions.

| RCM feature/attribute | RCM | | |
|---|---|---|---|
| | CMCC-CCLM4-8-19 | CNRM-ALADIN52 | GUF-CCLM4-8-18 |
| Driving field | CMCC-CM | CNRM-CM5 | MPI-ESM-LR |
| Ensemble member | r1i1p1 | r8i1p1 | r1i1p1 |
| Experiments | Historical/RCP4.5/RCP8.5 | Historical/RCP4.5/RCP8.5 | Historical/RCP4.5/RCP8.5 |
| Number of grid points | 130 × 95 *(original grid type)*<br>98 × 63 *(grid processing)* | 101 × 63 | 114 × 79 *(original grid type)*<br>98 × 63 *(grid processing)* |
| Number of vertical levels | 45 | 31 | 32 |
| Horizontal resolution | 0.44° × 0.44° | 0.5° × 0.5° | 0.44° × 0.44° |
| Grid type | Rotated pole projection | Lambert conformal projection | Rotated pole projection |
| CORDEX domain | MED-44 | MED-44 | MED-44 |
| References | http://www.cmcc.it/ | http://www.umr-cnrm.fr/ | http://www.clm-community.eu/<br>http://www.geo.uni-frankfurt.de/iau/meso/ |

### 2.4. Detection of deep depressions

#### 2.4.1. Identification of the mediterranean low-pressure systems

The deep depressions (low-pressure systems) over the Mediterranean Sea have been the subject of numerous studies over the past years. However, at first, their identification and localization were mostly based on empirical methods, including the subjectivity of researchers (Maheras, 1983; Radinovic, 1987; Flocas, 1988). Later, and since the 1990's, more objective methodologies were utilized to detect these centres of cyclogenesis at several domains of interest (*e.g.*, Alpert et al., 1990; Trigo et al., 1999; Maheras et al., 2001; Flaounas et al., 2018) over and around the basin. According to relevant literature (Flocas and Karacostas, 1996; Thorncroft and Flocas, 1997; Trigo et al., 1999; Maheras et al., 2001; Lionello et al., 2016) the main areas, characterized as "Cyclogenesis Centres", related to the Mediterranean domain are the following:

- The Gulf of Genoa; the depressions are mainly formed over the downhill sides of the Alps presenting quite stable frequency of occurrence throughout the year. The Gulf of Lions, as well as the Balearic Islands' region, are considered as extensions of the main centre and cannot be considered as separate cyclogenesis centres.
- The region at the south of the mountain range of Atlas; the most characteristic area is at the northwest Africa and the frequency of the cyclones is higher mainly during May and June.
- The Iberian Peninsula; it appears mainly during the mid-spring period until summer, when the temperature differences between sea and land favour the development of thermal depressions.
- The Aegean Sea; it is also characterized as a cyclogenesis centre, even though it is a rather limited area in comparison to the aforementioned ones.
- The eastern Black Sea; there, depressions can be formed throughout the year and mainly during the summer period (July and August).
- The broader Cyprus Region; the east-central Levantine Sea can produce cyclones of mid-intensity, usually observed during summer and autumn.
- The Middle East; the area over Syria and Iraq related to the formation of summer cyclones as a result of the easternmost extension of the Pakistan Low.

#### 2.4.2. Validation of Med-CORDEX RCMs for the simulation of deep cyclones over the Mediterranean Sea

In order to detect deep depressions (*i.e.*, cyclones with centre pressure lower than 1000 hPa; Trigo et al., 2002b), the methodology introduced by Rousi (2014) was applied. The proposed algorithm uses gridded data of daily SLP by both CERA and the three RCMs for the studied 30-years timespans (Reference and Future Periods). It computes the frequency of occurrence of deep depressions (*i.e.*, number of days within the 30-years period) after the identification of separate cyclonic circulation events. Results are illustrated on gridded maps of the study area (see Sections 3.3 and 5.1.2 for results). By comparisons of CERA to RCM produced maps, the ability of the climate models to reproduce both the locations of deep depressions and their frequencies can be assessed. The characterization of a daily time step in our analysis as "day of deep depression" relies on two criteria. Firstly, on this day SLP in a grid point must be lower than 1000 hPa. Secondly, it is also necessary for neighbouring grid points, within a threshold radius, to have higher atmospheric pressure values than that of the examined point to identify it as the centre of cyclogenesis.

As the Med-CORDEX project was very recent during the time of implementation of the presented research (2018–2020) and its evaluation is still ongoing, only a few validation reports were available in recent literature. These mainly focus on synoptic scale weather patterns, cyclones, barometric systems and aeolian processes, e.g., Belušić et al. (2018) examining wind variability over the Adriatic, Flaounas et al. (2018) exploring dynamical downscaling of regional winds and cyclogenesis, Obermann et al. (2018) investigating Mistral and Tramontane winds *in tandem* with large-scale pressure patterns, Gaertner et al. (2018) referring to seasonal shifts of Medicanes reproduced by an RCM ensemble, and Sanchez-Gomez and Somot (2018) seeking the variability of cyclone tracks.

### 2.5. Available field data for model validation

In the past, suitable *in situ* sea level observations in the Mediterranean basin, freely available by tide gauge measurements of National Hydrographic Services, *e.g.*, via the Global Sea Level Observing System (GLOSS; http://www.gloss-sealevel.org/), EMODnet (https://map.emodnet-physics.eu/) *etc.*, have been traced. These have been used for comparisons with MeCSS results to validate the model's performance for Control Run during different Reference Periods (see Androulidakis et al., 2015; Makris et al., 2015, 2016, 2021). Herein, for temporal sufficiency, homogeneity, and qualitative consistency reasons, data from the tide gauge network of the Hellenic Navy Hydrographic Service (HNHS; http://www.hnhs.gr/portal/page/portal/HNHS) are presented, namely by four stations in the Aegean Sea (Thessaloniki, Alexandroupoli, Heraklion and Chios) and one in the Ionian Sea (Lefkada). The available data cover an 11-year period from 1995 to 2005; to this end, the retrieved historical climatic dataset for the Reference Period was expanded by 5 more years from 2001 to 2005.

As comparisons of model-field data are based on daily averaged SSH values in this study, the measured *in situ* datasets were processed after subtraction of the calculated 11-year MSL with a high-pass filter operator using a cut-off frequency of 1/30 days, in order to exclude long-term sea level oscillations (Conte and Lionello, 2013). The latter can be primarily induced by the steric effects, due to the large-scale, low-frequency, thermohaline fluctuations and/or total mass variations of the enclosed basin under investigation (Carillo et al., 2012). These types of effects are not simulated by MeCSS, which considers the Mediterranean region as an enclosed aquatic body and, thus, it was necessary to exclude the effects of such processes from the observations

as well. Moreover, MeCSS model does not include modelling of tidal motions on all grid cells, as is typically done in short-term forecasts with HiReSS model, but only on the open straits as a Dirichlet type boundary condition. Astronomical tide signals are therefore removed from the used field data of SSH with the use of the T-Tide software (Pawlowicz et al., 2002). It is also noted that tides are of generally small amplitude in most parts of the Mediterranean Sea, compared to the extreme positive and negative free surface elevation due to storm surges. This is not necessarily true for the N. Adriatic where the tidal signal can add up to 30 cm on the 50-year return period SSH (Marcos et al., 2009). It is noted that no tidal gauge data in the Adriatic region were used for comparisons with model output in the present study.

### 2.6. Available climate reference data for RCM validation

For the evaluation of the used RCM outputs, datasets by the CERA-20C coupled assimilation system are used (please note that finer resolution datasets, *e.g.*, ERA5 were not yet available at the time of implementation). CERA-20C consists of a 10-member ensemble of coupled climate re-analyses of the 20th century from the European Centre for Medium-Range Weather Forecasts (ECMWF) and aims at reconstructing the past weather and climate of the Earth system including the atmosphere, ocean, land, ocean waves, and sea ice (Laloyaux et al., 2018). The timeseries cover the period from 1901 to 2010. It is based on the Coupled ECMWF Re-Analysis (CERA) coupled data assimilation system (Laloyaux et al., 2016), which assimilates only surface pressure and marine wind observations as well as ocean temperature and salinity profiles. It has been one of the crucial outcomes of ERA-CLIM2 project (https://www.ecmwf.int/en/research/projects/era-clim2).

The CERA-20C product describes the spatiotemporal evolution of the atmosphere (125 km horizontal grid with 91 vertical levels, between the surface and 0.01 hPa), the land-surface (125 km horizontal grid with 4 soil layers, the waves for the period 1901–2010), the ocean (110 km horizontal grid with meridional refinement at the equator, 42 vertical levels) and the sea ice. It should be highlighted that atmospheric data are not only available on the native 91 model levels, but also on 37 pressure levels (as in ERA-Interim), 16 potential temperature levels, and the 2 PVU potential vorticity level. The utilized spatial resolution of CERA-20C dataset was a downscaled version of $0.25° \times 0.25°$. The CERA assimilation system has the ability to produce a more balanced and consistent Earth system climate reconstruction, as it considers the interactions between the atmosphere and the ocean. More detailed information about the CERA-database can be found via the link: https://www.ecmwf.int/en/forecasts/datasets/archive-datasets/reanalysis-datasets/cera-20c.

To evaluate the skill of the three selected RCMs in simulating the main parameters that were used for MeCSS forcing, it was decided to execute comparisons during the 30-year Reference Period (1971–2000), on both an annual and seasonal basis.

## 3. Climatic data evaluation

In any respect, all researchers stress the need of consistent and quality-checked fine-scale observational datasets for the robust evaluation of RCMs. In the following, we present our own systematic validation of the Med-CORDEX SLP and wind data for the Reference Period 1971–2000 (Control Run simulations) via comparisons against CERA-20C datasets.

### 3.1. Validation of sea level pressure fields over the Mediterranean region

#### 3.1.1. Annual analysis

The spatial distribution of both re-analysis and RCM data for averaged SLP values on an annual basis is presented in Fig. 2. Regarding the mean annual SLP fields derived from CERA data it is found that the pressure values range from 1013 up to 1020 hPa with an increasing gradient from east to west-northwest. The minimum is located over Cyprus and the highest ones at the north in the Iberian Peninsula. The comparison with equivalent SLP fields, simulated by the three examined RCMs (CMCC, CNRM, and GUF; see Section 2.2), showed that all three models can capture the main characteristics of annual atmospheric pressure patterns with the lowest values at the easternmost part of the Mediterranean basin and the highest over to its western part. The calculated differences, which were evaluated applying *t*-test statistics at a level of significance 0.05, revealed that the CMCC tends to slightly overestimate the actual SLP values all over the domain of study. Small positive differences cover almost the entire Mediterranean region (up to 3 hPa) and only at a limited area near the north-western boundary the computed differences are negative.

However, even though the magnitude of the differences is small, most of the grid points were found to be statistically significant since the applied test considers the actual compared values of node-to-node SLP timeseries *in tandem* with the discrepancies in their variability. Regarding the CNRM model, the difference pattern divides the Mediterranean region in half. The northern continental parts are characterized by negative differences (*i.e.*, model underestimates SLP values), whereas the marine area shows small positive differences with higher overestimation over the south-eastern Mediterranean, central and eastern Levantine, southern Anatolia, and the Middle Eastern continent and coasts. Values of mean SLP deviations vary from −3 hPa to +3.5 hPa. The GUF model overestimates the annual atmospheric surface pressure towards the southern Mediterranean and the Iberian Peninsula (positive differences), while in the northern part of the domain the differences are negative (SLP underestimation). As in previous models, GUF modelled SLP differences are quite small, showing that the three models present an efficient skill in simulating mean SLP characteristics (main dynamics of barometric systems) during the typical annual cycle for a 30-years period.

#### 3.1.2. Seasonal analysis

The large-scale barometric system patterns during winter of the Reference Period (1971–2000), according to the CERA results, is characterized by four main high-pressure centres (above 1020 hPa), *i.e.*, over the Iberian Peninsula, Algeria, Balkans, and Turkey (Fig. 3). The central and eastern Mediterranean Sea, on the other hand, is characterized by lower values with a minimum over Cyprus. All models seem to be able to capture the location of these maximum centres (but with overestimated pressure values), while the minimum in all of them is found at the north-western parts of the domain. In spring (Appendix B, Figure A1.1), all over the Mediterranean, SLP values are much lower and more uniform, in comparison to winter. SLP varies from 1015 hPa at the south-eastern parts (Cyprus, Syria, Lebanon) and to 1017 hPa at the western parts of the Mediterranean (with SLP maxima covering a quite large area). The studied RCMs can reproduce the spring SLP fields, but the barometric highs are slightly more extended and intense compared to CERA datasets, especially for GUF's RCM. A stronger horizontal gradient characterizes the summer mean SLP fields over the Mediterranean, varying from 1005 hPa over its eastern parts up to 1019 hPa at the northwest.

Similar to aforementioned seasonal patterns, the three RCMs present high skills in reproducing the spatial pressure distribution, capturing the main characteristics of summer pressure over the Mediterranean. Finally, a more uniform distribution of the mean SLP values is illustrated in (Appendix B, Figure A1.2) during autumn, according to the CERA data. The minimum is located at the southeast of the Mediterranean region, while the highest mean pressure values are observed at the north, especially over the Balkan Peninsula. CMCC model can simulate this maximum but high-pressure values (1020 hPa) are found over France and Spain, too. Equivalent SLP autumn values are also observed over the western African coast. The CNRM simulations have a similar pattern with slightly lower values (they do not exceed 1018 hPa). Analogous results are found in the case of the GUF model, with the

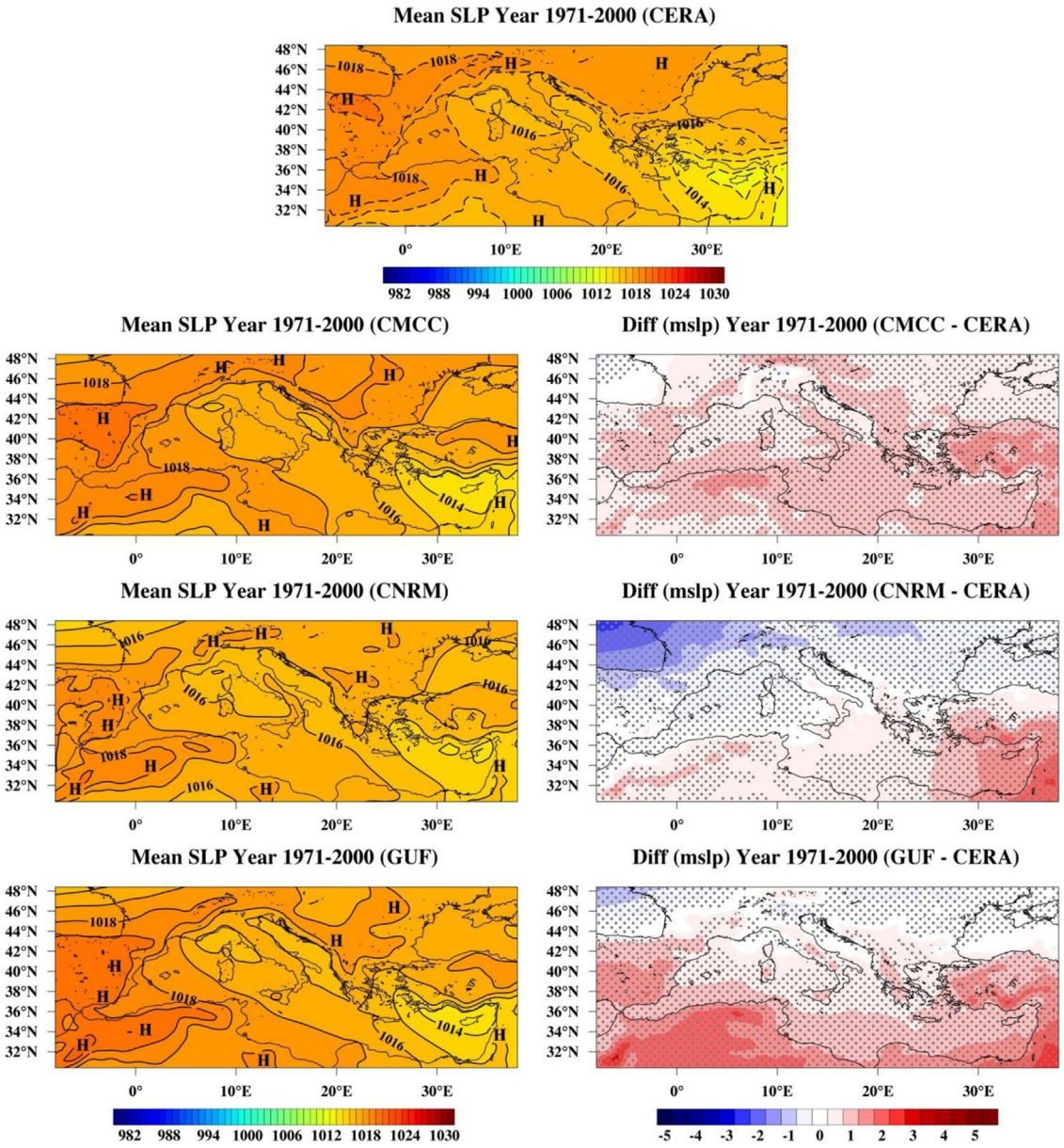


**Fig. 2.** Spatial distribution of re-analysis (CERA; top graph) and RCM mean SLP (mslp; in hPa) values on an annual basis during the Reference Period (1971–2000) for the three examined models by CMCC, CNRM, GUF (from top to bottom; left column graphs) and their differences in comparison to the CERA data (model – CERA; right column graphs). Grid cells with statistically significant differences ($t$-test: 0.05 level) are marked with grey point dots.

minimum over Cyprus and the maximums located over the same areas as the CERA pattern.

Moreover, the respective composite maps of mean SLP differences over the entire studied domain, comparing CERA to the three RCM datasets. The winter period is characterized by the largest differences compared to the rest of the seasonal patterns. Specifically, the CMCC model mainly overestimates the winter mean SLP, with the highest positive differences found over the central and eastern Mediterranean Sea, Turkey, and the south-eastern African coast. On the other hand, CNRM and GUF models overestimate the winter SLP mean values over the central and southern parts of the domain, while an underestimation (negative differences down to −5 hPa) is observed over the northern continental parts. In spring, CMCC can simulate the actual mean SLP values even better, since all over the study region the differences are very small (close to zero). CNRM underestimates the pressure values at the north-western parts of the Mediterranean, whereas positive differences are found at the south-eastern parts of the basin. Simulations seem more efficient over the marine areas than continental ones. The relevant map of the CNRM - CERA comparisons shows that negative differences prevail at the north-western, western, and central Mediterranean Sea, whilst positive ones at the southwestern African coast. In the case of GUF's RCM, the positive differences cover a more extended westernmost area up to the Iberian Peninsula (Appendix B, Figure A1.1).

As regards summer differences, both CMCC and CNRM models slightly underestimate summer mean SLP fields over the maritime Mediterranean area and the African coast, and slightly overestimate them over the continent (mainly CMCC). Conversely, GUF model overestimates the Reference Period's mean SLP values almost all over the examined domain with the positive differences increasing from north to south (Fig. 3). Finally, the computed autumn difference maps show that CMCC and GUF models have a similar performance in simulating the mean SLP values and overestimate them all over the domain of interest. In the case of CNRM model, positive differences cover only a very limited part of the Mediterranean at the southeast and negative

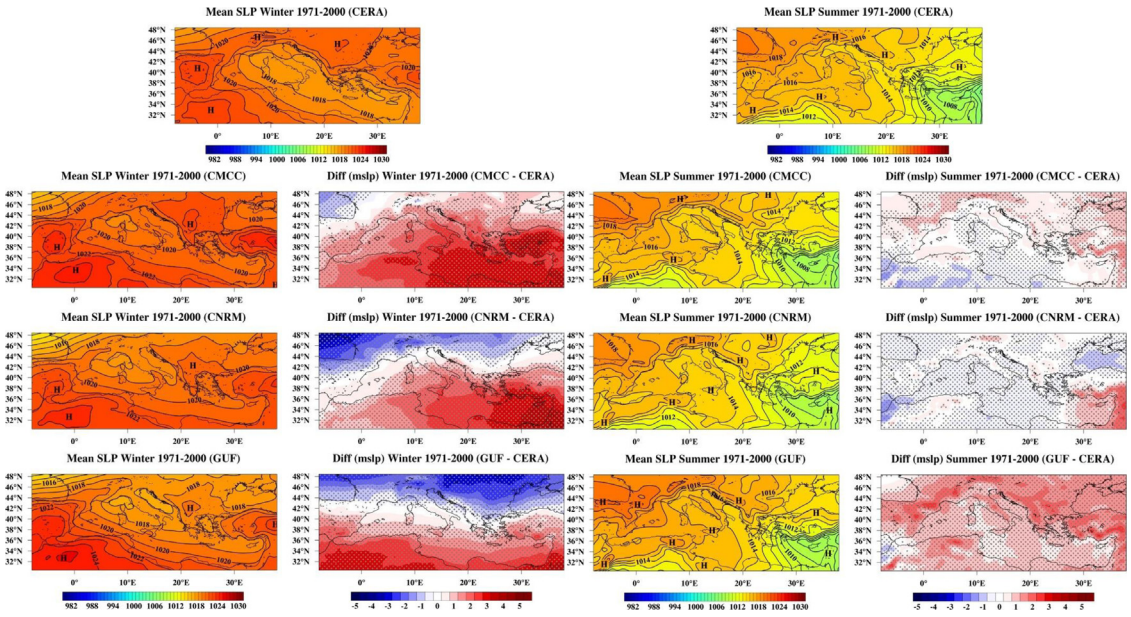


**Fig. 3.** As Fig. 2 but in the case of winter (left) and summer (right).

differences dominate. The largest deviations (being statistically significant) are found at the north-western parts of the region (Appendix B, Figure A1.2).

### 3.2. Validation of wind fields over the Mediterranean region

#### 3.2.1. Annual analysis

Fig. 4 displays the 30-years' mean climatic patterns of wind speed over the study domain, based on annual cycle analysis. According to CERA data depictions, the prevailing pattern refers to more intense winds over the marine areas than overland. Maximum values of mean wind speeds reach up to 8 m/s over the Aegean Sea, as expected. A secondary maximum of mean atmospheric circulation can be seen over the broader Gulf of Lions area, as well as in the southwestern Mediterranean region between Sardinia and Tunisia. The occurrence of wind maxima over the Aegean region could be attributed to the Etesian winds during summer, as well as to the strong north winds prevailing in winter. Moreover, the western maximum over the broader region around Marseille is found in one of the most characteristic (cyclogenetic) centres of deep depression formation over the Mediterranean, which should be associated with high-speed winds.

The evaluation of the three examined RCMs in simulating the wind fields over the Mediterranean showed in general an efficient skill in reproducing the spatial distribution of their velocities (Fig. 4). The Gulf of Lions is the region where all climate models reproduce the highest mean wind speed values, up to 8 m/s, while the Aegean Sea is the second Mediterranean area, where high winds blow. However, discrepancies can be traced, *e.g.*, RCMs could not reproduce the intense wind regime above and around the island of Crete, conversely to CERA output. Another differentiation of the RCM simulation outputs from the CERA annual wind maps is the existence of more intense winds at the Strait of Gibraltar (Fig. 4; left column). Regarding the continental parts of the study domain, CMCC and GUF models simulate slightly higher wind speeds especially in some parts of the Balkan Peninsula and the mountainous areas of the Iberian Peninsula. On the other hand, the CNRM model reproduces quite weaker winds over Spain, Italy, and Greece.

The equivalent composite maps of mean wind speed differences, between RCMs and CERA values, reveal several relatively small areas, where the differences are rather significant (Fig. 4; right column). All models underestimate (negative differences) the wind speeds at the Mediterranean coasts of Spain and France, over Corsica and Sardinia, the southern parts of Italy, in Greece above Peloponnese and Crete, and in the south-eastern coastal area of Turkey. Moreover, negative differences up to −2.5 m/s can be found over Cyprus. The above findings could be attributed to inadequacies in schemes and resolutions of the RCMs in simulating regional peculiarities of aeolian patterns and local complexities of the geographical characteristics in the Mediterranean region, especially in areas with diverse island formations and intense changes in land–sea sequence.

Regarding the main body of the Mediterranean Sea, the three examined RCMs seem to slightly overestimate the average wind speed patterns, with small positive differences all over the region. CMCC model results portray the highest overestimations, while for GUF model positive differences are very close to zero, except for the Gibraltar Strait. The latter is an area where highest positive differences are traced (up to 2 m/s). As mentioned above, the Gulf of Lions is another area where RCMs overestimate the mean wind speed climate, as well as the Ionian Sea, the eastern and south-eastern parts of the Aegean Sea. GUF model seems to underestimate the annual-basis mean wind speed regime of the northern parts of continental Africa, even though it presents the smallest differences in comparison to the other two RCMs (Fig. 4; right column).

#### 3.2.2. Seasonal analysis

During winter, the CERA mean wind speed fields over the Aegean Sea reach up to 9 m/s, representing an apparent local maximum throughout the Mediterranean region, followed by the local high wind speed potential in the Gulf of Lions (Fig. 5). In spring, the winds in these two areas are much weaker and the domain of study presents a much more uniform wind speed pattern. In summer, a dipole is detected with strong winds in the Aegean region (Etesians over the central and southern parts) and significantly weaker winds over the central Mediterranean, Tyrrhenian Sea and Sicily. Finally, in autumn, the two maxima winter pattern remains, but with significantly lower wind speeds (Appendix B, Figure A1.3).

The equivalent maps of the CMCC model output reveal its ability to reproduce the main features of the horizontal wind speed distribution during winter months, when maxima are correctly represented over the Gulf of Lions and the Aegean Sea. However, it is noteworthy that strong winds are also detected over the Black Sea, especially at its north and north-western parts as well as in the central part of the Mediterranean

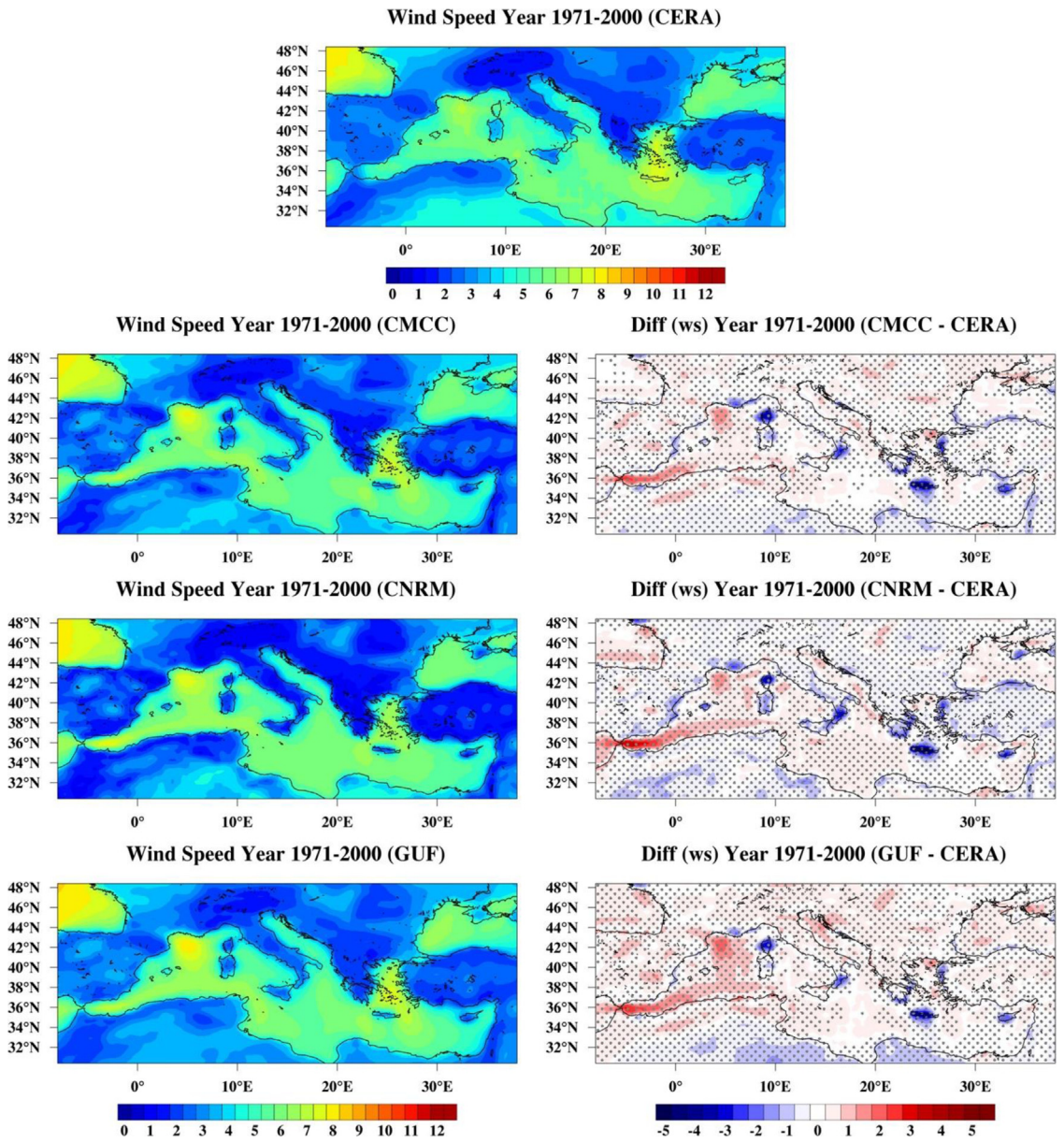


**Fig. 4.** Spatial distribution of re-analysis (CERA; top graph) and RCM wind speed (m/s) values on an annual basis during the Reference Period (1971–2000) for the three examined models by CMCC, CNRM, GUF (from top to bottom; left column graphs) and their differences in comparison to the CERA data (model – CERA; right column graphs). Grid cells with statistically significant differences (*t*-test: 0.05 level) are marked with grey point dots.

Sea between Sardinia and Sicily (Fig. 5). A more homogeneous wind speed pattern is reproduced during spring period, in accordance with CERA data, yet with persistent stronger winds over the Gulf of Lions (Appendix B, Figure A1.3). In summer, the CMCC's RCM can reproduce the Etesian winds' regime in the Aegean, but with lower speed values. On the other hand, in autumn depictions the two aforementioned maxima are higher than CERA results (Fig. 5).

CNRM simulations diversify in terms of winter patterns, as the model can capture strong wind fields over the Gulf of Lions, but the maximum over the Aegean Sea is much weaker than the CERA one. For the rest of the seasons, more homogeneous wind speed patterns are detected. Apart from the southern French continental shelf maximum, the rest of the Mediterranean Sea is characterized by speeds from 6 to 7.5 m/s.

Finally, the GUF model seems to reliably simulate the actual pattern of winds' distribution over the study domain, yet especially winter wind fields are estimated to be much stronger. On the other hand, the summer dipole (mentioned in the above paragraph) is more extended, especially its minimum pole, and the greatest part of central Mediterranean Sea is covered by wind speed values that do not exceed 3 m/s (Fig. 5). The composite maps of wind velocity differences (Fig. 5) show in general the same positive and negative poles as in the previous maps. It is worth mentioning that the highest positive differences (overestimation) of the GUF model refer to wintertime, and that the overestimation of wind speeds over the Strait of Gibraltar corresponds to all seasons for all three RCMs (Fig. 5).

### 3.3. Evaluation of extreme sea level pressure systems

According to the annual scale analysis of CERA data (Fig. 6), deep cyclones can be found in a quite large part of the Mediterranean region, especially over the sea. For most of the grid points, the frequency of

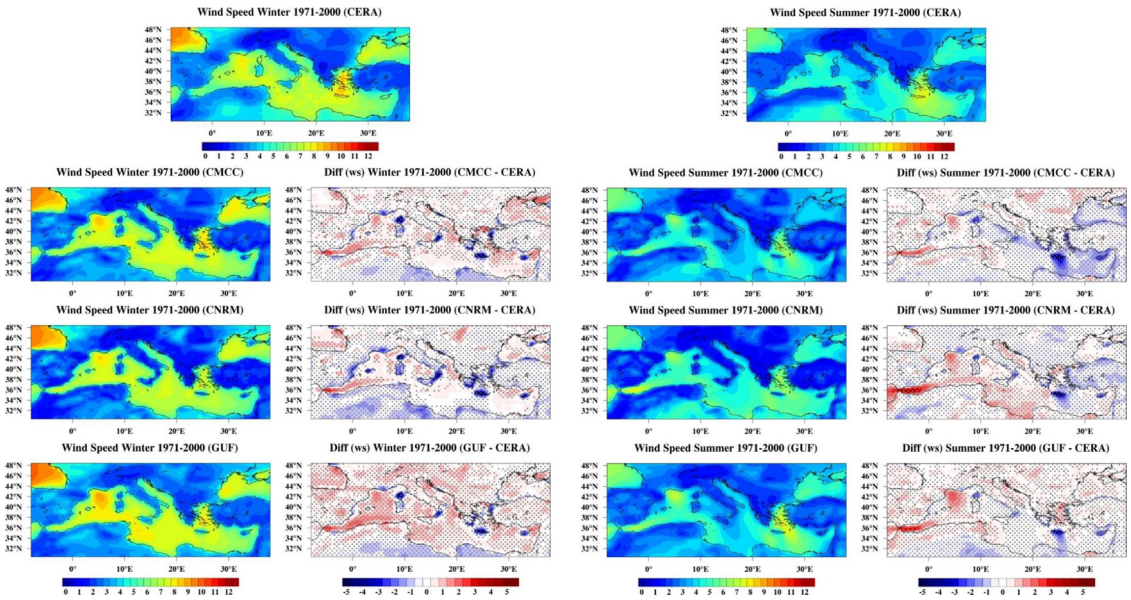


**Fig. 5.** As in Fig. 4 but for winter (left graphs) and summer (right graphs) seasons.

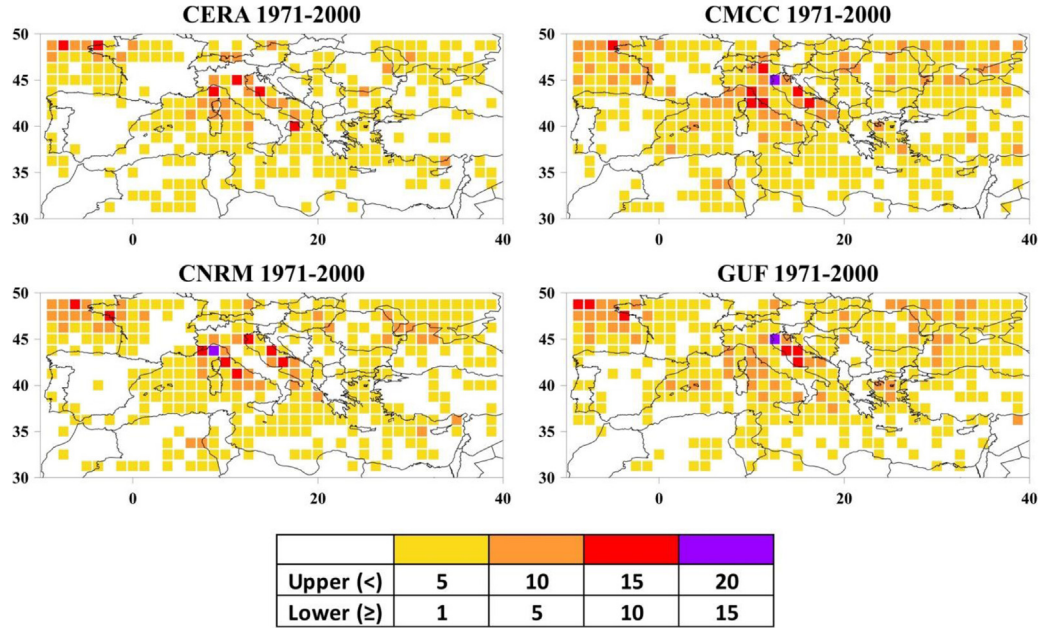


**Fig. 6.** Gridded map of frequencies of occurrence (in number of days) for the deep depressions over the Mediterranean Sea on an annual basis, regarding re-analysis (CERA) and RCM (CMCC, CNRM, GUF) from top to bottom graphs for the Reference Period (1971–2000). Colour palette is divided in four classes according to lower and upper margin for recorded number of days: 1st 1–5 days, 2nd 5–10 days, 3rd 10–15 days, 4th 115–20 days.

occurrence of deep depressions does not exceed five days during the Reference Period (1971–2000). However, it is obvious that there are regions of depression centres, especially over Italy in the Apennine Peninsula, where these frequencies are higher (Fig. 6). The maximum is found over two of the most well-known regions of Mediterranean cyclogenesis, such as the Gulf of Genoa (Ligurian Sea) and the Gulf of Venice in the Adriatic Sea. In these areas, the frequency of "extreme" depressions reaches 10 days (2nd class). For some grid points (in the aforementioned regions, as well as the Gulf of Taranto in southern Italy) the frequency is even higher, up to 15 days (3rd class). Finally, grid points with 2nd class frequency of occurrence are detected in the north of Cyprus, at the northeast of the Black Sea, as well as in the centre of the Tyrrhenian Sea. It should be underlined that these centres are in accordance with previous studies (Trigo et al., 1999; Maheras et al., 2001).

Regarding CMCC model results, its ability to reproduce the main centres of the deep depression formation over the domain of study is rather plausible. However, the grid points of the domain, which satisfy the suggested criteria for deep depression identification, are more than the relevant CERA-based results. Furthermore, a larger number of grid points have frequencies of the 2nd class (5 to 10 days).

The deep cyclone centre over the Gulf of Venice presents the largest recurrence pattern with 20 days of "extreme" depressions (Fig. 6). For CNRM model, the spatial distribution of incident frequencies of deep cyclones is quite similar to the CERA one, with the main cyclonic centres over the Gulfs of Genoa and Venice, the middle of the Tyrrhenian Sea and the centre of the Adriatic Sea (Fig. 6). However, the hotspot of deep depressions with a maximum frequency of 20 days is shifted to the west, at the Gulf of Genoa, in comparison with the CMCC

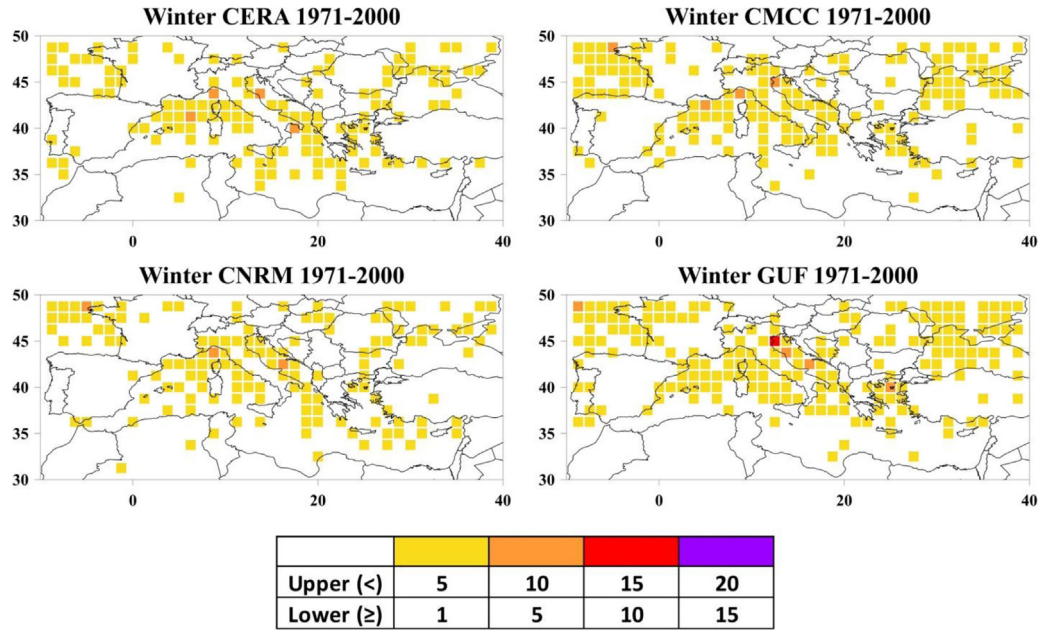


**Fig. 7.** As in Fig. 6 but in the case of winter.

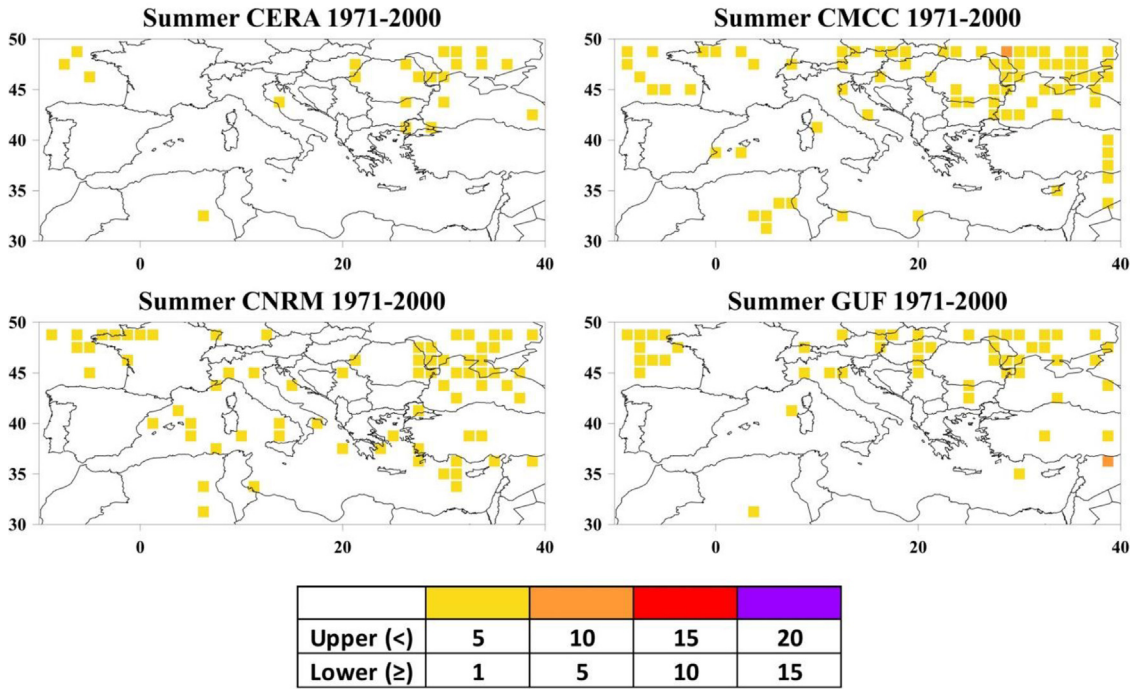


**Fig. 8.** As in Fig. 6 but in the case of summer.

model. Finally, the equivalent annual-scale results of the GUF model are mainly analogous to the CMCC model output, regarding especially the frequency maximums (Fig. 6).

In general, GUF's RCM is capable in reproducing the deep depression areas, also indicating three neighbouring grid points over the central and northern Aegean Sea with frequencies of occurrence up to 10 days, and one more over the northern Black Sea with barometric low incident frequencies in the 3rd class (10 to 15 days).

Figs. 7–8 (and A1.5–6 in the Appendix B) present the spatial distribution of the grid points, corresponding to locations with sufficient days of incident deep depressions (<1000 hPa) on a seasonal basis. For the winter season (Fig. 7) the largest percentage of deep cyclogenetic areas are located over the sea, rather than the continental parts of the Mediterranean region. The grid points with the maximum frequencies are found over the Adriatic Sea, the Gulf of Genoa, at the west of Corsica and at the Gulf of Taranto. Respective results were found for the CMCC's RCM simulations with a more extended cyclogenesis area over the Black Sea. In general, the winter deep depression frequencies do not exceed the five days threshold during the Reference Period. In the CNRM case, RCM results are very similar once again to the CERA data, indicating that the model can capture the deep depression occurrence frequencies (in both location and magnitude). In the Aegean Sea, the number of CNRM grid points with deep depressions is smaller than the CERA-based ones, while there is an overestimation of them over the Balkan Peninsula. Moreover, the GUF model results show that rather few grid points in the southern Mediterranean Sea fulfil

the criteria of the extreme cyclone incidence, while the maximum is reasonably located over the Gulf of Genoa with winter incidence frequency reaching up to 15 days (Fig. 7).

During springtime, CERA results show that the main pattern of the deep depression grid points is quite similar to the winter one, even though their number is higher, and they are more extended to the south. It is noteworthy that frequency maxima are traced over the continental parts of the study domain. The most important differentiation of the CMCC simulations is the exaggerated number of cyclogenetic grid points with deep depressions covering a very large part of the Mediterranean region. However, the incident maxima are located at the same areas as the winter ones (Appendix B, Figure A1.5). Analogous overestimating results were found for the other two RCMs (from CNRM and CUF). The summer results both for CERA and RCM simulations show that the deep depressions are quite fewer than the rest of the seasons, and the areas that are generally characterized by extreme depressions are limited over the northeast of the study domain (Fig. 8). Lastly, CERA results for the autumn season show that most of the deep cyclone grid points are gathered over the central parts of the Mediterranean Sea with the maximum frequency location over the northern Adriatic Sea, while very few grid points are found in the southern Mediterranean. All RCMs seem to simulate this pattern efficiently (Appendix B, Figure A1.6).

## 4. Storm surge model validation

The rigorous evaluation of MeCSS model, and its operational forecasting counterpart, HiReSS, has been extensively performed during the last decade, especially within the Mediterranean basin including datasets form Greek, Spanish, Italian and French tide-gauges (Androulidakis et al., 2015; Krestenitis et al., 2015, 2017; Makris et al., 2015, 2016, 2019, 2021). For the sake of coherence, brevity, and fulfilling the need for continuous datasets during an adequate timespan (at least 10 years within a climatic study) of the Reference Period (1971–2000), herein we focus on comparisons of MeCSS results against field data of SSH in five selected Greek stations. Data from other Mediterranean hydrographic services are not freely available for the specific timeframe, at least within the classic sea level data sources. The utilized datasets refer to uninterrupted, long-term, and extensively pre-validated, *in situ* hydrographic information by tide-gauges of the HNHS. Herein, the MeCSS model runs were extended to 2005 to at least cover a decadal period (1995–2005) for validation purposes, forced by the same set of CMCC, CNRM, GUF RCMs' produced atmospheric conditions. In evaluations of climatic mode runs of storm surge models, researchers usually pursue the agreement of model results and field observations, mainly based on statistical measures of either seasonal or annual and inter-annual maxima values and their correlations, rather than day-to-day comparisons of modelled and *in situ* SSH timeseries, as commonly done in operational forecasts. This is because the atmospheric forcing data from RCMs does not reproduce the daily weather patterns as in meteorological forecast modelling, but rather seeks to capture the long-term climatic patterns of atmospheric circulation.

### 4.1. Storm surge index and SSH maxima

In the present analysis, we focus on inter-annual maxima of storm surges, in order to trace 30-year long changes of sea level variations. Therefore, the Storm Surge Index (SSI) is used as it refers to the average of the three highest independent storm surge maxima per year (Conte and Lionello, 2013; Androulidakis et al., 2015; Makris et al., 2016; *etc.*). Only incidents of maximum SSH separated by at least 120 h (estimation of the maximum duration of a typical storm in the Mediterranean) are considered as independent storm surge events to avoid overestimations of SSI due to the occurrence of multiple conjugate peaks within a unique storm incident in the SSH timeseries. The SSI for both simulated and observed timeseries was calculated for each of the five stations, along with corresponding Percent Error ($E$), Error Index ($EI$), Root-Mean-Square Error ($RMSE$), Pearson product-moment correlation coefficient $COR(x)$, and Willmott Skill Score ($WSS$) or Index of Agreement ($IoA$) (see Appendix A.1 for analytic definitions of statistical parameters).

Fig. 9 presents the comparisons of the decadal (1995–2005) average SSI (m) and $SSH_{max}$ (m) in five selected Greek stations between field and model (CMCC-, CNRM-, and GUF-forced MeCSS) data. All MeCSS model implementations follow the same geographical pattern as the one referring to field observations, *i.e.*, higher storm surge levels in the northern part of the studied area and lower SSHs towards the south. The model's performance is better in the central Aegean and Ionian Seas (Chios and Lefkada) followed by the northern part of the Aegean Sea (Alexandroupoli and Thessaloniki), while in Heraklion the MeCSS runs seem to behave like an outlier. This is attributed to peculiarities of the computational domain's coastal bathymetry in the southern Aegean Sea on the northern coast of the island of Crete. The GUF-forced MeCSS model runs perform quite adequately in almost all locations. In general, MeCSS model implementations forced by Med-44 resolution Med-CORDEX climatic data for the Reference Period slightly underestimate the magnitudes of annual SSH maxima and SSI, except from GUF-MeCSS in the central Aegean.

Table 2 presents the aggregate estimation of MeCSS model's performance, forced by the three RCMs (CMCC, CNRM, and GUF), in the form of overall statistical measures and skill metrics ($E$, $EI$, $RMSE$, $COR$, and $WSS$) for comparisons between field and model data. These are based on decadal (1995–2005) averages of SSI and $SSH_{max}$ at five Greek stations. Corroborating several previous works (*e.g.*, Androulidakis et al., 2015; Makris et al., 2015, 2016), the highest SSI values occur over the northern Aegean coastal region (Alexandroupoli), where both modelled and observed SSIs are >23 cm. The median Percent Errors range from quite small to tolerable ($-13\% < E_i < -6.2\%$ for $SSI$ and $-22\% < E_i < -12\%$ for $SSH_{max}$) with generally low values in certain parts of the Mediterranean basin. This supports the good performance of MeCSS model during the Reference Period. Even though the model underestimates the SSI at all stations (negative $EI$ values), the error is generally acceptable and differences between modelled and observed SSI values are plausible. Conte and Lionello (2013) also showed results of storm surge climate simulations with rather high errors, *e.g.*, $E > 40\%$ and similar underestimations of the simulated SSH over coastal regions of the western Mediterranean. The model resolution might be the prime reason for this discrepancy yet refining the discretization of storm surge models for long-term climatic runs, drastically increases the need for computational resources and times, undermining the feasibility of adequate combinations of RCMs/RCPs implementations. Similar analytic comparisons of storm surge intra-annual extremes were performed based on the absolute yearly maxima of sea level variations, giving an average of annual $SSH_{max}$ for both simulated and observed timeseries. Same comparisons as for the SSI were performed providing similar results. Overall, the cumulative comparisons reveal quite high Pearson correlation coefficients (>0.8), with RMSE ranging from only 3 to 4.3 cm, namely a rough 12%–18% of the average $SSH_{max}$ and <7% of the absolute observed $SSH_{max}$. The $IoA$, based on $WSS$, reveals a high correlation of GUF-forced MeCSS model (>0.8) with field data in terms of the interdecadal $SSH$ extremes. The skill scores of the CMCC- and CNRM-forced MeCSS are lower, rendering the GUF-forced MeCSS model setup as generally (but not locally) most reliable in performing estimations of the extreme climate of storm surges (large SSH), at least for the east-central Mediterranean.

### 4.2. SSH percentiles and HRP index

To enhance our validation of MeCSS runs for the Reference Period, comparisons of simulated SSH with corresponding field data were expanded to other types of storm surge maxima and mid-range values of storm-induced sea levels. Thus, the performance of MeCSS model implementations was also evaluated using mid- to high-order percentiles

**Table 2**
Statistical measures and skill metrics of the comparison based on decadal (1995–2005) averages of SSI (m) and $SSH_{max}$ (m) at five Greek stations for field and model (CMCC-, CNRM-, and GUF-MeCSS) data. Definition of parameters in text and Appendix A.1.

| SSI | RCM | Pearson correlation | Willmott skill score | RMSE (m) | RMSE/SSI (%) | MEDIAN $E_i$ (%) | MEDIAN $EI_i$ |
|---|---|---|---|---|---|---|---|
| | CMCC | 0.849 | 0.735 | 0.039 | 17.98% | −10.54% | −0.342 |
| | CNRM | 0.840 | 0.664 | 0.039 | 17.97% | −12.97% | −0.420 |
| | GUF | 0.793 | 0.816 | 0.029 | 13.10% | −6.29% | −0.206 |
| | RCM | Pearson correlation | Willmott skill score | RMSE (m) | RMSE/$SSH_{max}$ (%) | MEDIAN $E_i$ (%) | MEDIAN $EI_i$ |
| $SSH_{max}$ | CMCC | 0.884 | 0.780 | 0.037 | 15.69% | −17.11% | −0.618 |
| | CNRM | 0.828 | 0.582 | 0.043 | 18.70% | −21.20% | −0.566 |
| | GUF | 0.810 | 0.802 | 0.030 | 12.65% | −12.90% | −0.468 |

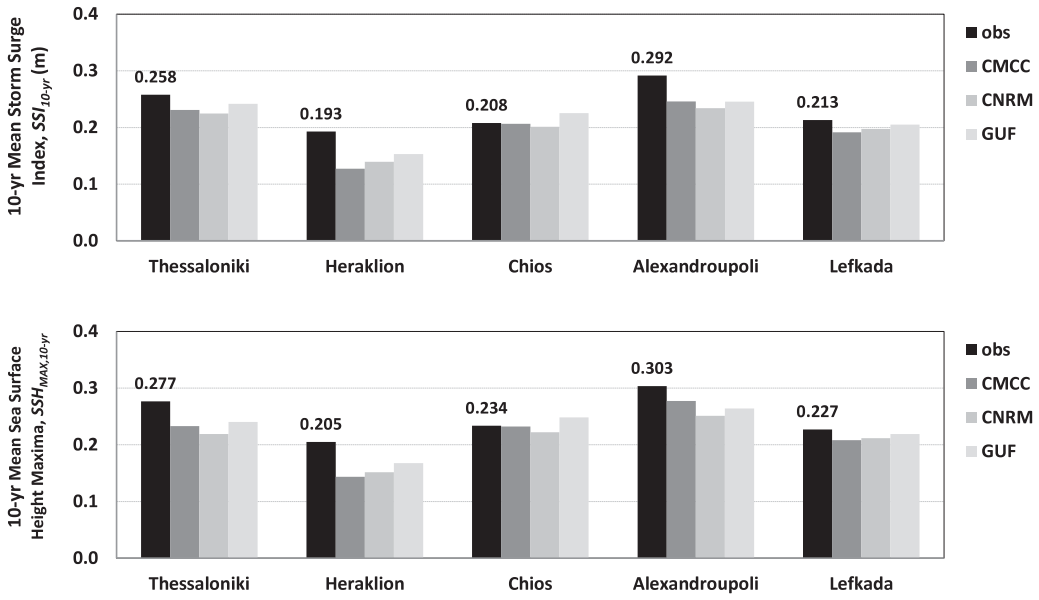


**Fig. 9.** Comparisons of the decadal (1995–2005) average SSI (m) and $SSH_{max}$ (m) [upper and lower graphs, respectively] in five Greek stations for field (obs) and model (CMCC-, CNRM-, and GUF-MeCSS) data.

**Table 3**
HRP index and its median metric for the ranked percentiles of the entire decadal (1995–2005) SSH (m) timeseries at five Greek stations by comparisons of field and model (CMCC-, CNRM-, GUF-MeCSS) data.

| RCM | CMCC-MeCSS | | CNRM-MeCSS | | GUF-MeCSS | |
|---|---|---|---|---|---|---|
| Coastal site | HRP index | MEDIAN | HRP index | MEDIAN | HRP index | MEDIAN |
| Thessaloniki | 0.98 | | 0.96 | | 0.98 | |
| Heraklion | 0.79 | | 0.86 | | 0.85 | |
| Chios | 0.95 | **0.95** | 0.96 | **0.96** | 0.94 | **0.95** |
| Alexandroupoli | 1.00 | | 0.95 | | 0.98 | |
| Lefkada | 0.95 | | 0.96 | | 0.95 | |

(80th, 90th, 95th, 97.5th, 99th, 99.5th, *etc.*) of SSH for both modelled and observed timeseries. As SSI and $SSH_{max}$ values lie around the 99th and 99.5th percentiles, for the sake of brevity, only comparisons of the decadal (1995–2005) 97.5th and 90th Percentiles of SSH for field against CMCC-, CNRM-, and GUF-MeCSS data are presented in Fig. 10. The highest modelled values were derived again for the northern Aegean Sea (Alexandroupoli), in agreement with the analysis of intra-annual maxima (SSI and $SSH_{max}$). It is although obvious that, unlike the case of SSH maxima, all model runs tend to overestimate the SSH for mid-range values, *i.e.*, for the 90th and lower percentiles. In general, all model implementations perform very well (for the 97.5th percentile of SSH) to acceptably (for the 90th percentile of SSH); the rest classes of percentiles are not shown for the sake of conciseness. The case of Heraklion is still considered to be an outlier compared to other locations of focus, *e.g.*, MeCSS model skill in SSH percentile comparisons is very good for Lefakda, Chios and Alexandroupoli sites, and occasionally for Thessaloniki. We note that the Hreaklion *in situ* measured timeseries is the most unreliable out of the bunch of the HNHS observations, as it is incomplete lacking continuous information about the 1995–1997 period. It is also evident that all model implementations perform very well in reference to the decadal 97.5th percentile of SSH. Therefore, it can be deduced that the agreement of the MeCSS model runs for all model implementations is high in terms of the unfiltered SSH mid and extreme values reproduced within the 1995–2005 period.

Aiming to quantitatively assess the ability of the MeCSS model to reproduce a wide range of the SSH values within its simulated timeseries, and further decide on the essentiality of a possible bias correction of modelled results, we also calculated the Hit-Rate-of-Percentiles (HRP) index (Schoetter et al., 2012; Makris et al., 2016) as a model evaluation metric (see Appendix A.1). In general, if HRP index is greater than 0.95, then bias correction is not necessary for model results. The closest that HRP values are to 1, then it can be deduced that MeCSS model should efficiently reproduce the most classes of SSH in the simulated dataset. This applies to maxima, mid-range, and minima of modelled SSH, *i.e.*, for both positive and negative surges. The HRP index for the five Greek stations is presented in Table 3, regarding CMCC-, CNRM-, GUF-forced MeCSS model runs. It was found that the MeCSS model simulates the statistical properties of the ranked percentiles of SSH in four of the characteristic locations adequately (Heraklion continues to be the outlier reference spot), since HRP exceeds the limit of 0.95 everywhere and reaches the value of 0.98 and 1.00 in Thessaloniki and Alexandroupoli for the CMCC- and GUF-MeCCS setups. The latter however seems to slightly outperform the CMCC- and CNRM-forced MeCSS simulations in terms of mean HRP values, yet the median HRP index reveals that differences are marginal (0.95–0.96 for all three model implementations) and not able to offer a definite reason for

**Table 4**
Differences of future–Reference storm surge maxima, $DSSH_{max}$, and meteorologically induced component of MSL deviation, $DSSH_{mean}$, (both in m and %) for 28 Mediterranean stations during the Future Period of study (2071–2100) for the two RCP (4.5 and 8.5) climate scenarios, separated by CMCC-, CNRM-, and GUF-forced MeCSS results. (Detailed datasets and calculations in Appendix B, A3; Figures A3.1-3).

| RCM-forced | Average of 28 locations | | | | |
|---|---|---|---|---|---|
| MeCSS | Scenario | $DSSH_{max}$ (m) | $DSSH_{max}$ (%) | $DSSH_{mean}$ (m) | $DSSH_{mean}$ (%) |
| CMCC | RCP4.5 | −0.012 | −3.54% | −0.008 | −47.93% |
| | RCP8.5 | −0.024 | −7.05% | −0.017 | −107.283% |
| CNRM | RCP4.5 | −0.027 | −7.63% | −0.004 | −17.71% |
| | RCP8.5 | −0.017 | −4.35% | −0.009 | −42.00% |
| GUF | RCP4.5 | −0.028 | −7.42% | −0.006 | −20.41% |
| | RCP8.5 | −0.037 | −9.56% | −0.012 | −41.95% |

All differences refer to "Future – Reference" (2071–2100)–(1971–2000) subtractions of $SSH_{max/mean}$.

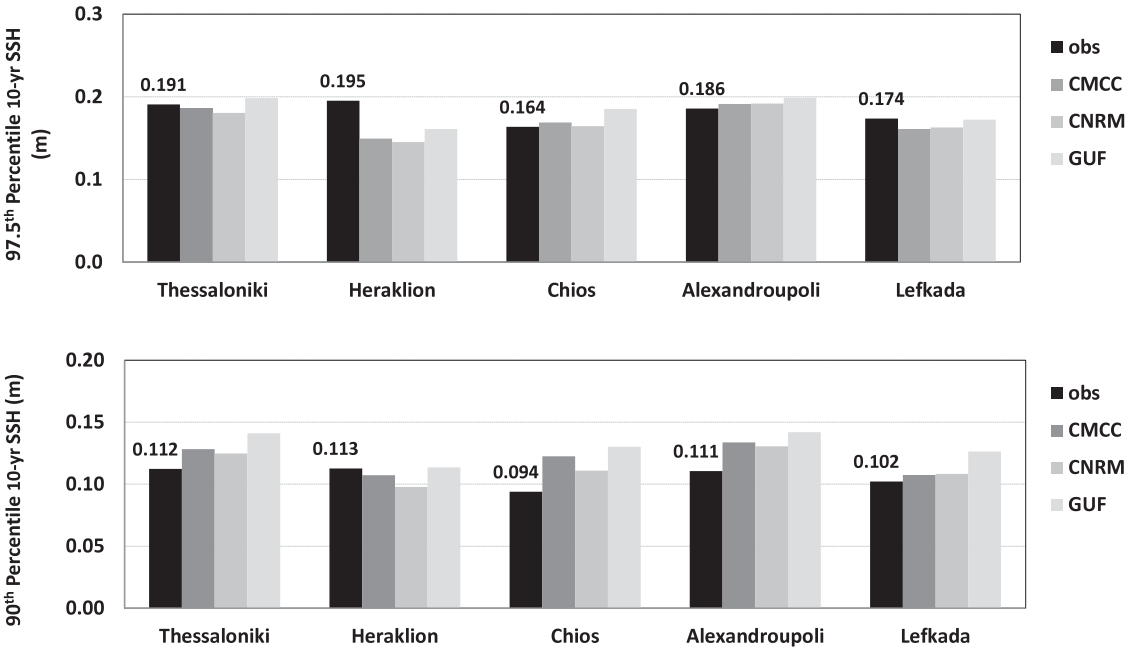


**Fig. 10.** Comparisons of the decadal (1995–2005) 97.5th and 90th Percentiles of SSH (m) [upper and lower graphs, respectively] in five Greek stations for field (obs) and model (CMCC-, CNRM-, and GUF-MeCSS) data.

discarding the one or the other setup. Altogether, it can be concluded that the MeCSS model can reproduce the storm surge patterns for all the classes of percentiles in an adequate way, and thus the statistical distributions of the modelled SSH data are considered to be reliable for further use in future projections during the 21st century, by a combination of RCMs/RCPs implemented MeCSS.

### *4.3. Probabilistic analysis of SSH maxima occurrence and threshold values exceedance*

A heuristic approach is used in the present study to define "statistically coherent" events, as these storm surge incidents having values of $SSH_{coh} \geq (\mu_{SSH} + \sigma_{SSH})$, where $\mu$ is the mean of the SSH timeseries over the entire study period (1995–2005), and $\sigma$ is the corresponding standard deviation (Makris et al., 2015, 2016; Skoulikaris et al., 2021). The exceedance probability, $P_{coh}$, of the critical value for coherent events together with the respective calculated thresholds $SSH_{coh} = \mu_{SSH} + \sigma_{SSH}$ for all Greek stations are presented in Fig. 11 (top and mid graphs), as derived from both simulated and observed timeseries of SSH.

The simulated values are correlated well with the measured ones in all stations except the Heraklion site, with lower frequencies of occurrence (shown here by probabilities of exceedance) of coherent events over the Ionian and central Aegean Seas (Lefkada and Chios) compared to the northern Aegean regions (Thessaloniki and Alexandorupoli). It follows that these areas show more frequent, either lower or higher in magnitude SSH. Both model and *in situ* values support this finding, indicating the good performance of the MeCSS model between different areas. It is also noted that the "coherent" threshold is adequately estimated or slightly overestimated everywhere, except from the Heraklion station, where model results exactly fit to the field data. Overall, it can be deduced that the MeCSS model can adequately reproduce the statistical storm surge patterns corresponding to heuristically defined coherent events. A tendency is traced for the MeCSS model implementations to mostly overestimate small values of SSH and perform better for the estimation of statistical features for larger SSH values (not shown here for brevity), representative of intense storm surge events. Therefore, the reproduced probabilistic parametric features of the modelled SSH data can be considered reliable for further use in future projections under several RCP climate change scenarios.

We have also calculated the probabilities of occurrence of local peaks in the SSH timeseries at the five Greek stations, in order to assess the performance of MeCSS model in terms of the "local maxima" of sea level variations in coastal regions with different topographic characteristics. The local maxima computation is based on the minimization of the SSH distribution gradient in "local" short frames of the timeseries, where there is a flat tangent line. The probability of occurrence of SSH local maxima is shown in Fig. 11 (lower graph) as derived from the number of days that they appeared in the SSH timeseries, divided by the total number of days of each study period. For each station, all local peak points (maxima) with SSH that exceed 10, 20 and

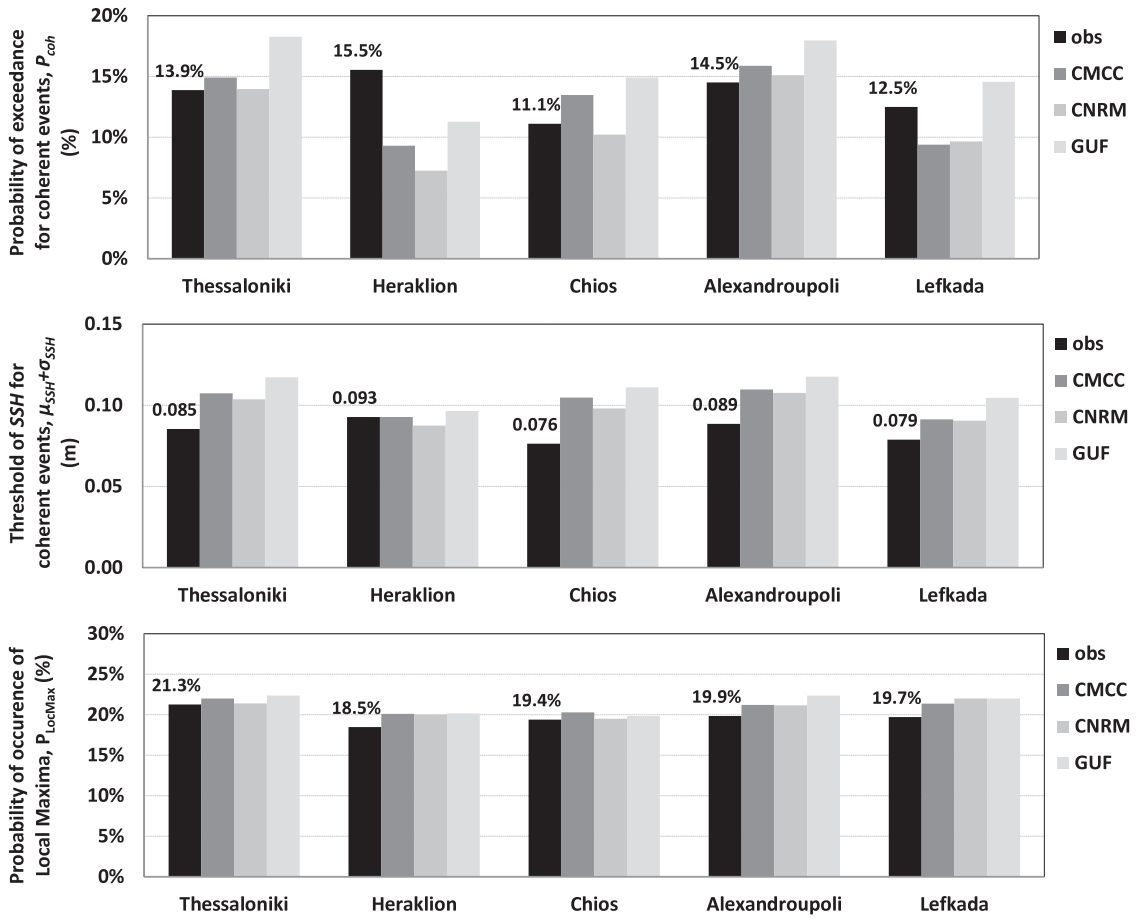


**Fig. 11.** Comparisons of the decadal (1995–2005) exceedance probability of the threshold SSH for statistically coherent storm surge events, $P_{coh}$ (%), the calculated threshold $\mu_{SSH} + \sigma_{SSH}$ (m), and the occurrence probability of 'local' maxima in SSH timeseries (%) [upper, mid, and lower graphs, respectively] in five Greek stations for field (obs) and model (CMCC-, CNRM-, and GUF-MeCSS) data.

30 cm were also computed to evaluate the MeCSS model performance during events of extreme surges (not shown here for conciseness). The comparison between model and field data shows that the agreement is very satisfactory in all stations for all three MeCSS implementations. This observation agrees with previous studies (Androulidakis et al., 2015; Makris et al., 2015, 2016; for the SRES-20C3M historical dataset) that have also found the highest *SSH* values of the Aegean over the northern part of it.

In general, it can be concluded that the MeCSS model can well reproduce the probabilistic features of storm surge patterns in terms of the amount and occurrence frequency of surge events leading to a prominent peak in the modelled SSH timeseries. The latter correspond to temporally local events of high sea levels on the coast induced by meteorological phenomena. Therefore, the estimated probabilistic features of the modelled SSH data are considered reliable for further use in a climatic study of storm surge patterns' estimation in the 21st century.

## 5. Results

In the following, projections of the RCM simulation results are provided over the Mediterranean region. We provide estimations on a 30-year level of analysis for the cyclonic patterns and synoptic scale atmospheric dynamics that serves as input in high-resolution hydrodynamic modelling with MeCSS model. We further analyse the sea level response to RCM projections in the entire Mediterranean basin, and present climate change signals of the maxima and mean SSH due to storm surges on the shoreline and correlations of deep depressions to episodic elevations of coastal sea level.

### 5.1. Weather patterns by RCM projections in the 21st century

The climatic projections of mean and extreme barometric systems, *i.e.*, the projected changes of respective SLP and wind fields, over the Mediterranean region for the 21st century per RCM implementation and RCP scenario used is presented herein. This is done to correlate the future trends and climate change signals of synoptic scale patterns (barometric systems and aeolian regimes) to the respective projected trends of episodic *SSH* and storm surge-induced changes in MSL on the coastal zone of the Mediterranean basin.

#### 5.1.1. Mean barometric systems over the mediterranean region: future climate projections for sea level pressure and wind fields

An attempt is made to analyse the potential future changes as estimated by the three RCMs used, regarding the two main parameters that are widely used: SLP and Wind (speeds). Since this is a primer analysis on the model's future projections it is selected to present the results regarding the last 30-year period of the century and to show the RCM estimations under the "high emission/concentration" scenario, RCP 8.5. According to the IPCC Synthesis Report (2014) the RCP 8.5 is characterized by increasing greenhouse gas emissions that lead to high greenhouse gas concentrations over time, estimating that $CO_2$ levels will triple by the end of the century accompanied by a rapid increase of the $CH_4$ emissions. The future estimations of the SLP and wind changes were computed by calculating the biases (differences) of the mean annual and seasonal values of the two examined parameters (Future Period; 2071–2100) in comparison with the equivalent values of the Reference Period (1971–2000), which are analysed in Section 3. Fig. 12 illustrates both the mean annual spatial distribution of the SLP values

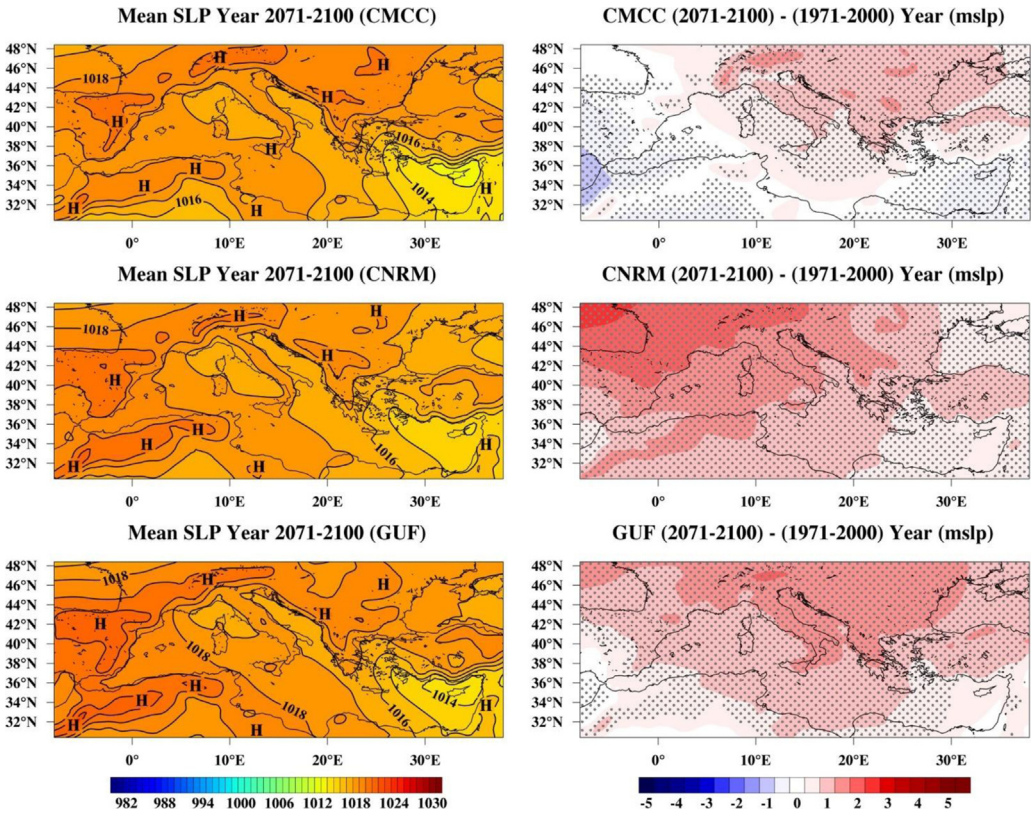


**Fig. 12.** Spatial distribution of estimated future mean SLP (hPa; left column graphs) during the Future Period (2071–2100) and difference composite maps of mean SLP (hPa; right column graphs) in comparison to the Reference Period (1971–2000), by each examined RCM (CMCC, CNRM, GUF; from top to bottom), based on annual scale analysis. Grid cells with statistically significant differences (t-test: 0.05 level) are marked with grey point dots.

over the Mediterranean region as well as the calculated difference (Future–Present) for each model under study. All models agree in general that the SLP values are estimated to present an increasing gradient from the south-eastern part of the region to the northwest in the future. The values range from 1012 hPa over Cyprus up to 1020 hPa at the north of the Iberian Peninsula. However, even though the spatial distribution does not seem to differ much from one model to the other, the estimated future differences present some discrepancies. Overall, all models agree that SLP values are going to increase in the future since positive differences (up to 3.5 hPa) characterize the largest part of the Mediterranean region. Yet, in the case of the CMCC model, these positive differences are observed mainly over Italy and the Balkan Peninsula while over the west and south the differences are very small and, in some parts, almost zero. For CNRM, the maximum of the positive differences is located at the northwest of the region and the smallest ones at the south-eastern Mediterranean Sea. Finally, for GUF's RCM, the positive differences decrease moving to the south (Fig. 12).

The winter future SLP values are quite higher than the annual ones and with a difference in spatial distribution. All models estimate that the minimum sea level pressures will be observed at the northwest of the domain of interest while the maximum will be found at the southwest (over north Africa) (Fig. 13). It is worth mentioning that a large part of the Mediterranean area is estimated to present SLP values that will exceed 1020 hPa in the future. On the other hand, the estimated differences between the Future and Reference Period vary between model implementations. In the case of CMCC's RCM, a characteristic dipole is observed with positive difference (increase of the SLP) over the Balkan Peninsula and the Eastern Europe and negative ones (decrease of the SLP values) at the northwest. Also, some regions over the central Mediterranean are estimated according to the model to have no future changes regarding SLP. For CNRM, the increase of the examined parameter is clear all over the domain of study. The most intense future changes are expected to be found at the northwest and the smallest ones over the Cyprus area. In the case of GUF, the centre of positive differences is located over Greece (up to almost 5 hPa) which seem to decrease perimetrically with the smallest positive difference found at the west (Fig. 13).

The future spring SLP values are smaller in comparison to the winter ones. The spatial distribution is very similar to the annual one with the smallest values 1012 hPa observed over Cyprus and the highest ones over the northwester part of the Mediterranean region. Regarding the actual sea, the future SLPs are estimated to present a gradient from east (minimum) to west (maximum). All model results indicate that the spring pressures will increase during the last 30 years of the 21st century. Positive differences cover the whole area under study, while the most intense future changes are found in the CMCC model over the central continental areas of the Mediterranean (Appendix B, Figure A1.7).

Regarding summer, the mean seasonal SLP future values are lower than the other two seasons. The smallest pressures are found at the southeast of the region (lower than 1010 hPa), increasing over the sea area, and the maximum is found at the north-northwest (up to 1018 hPa). All models agree on that spatial distribution (Fig. 14). The equivalent estimated changes in comparison with the Reference Period's summer ones show that summer will be the only season where SLP is estimated to decrease in the 21st century. Especially in the case of the CMCC model, quite large negative differences (decrease) cover the sea area of the Mediterranean as well as the north continental parts of Africa. The CNRM projections present a weaker climate signal with small positive differences at the northwest and central continental parts of the Mediterranean and small negative ones over the Balkan Peninsula and Eastern Europe (Fig. 15).

In the case of autumn, during the last 30-years of the 21st century, all models agree that higher pressures will characterize the continental parts of the region under study, while lower pressures will be observed over the sea. The SLP values range from 1015 hPa up to 1022 hPa in limited areas over the Iberian and the Italian Peninsulas (Appendix

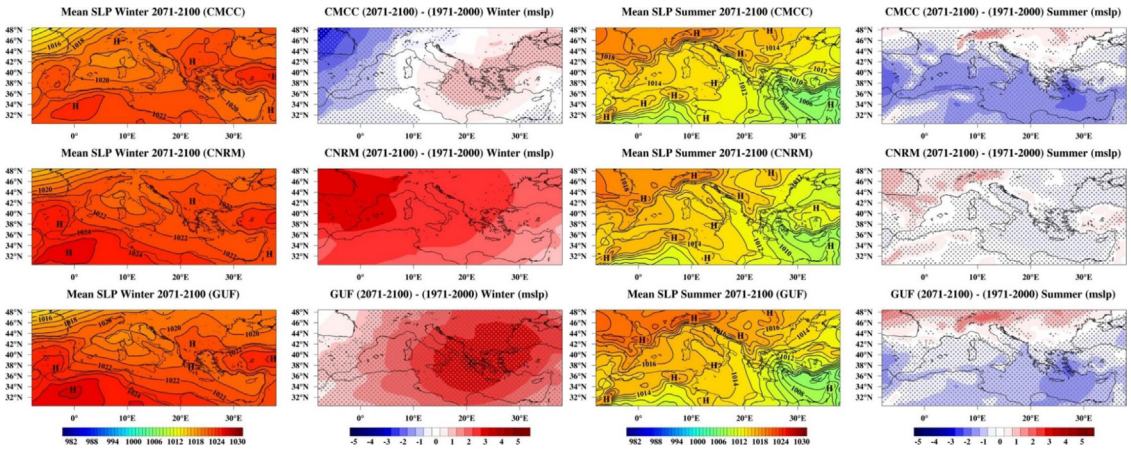


**Fig. 13.** As in Fig. 12 but for the seasonal analysis of winter (left graphs) and summer (right graphs).

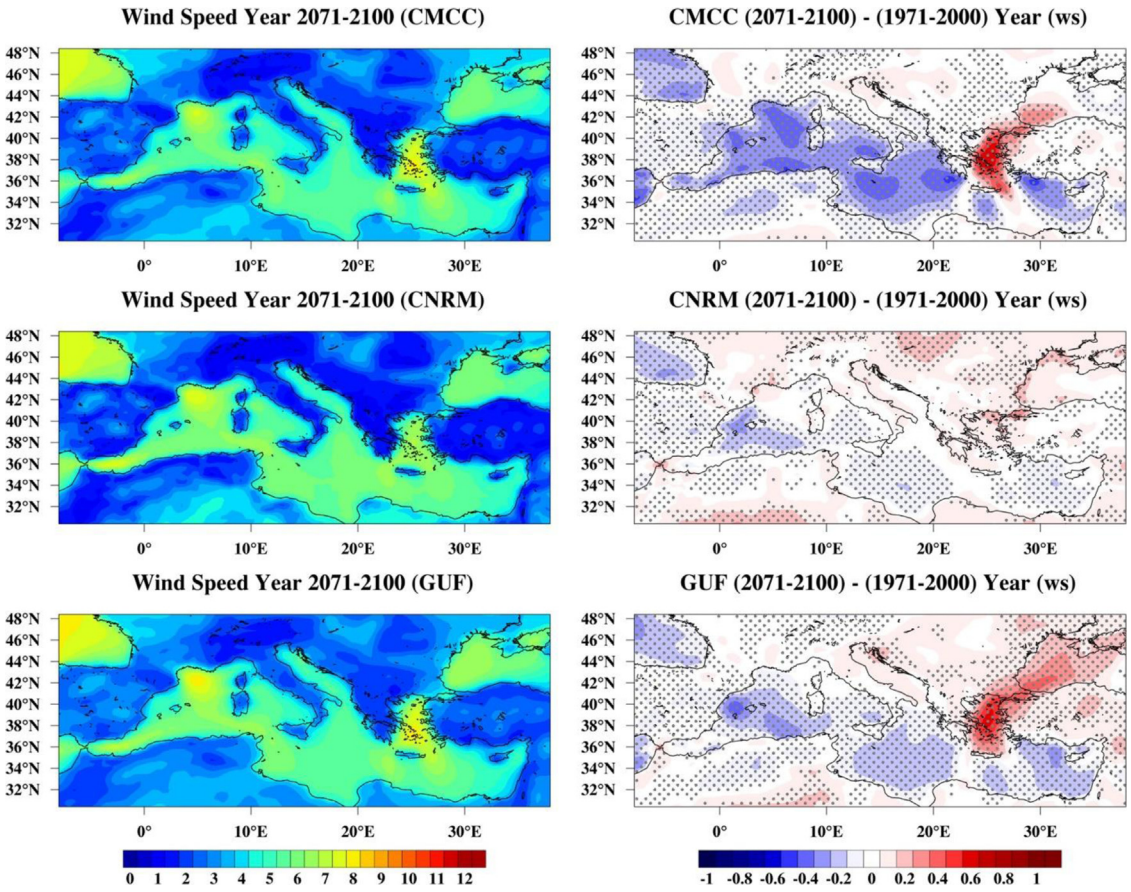


**Fig. 14.** Spatial distribution of estimated future patterns of wind speed (m/s; left column graphs) fields during the Future Period (2071–2100) and difference composite maps of wind speed (m/s; right column graphs) in comparison to the Reference Period (1971–2000), by each examined RCM (CMCC, CNRM, GUF; from top to bottom), based on annual scale analysis. Grid cells with statistically significant differences ($t$-test: 0.05 level) are marked with grey point dots.

B, Figure A1.8). In comparison to the Reference Period's SLP autumn values, it is estimated that pressure will generally increase over the Mediterranean. According to the CMCC future projections the autumn SLP is estimated to increase (small positive differences) especially in Italy and the Balkan Peninsula. Over the sea area, these positive differences are even smaller and, in some regions, very close to zero (no future climate signal). Only over Cyprus the examined parameter is expected to slightly decrease. Regarding CNRM, the future SLP increase is more intense. Positive differences cover the whole of the study region with the highest ones at the north and northwest. As previously, over Cyprus the change of the autumn SLP values is zero (no future pressure change). Analogous is the distribution of the positive differences for GUF model, but the pressure increase is slightly weaker (smaller positive change) (Appendix B, Figure A1.8).

The future projections of the three examined models regarding the wind speeds over the Mediterranean domain present many similarities especially in the spatial distribution of their patterns. The most intense wind speeds are expected to prevail mainly over the sea areas

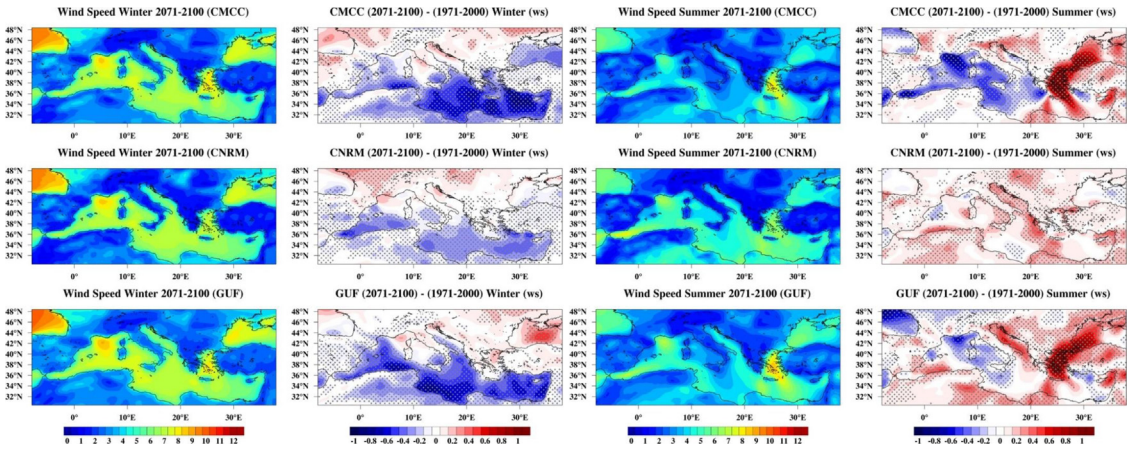


**Fig. 15.** As in Fig. 14 but for winter (left graphs) and summer (right graphs).

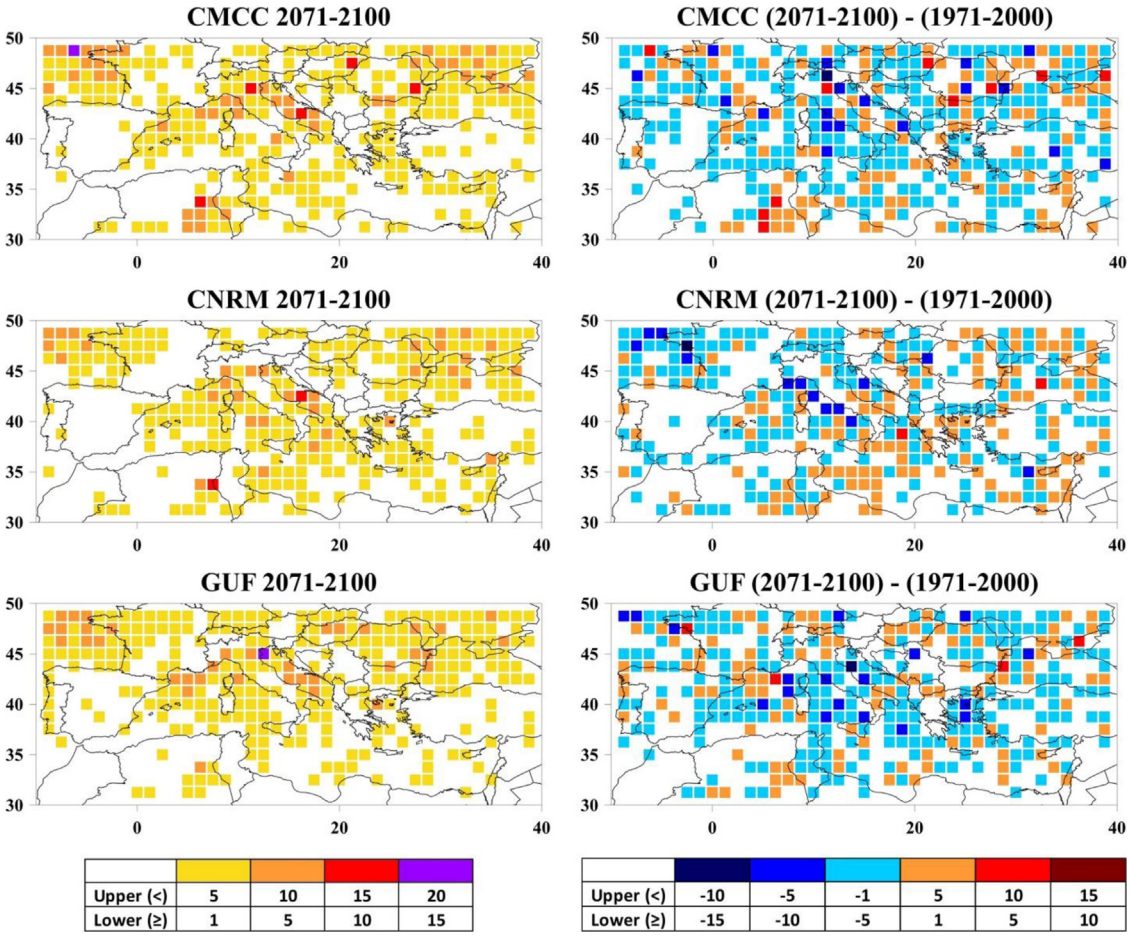


**Fig. 16.** Gridded map of estimated frequencies of occurrence (number of days; left column graphs) for the deep depressions over the Mediterranean Sea during the Future Period (2071–2100) on an annual basis; colour palette is divided in four classes according to lower and upper margin for recorded number of days: 1st 1–5 days, 2nd 5–10 days, 3rd 10–15 days, 4th 15–20 days. The relevant difference composite maps of occurrence frequencies (number of days; right column graphs) for deep depressions in comparison to the Reference Period (1971–2000) are also presented; colour palette is divided in six classes according to lower and upper margin for recorded differences in number of days: 1st −15–−10, 2nd −10–−5, 3rd −5–−1, 4th 1–5, 5th 5–10, 6th 10–15. All graphs refer to RCM (CMCC, CNRM, GUF; from top to bottom).

(especially over the Aegean Sea and the Marseille Gulf, reaching up to approximately 8 m/s) while over the continents, the winds are estimated to be weaker in the future (Fig. 15). The composite maps of the differences in comparison to the Reference Period are not very strong. In general, it could be mentioned that there is a small strengthening of the wind speeds over the Balkan Peninsula as well as over Spain, with positive differences that in most of the areas are statistically significant. It should be highlighted that mainly CMCC and GUF model project stronger winds also over the Aegean Sea (statistically significant, too).

The future pattern of the wind speeds during the winter months is quite similar to the annual one regarding the spatial distribution of the velocities. Weak speeds are estimated to be found over the continent while the sea is going to present larger values. Conversely to the year analysis, the maximum this time is observed over the Marseille gulf (up to 8 m/s), while the secondary one is located in the Aegean Sea. Moreover, strong winds are predicted by the models over the northwest of the domain of interest (over the Atlantic Ocean) as well as in the Black Sea region (Fig. 14). The computation of the differences between the future and the Reference mean values revealed that the climate signal is quite weak. Small positive (yet statistically significant differences) are expected over land, especially in Italy, central Europe, and the Balkan Peninsula. On the other hand, the wind speeds are not estimated to change drastically over the sea and in some case, there are going to be slightly weaker (small negative differences).

As in winter, the future spring winds are expected to present their maximum speeds over the sea during the last 30 years of the century. However, they are quite smaller than the respected winter ones (Appendix B, Figure A1.9). Also, the selected models predict that overall winds in the future are going to be a little stronger. Small positive difference prevails especially over the continental parts of the Mediterranean region. The only exception is in the case of the CMCC model, where a more significant positive change (strengthening of wind speeds) is projected over the Aegean Sea region.

In summer, the regions with future winds lower than 3 m/s are more extended over the sea particularly in the cases of CMCC and GUF models. However, these two models estimate a maximum of wind speeds over the Aegean Sea meaning that the Etesian winds will also be detected during the future years. Moreover, from the difference maps, the Etesian winds are estimated to become even stronger in the future with larger positive differences over the area of the Aegean Sea. This intensification of the winds over this area is mainly found in the case of the CNRM model and the maximum is extended over the southern Black Sea and over the southeast of the island of Crete (Fig. 15).

Finally, in the case of the future autumn estimations the spatial distribution of the wind speeds is similar to the winter spring and annual ones where, the land is expected to be characterized by weak winds and the sea with stronger ones. All models also detect two future maxima (the first in the Aegean Sea and the second in Marseille) which is expected to be more intense according to the future CMCC and GUF projections. The future climate signal of the examined parameter is weak, and the calculated differences are in general quite small. Positive differences are mainly observed over the eastern parts of the Mediterranean region (especially the Aegean Sea) meaning that the autumn winds over these regions are expected to be slightly stronger in the future (Appendix B, Figure A1.10).

#### *5.1.2. Extreme barometric systems over the mediterranean region: future climatic projections of deep depressions*

The future projections of the three models in estimating the frequency of occurrence of deep depressions (centre <1000 hPa) is also presented. The methodology, described in Section 2.4, was followed to define the centres of these deep depressions (low barometric pressure systems) and the grid points on which these low-pressure centres will occur in the future were mapped for the future period 2071–2100. Moreover, the differences on the days of occurrence of these depressions (Future–Reference) were also computed and illustrated both on an annual and seasonal basis. The annual results showed (Fig. 16) that all three models estimate the occurrence of these deep cyclones in the largest part of the Mediterranean region. In the case of CMCC and GUF model these cyclones are expected to have their centres mainly over land while according to the CNRM model their occurrence is also over the sea area. It should be mentioned that their frequency in most of the cases does not exceed 5 days, however scattered grid point, both over the continental as well as the sea areas present a higher frequency of occurrence.

From the "differences" maps it becomes obvious that cyclones, even though, they will still occur in the future, are estimated to present a general frequency decrease. For a high percentage of the grid points, the calculated differences are negative, meaning either that there is a decrease of these deep cyclones (for Future projections compared to the Reference Period) or that the centres of these cyclones are estimated to be found in different areas during the 21st century, creating negative differences (Fig. 16). Yet, it should be considered that there are also grid points with an increasing frequency of occurrence of extreme pressures (up to almost 10 days), but their locations differ by model application.

The winter future projections showed that for all three RCMs the number of grid points that will present deep depressions by the end of the 21st century, is much lower than the annual ones (Fig. 17). As expected, their frequency of occurrence is also smaller (does not exceed 5 days) than the equivalent frequencies found in the annual analysis. The deep depression centres are mainly located over the continental land rather than the sea. According to the difference maps, it should be noted that the extreme cyclones are expected to be less frequent since negative differences prevail over the Mediterranean. However, the maximum of the frequency of occurrence detected for the GUF model over the north Adriatic Sea (and the intense positive differences at the same grid point and intense negative difference at the next one) shows that this centre of extreme cyclogenesis remains strong over the area.

During spring, the regions that will present deep depressions in the future are more extended, also covering several parts of the Mediterranean Sea. As in winter, the frequency of occurrence mainly belongs to the first class (Appendix B, Figure A1.11). Moreover, these extreme cyclones will be rarer in the future (from the projections of the CMCC and GUF models), while in the case of the CNRM one, numerous grid points over the sea are expected to present more deep depressions at the last 30 years of the century.

Regarding summer and autumn (Fig. 17 and Figure A1.12 in Appendix B) all models project in the future a very limited number of grid points (areas) where in the future very low-pressure systems will occur. Especially for summer, the eastern and north-eastern Mediterranean region is the one that will generally experience in the future deep depressions. The respected differences over this area are either positive or negative due to the slight change of the geographical location of the grid points with extreme pressures and not to an actual change of their frequency. For autumn, the deep depressions are also expected to become less frequent mainly over central Mediterranean Sea. An exception can be observed over the north Adriatic Sea, in the case of the GUF model, where the grid points over the area present positive differences indicating that the frequency of the extreme cyclones is expected to increase in the future (Appendix B, Figure A1.12).

### *5.2. Storm surge projections in the 21st century by mecss model output*

We investigate the estimated evolution, the projected future trends and variability of SSH maxima and averages *in tandem* with their correlation to the main forcing mechanisms (deep depressions) that can induce high surges in the Mediterranean coastal zone under the effects of possible climate change.

#### *5.2.1. Maps of inter-annual SSH maxima: future projections under combinations of RCMs and RCPs*

The main output of the storm surge model is presented in the form of horizontal maps of $SSH_{max}$ (m) portraying the entire coastal zone of the Mediterranean basin. The presented $SSH_{max}$ values correspond to model output of 30-year averages of annual maxima of SSH for the two main time-windows of simulations for Reference and Future Periods (Figs. 18–20). The graphs are firstly separated by model implementation/setup, *i.e.*, for CMCC-, CNRM-, and GUF-forced MeCSS (Figs. 18, 19, and 20, respectively) for the historical time window (Reference

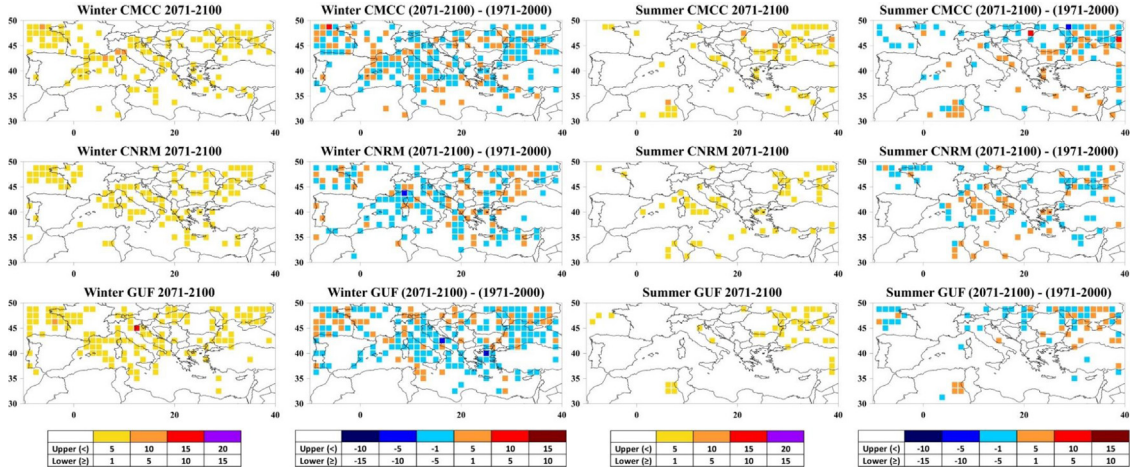


**Fig. 17.** As in Fig. 16 but in the case of winter (left graphs) and summer (right graphs).

Period; upper graphs). Secondly, they are separated by future climatic scenario, *i.e.*, RCP4.5 based runs (middle graphs) and RCP8.5 based runs (lower graphs); the latter two refer to percentage differences (Future–Reference Period) of estimated $SSH_{max}$ for each discrete model implementation for the end of the 21st century (2071–2100) along the coastline from the baseline/historical (1971–2000) control run of MeCSS.

The 30-year averaged $SSH_{max}$ for every RCM-forced MeCSS model implementation follows a similar and rather consistent pattern in terms of geographical distribution. The largest storm surge maxima ($SSH_{max}$) are observed in the northern Adriatic Sea, followed by the Gulfs of Gabes and Alexandretta (south-central Mediterranean and north-eastern Levantine, respectively). The peak values of $SSH_{max}$ score 0.43–0.45 m (Reference), 0.41–0.43 m (Future RCP4.5), and 0.43–0.44 m (Future RCP4.5), reaching up to SSH = 0.58–0.65 m locally (*e.g.*, Venice lagoon) during certain years of simulation. In the coastal zones of the northern Aegean Sea and southern France, storm surge maxima range from 0.24 to 0.38 m, while in the area around the Gibraltar strait and the outer western boundary of the Mediterranean $SSH_{max}$ may extent up to 0.35 m. The mid-latitude regions and the rest of the north-African coasts show a consistent pattern for all climate implementations with $SSH_{max}$ < 0.25 m. In general, the GUF-forced MeCSS results reveal the more pronounced $SSH_{max}$ values (0.42–0.44 m) all over the Mediterranean compared to the second and third, CMCC- and CNRM-forced MeCSS (0.40–0.42 m and 0.37–0.38 m), respectively.

For the RCP4.5 scenario during the Future Period 2071–2100 (mid graphs of Figs. 18–20), the storminess patterns and the consequent coastal surges are estimated to decrease by a percentage of −5% down to −15% (depending on RCM) in most of the Mediterranean littoral areas (Adriatic, Alboran, Aegean, and Ionian Seas, Sardinia, Sicily, Corsica, Crete, Cyprus and almost all African coasts). The regions with a possible small increase of <5%–7% for estimated future $SSH_{max}$ towards the end of the 21st century are the French coasts of the Balearic Sea, the Gulf of Lions, the Ligurian Sea coasts (only for CNRM and GUF implementations), the south-western Italian coasts (only for CMCC and GUF implementations), the Gulf of Gabes (only for CMCC implementation), the northern Aegean Sea (only for GUF implementation), the north-western Cyprus and southern Anatolia coasts (both only for CMCC and GUF implementations). We observe that climatic projections tend to generally favour the future increase of local surge maxima only in areas of mid to low coastal sea level extremes, while $SSH_{max}$ is estimated to slightly decrease in the 21st century in areas of the highest observed storm surges (conditionally except from the Gulf of Gabes). Therefore, an occasional projected attenuation of storminess over the entire Mediterranean basin under the RCP4.5 Scenario is rather prevalent for the last 30 years of the 21st century, as also suggested by other researchers in the past (*e.g.*, Marcos et al., 2011; Jordà et al., 2012; Conte and Lionello, 2013; Androulidakis et al., 2015; Makris et al., 2016; all based on former SRES). The latter is further corroborated by the spatially averaged (over the Mediterranean coastline) difference of $SSH_{max}$ from Future to Reference Period, which marginally reaches values of −3.72%, −9.92%, and −4.66% for CMCC, CNRM, and GUF implementations, respectively.

For the RCP8.5 scenario during the Future Period 2071–2100 (lower graphs of Figs. 18–20), the storminess patterns and the consequent coastal surges are also estimated to decrease by generally "higher" negative percentages than the RCP4.5 driven output, *i.e.*, by a percentage of −10% down to −20% (depending on RCM, almost except from CNRM) in most of the Mediterranean littoral areas (Adriatic, Alboran, Aegean, and Ionian Seas, Sardinia, Sicily, Corsica, Crete, Cyprus and almost all African coasts). The only regions with a possible small increase of <5% for estimated future $SSH_{max}$ towards the end of the 21st century are the French coasts of the Balearic Sea (only for CNRM implementation), the Ligurian Sea coasts (only for GUF implementation), the western Italian coasts (only for GUF implementation), the Alexandroupoli coastal area in the northern Aegean Sea (only for CNRM implementation). Finally, a rather large possible increase >15% for the Gulf of Gabes (only for CMCC implementation) is also expected. We again observe that climatic projections tend to generally favour a slight future increase of local surge maxima only in areas of mid to low coastal hazards related to storms, while $SSH_{max}$ is estimated to decrease towards the end of the 21st century in high-surge areas (conditionally except from the Gulf of Gabes). However, it is noted that in the Reference Period, CMCC- and GUF-forced MeCSS model results were higher than the CNRM-driven ones, hence the occasional larger projected attenuation of storminess over the entire Mediterranean basin under the RCP8.5 scenario. Our inferences are further confirmed by the spatially averaged (over the Mediterranean coastline) differences of $SSH_{max}$ from Future to Reference Period by RCP8.5, which score −11%, −6.44%, and −8.76% for CMCC, CNRM, and GUF implementations, respectively.

Essentially, a similar spatiotemporal pattern of estimated $SSH_{max}$ evolution in the 21st century can be observed between CMCC-, CNRM- and GUF-forced MeCSS model outputs. Namely, the averaged $SSH_{max}$ for every 30-year period follows a similar and consistent trend in its geographical distribution. A conditional small rise in magnitude for the 21st century in certain mid-level surge areas can be traced together with a respective generalized attenuation of $SSH_{max}$ almost everywhere around the basin, especially in locations with observed strong surges in the past. The GUF-model runs tend to overestimate the surge level maxima and their projected variations in the Future Period compared to the other two RCMs, yet except for the Gulf of Gabes within the CMCC-forced simulations that assess a possible 15%–20% increase

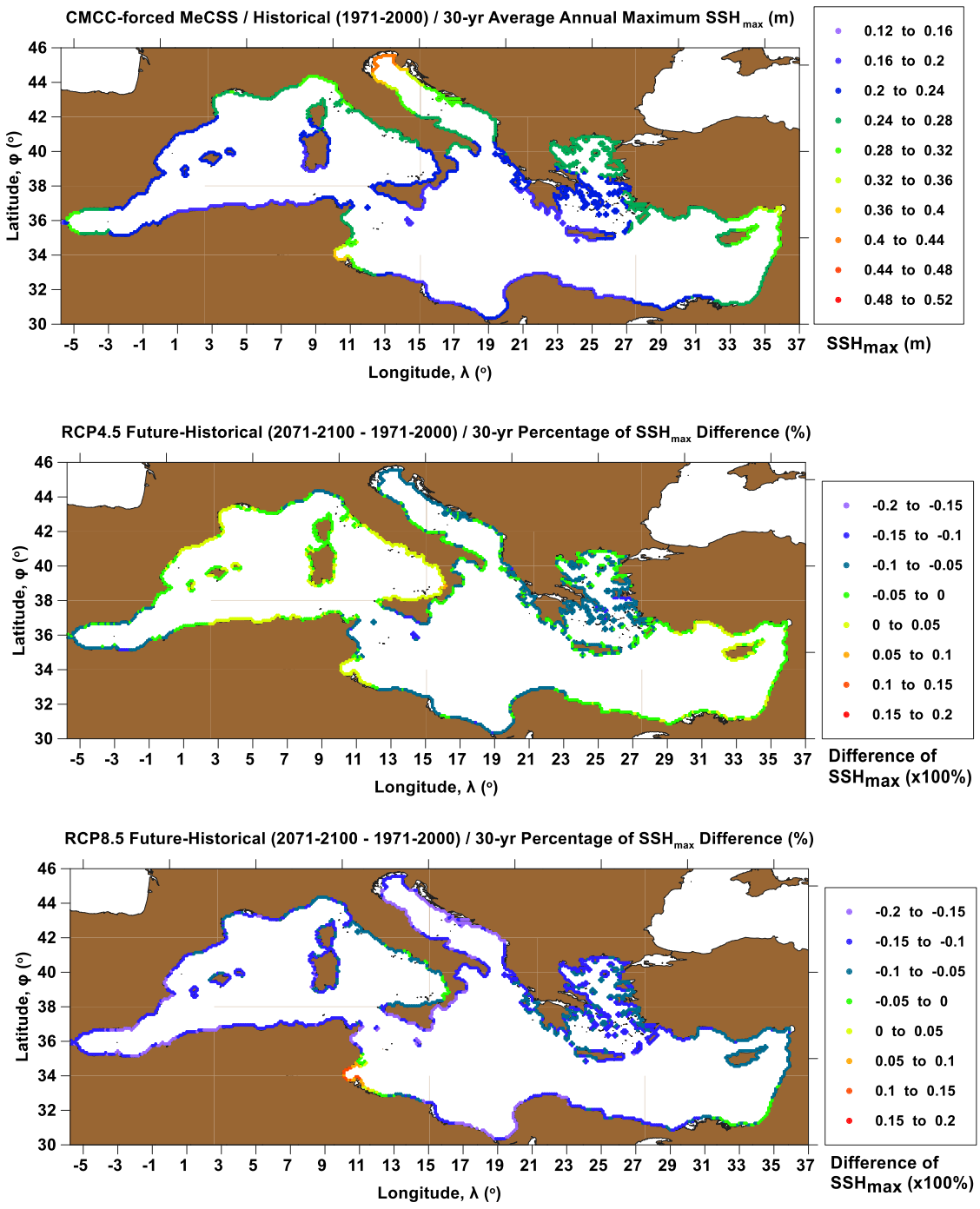


**Fig. 18.** Map of horizontal spatial distribution of: 30-year averaged annual maxima of SSH (m) during the Reference Period (1971–2000; top graph); differences of $SSH_{max}$ (×100%) between Future Period (2071–2100) and Reference Period for the RCP4.5 and RCP8.5 scenarios (mid and lower graphs, respectively) by the CMCC-forced MeCSS model.

in storm-induced coastal hazard (only under the pessimistic RCP8.5 scenario). The inter-scenario differences (RCP8.5-RCP4.5) also reveal a stable pattern for all RCM-forced model performances, *viz.* giving a slight increment of the pessimistic scenario compared to the modest one, by 4.76%, 2.63%, and 4.55%, respectively, for the evaluated storm surge maxima.

In general, a plausible increase of SSH maxima may be estimated for the 21st century, compared to those of the Reference Period, only in specific areas under certain projected climatic conditions. Overall, the spatial distributions of storm surge levels are estimated to remain similar to those of the past period throughout the entire Mediterranean coastal zone. However, a generalized storminess enfeeblement is more likely to occur in the study area towards the end of the 21st century. Moreover, a reduction of averaged (meteorological residual) storm-induced sea level ($SSH_{mean}$; not shown here for the sake of brevity) is also apparent throughout the 21st century. The extreme magnitudes of SSH range between 0.4 m and 0.6 m in the Mediterranean with higher values along parts of the Adriatic Sea and the Gulf of Gabes. The differentiations between the two scenarios used are obvious, not so much related to the spatiotemporal distribution of $SSH_{max}$, which show a very stable pattern, but in terms of magnitudes of surge-induced sea levels. For these, a mild decrease of $SSH_{max}$ values can be observed for the 21st century for both RCPs 4.5- and 8.5-driven MeCSS simulations. The largest SSHs of the entire Mediterranean coastal region seem to occur in the Adriatic Sea, probably due to the reinforcement of the

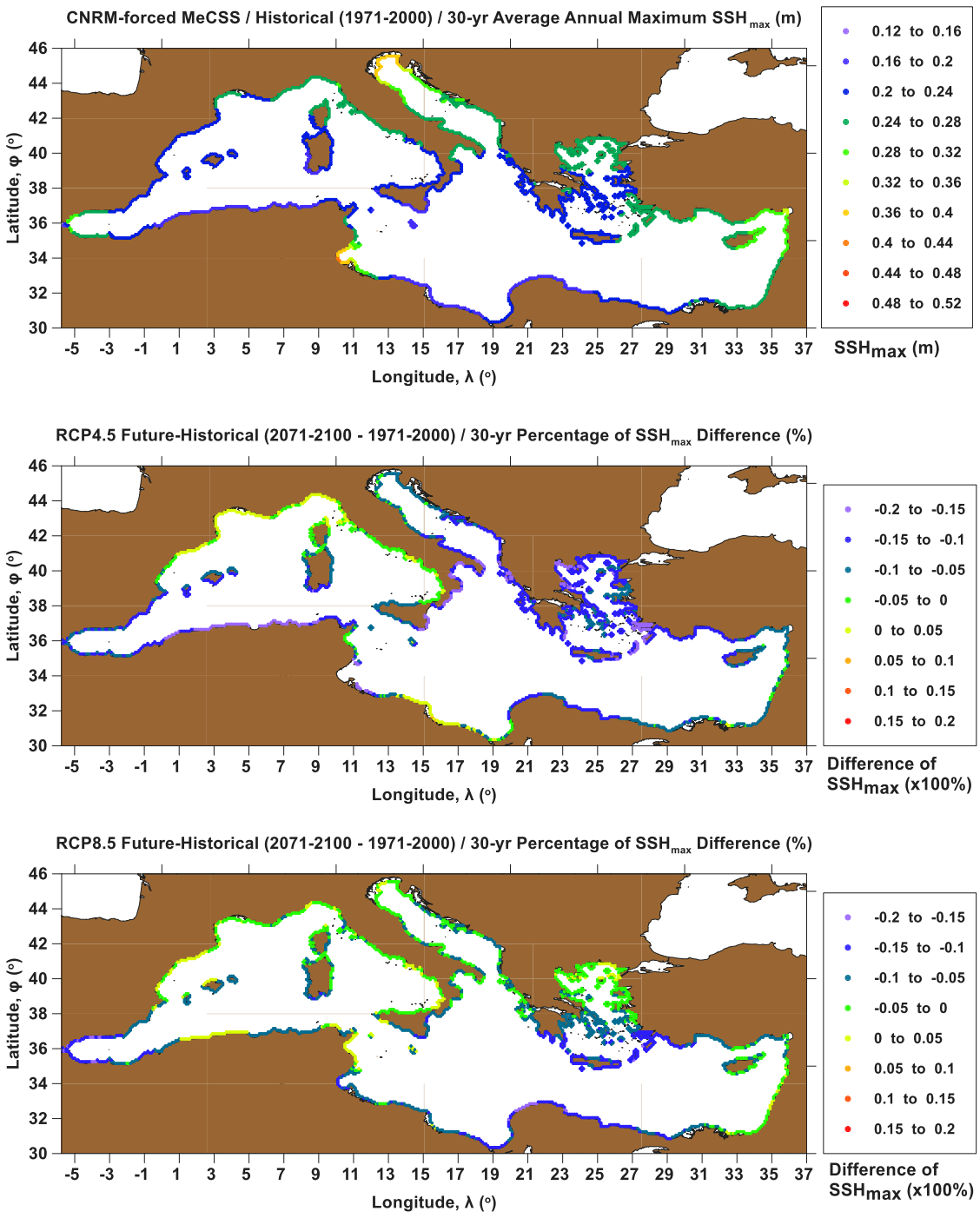


**Fig. 19.** Map of horizontal spatial distribution of: 30-year averaged annual maxima of SSH (m) during the Reference Period (1971–2000; top graph); differences of $SSH_{max}$ (×100%) between Future Period (2071–2100) and Reference Period for the RCP4.5 and RCP8.5 scenarios (mid and lower graphs, respectively) by the CNRM-forced MeCSS model.

inverse barometer effect by intense local wind forcing mechanisms (*i.e.*, Scirocco).

### 5.2.2. *Climate change signals of SSH maxima in the 21st century*

The Climate Change Signals (CCS) are also defined locally, *i.e.*, at 28 Mediterranean locations, as variations in the timeseries of annual storm surge maxima, $SSH_{max}$, and annual meteorologically induced MSL, $SSH_{mean}$, averaged over the two 30-year periods of study (1971–200 and 2071–2100) for the two RCPs (4.5 and 8.5). The 28 locations refer to coastal cities such as Kavala, Thessaloniki, Heraklion, Lefkada, Chios, and Alexandroupoli in Greece; Zadar, Dubrovnik, Split, Rovinj and Bakar in Croatia; Marseilles, Nice and Toulon in France; Genova, Catania, Naples, Cagliari, Ancona, Otranto, Venice, and Trieste in Italy; Alexandria in Egypt; Ajaccio in Corsica; Tarifa, Ibixa, Barcelona in Spain; and Antalya in Turkey (see Appendix B, A3). $SSH_{max}$ relates to the annual maximum of SSH as storm surge-induced high seas and $SSH_{mean}$ relates to the average SSH defined as the meteorologically induced residual of deviation from MSL. The analysis is separated to three discrete MeCSS model implementations (CMCC-forced, CNRM-forced, and GUF-forced). The raw data of calculations for the CCS of storm surge patterns for the 28 Mediterranean coastal sites are provided in Appendix B, A3 (Figures A3.1-3) together with differences of Future–Reference $SSH_{max/mean}$ and their percentages compared to the respective Reference period values.

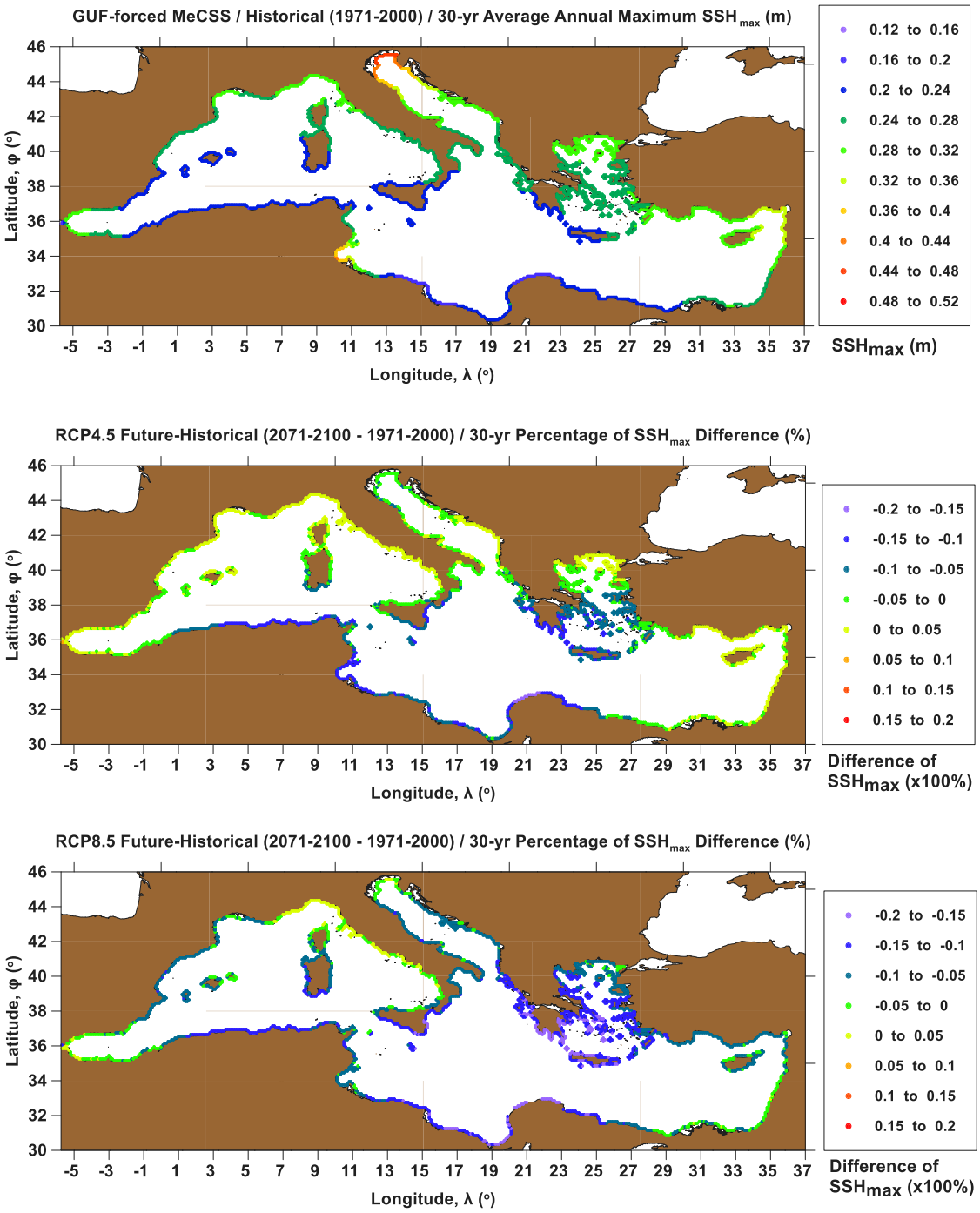


**Fig. 20.** Map of horizontal spatial distribution of: 30-year averaged annual maxima of SSH (m) during the Reference Period (1971–2000; top graph); differences of $SSH_{max}$ (×100%) between Future Period (2071–2100) and Reference Period for the RCP4.5 and RCP8.5 scenarios (mid and lower graphs, respectively) by the GUF-forced MeCSS model.

Table 4 presents the mean values (averaged over the 28 locations) of differences from a "Future – Reference" subtraction for $SSH_{max}$ and $SSH_{mean}$ ($DSSH_{max}$ and $DSSH_{mean}$, respectively) together with their percentages compared to the values of the Reference period (*e.g.*, $DSSH_{max}/SSH_{max,Ref}$ in %). In general, for all RCM-forced MeCSS runs both scenarios RCP4.5/8.5 show small decreases in $SSH_{max}$ of −3.5% to −9.5% (*i.e.*, from 12 mm to 3.7 cm) compared to the Reference Period. Thus, RCP scenario-based projections of storm surge maxima offer a bulk estimate of coastal storminess attenuation (in terms of surges) for the Mediterranean basin towards the end of the 21st century. Nevertheless, this is a spatially averaged assessment that presumes equal contribution of each location to the CCS calculation. Either weighted averaging or a spread-out derivation at more representative coastal sites around the Mediterranean littoral zone could maybe change this perception (for larger or smaller decrease).

Moreover, when referring locally at certain stations, for many of these coastal sites, such as Rovinj, Bakar, Toulon, Trieste, Ajaccio, Genova, Marseilles, Naples, Venice, Cagliari, Ancona, Ibixa, and Barcelona, the $SSH_{max}$ is expected to increase from 1% up to 22%. The change in $SSH_{mean}$ seems to be negative everywhere around the Mediterranean basin. At the rest of the locations, the $SSH_{max}$ decrease towards the end of the 21st century ranges from −30% to −2%. The aforementioned values refer to the CMCC-forced MeCSS implementation. Similarly, proportional changes are found for the CNRM- and GUF-forced MeCSS simulated results, although with a more pronounced attenuation pattern for these cases and specific differentiations of positive/negative

CCS given the different locations. For the storm-induced component of MSL rise, based on the calculation of $SSH_{mean}$, the general attenuation pattern is also prevalent for all cases of any RCM-forced MeCSS run. All the above signify that there is a need to assess if the calculated CCS is robust in our implemented projections, i.e., trace if there is a strong agreement between the results produced based on the three RCMs.

The robustness of the local CCS values (for each coastal city) was defined as the agreement of results per RCM-induced (CMCC-, CNRM-, GUF-forced) MeCSS model results for at least one (or even both) of the RCP-based (4.5 and 8.5) implementations. As "agreement" we consider the case of e.g., both CMCC- and CNRM- (or GUF-forced) MeCSS to produce results that show a decrease or increase (negative or positive rate of change as CCS %, respectively) when comparing the Future projections of $SSH_{max/mean}$ to the respective Reference Period values. The 30-year average of the annual meteorologically induced MSL, $SSH_{mean}$ tends to robustly decrease everywhere (in the 28 examined coastal sites) for all the possible RCM and RCP combinations tried in our analysis. Therefore, the reducing CCS concerning the meteorological residual of MSL deviation can be considered fully robust. For the 30-year average of the annual storm surge maxima, $SSH_{max}$, 18 out of 28 sites (>64%) present a robust agreement in the tendency to a storminess attenuation towards the end of the 21st century, i.e., all RCM-RCP combinations of MeCSS runs reveal an accordance about the trend for negative CCS values (%) either for one of the RCPs or for both. Especially for the coastal cities of Kavala, Alexandroupoli, Toulon, Ajaccio, Genova, Marseilles, Naples, Venice, Ibixa, and Barcelona, all RCM-forced MeCSS implementations do not agree with each other but at least two out of the three RCM-based runs tend to show the same behaviour. Analytic datasets are provided in Appendix B, A3.

### 5.3. Impact of mediterranean deep depression systems on storm surges

The statistically significant correlation ($p_{value} < 0.01$ with Mann–Kendall test) between the occurrence of storm surge maxima, $SSH_{max}$, and deep depressions, $SLP_{min}$, (see Sections 2.4.2, 3.3–Fig. 6, and 5.1.2 – Fig. 16 for identification/calculation methodology, evaluation, and derivation, respectively), is quantified by the Pearson product moment coefficient of the SLP timeseries on the nodal points of the RCM grid to SSH timeseries on all coastal cells of MeCSS model. These refer to entire the Mediterranean coastline, yet specifically for the time window of occurrence of separate deep depression events. Therefore, correlation maps on the Mediterranean coastal zone are produced for each one of the identified deep cyclone events (Section 5.1.2). These are divided in two 30-year (Reference and Future) simulation periods, by RCM-forced implementations only for RCP8.5 (worst case scenario) for the sake of brevity. In our case, the negative Pearson coefficient values reveal a large correlation of coastal SSH to the SLP, due to physical process of the inverse barometer effect (lowest SLPs induce highest sea levels in the vicinity of the cyclone's "eye"). Thus, the minima of correlations are then derived on every MeCSS coastal cell for each 30-year model run and compared against each other in respective pairs (*e.g.*, see intercomparisons in Section 5.2.1). Hence, a cumulative portrayal of the effect of synoptic scale climatology on the coastal storm surges is achieved in a heuristic way. This allows the mapping of vulnerable coastal areas due to storm surges, exposed to specific identified atmospheric patterns of extreme low-pressure systems. Figs. 21–23 present maps of the calculated Pearson correlation minima, $COR_{min}(SLP_{min}$-$SSH_{max})$, for the *SSH* on all coastal cells of the MeCSS model domain with the low SLP values of the identified deep depression systems. This way, we produce a display of topographic variability of the influence that "deep depression" low-pressure barometric systems exert on the entire Mediterranean coastal zone in terms of storm-induced sea level elevation. The results are separated by model implementation/setup, *i.e.*, for CMCC-, CNRM-, and GUF-forced MeCSS (Figs. 21, 22, and 23, respectively) presenting $COR_{min}(SLP_{min}$-$SSH_{max})$ on Reference and Future Period (RCP8.5) maps (upper and mid graphs). The lower graphs in Figs. 21, 22, and 23 refer to the algebraic differences (Future–Reference Period) of estimated correlation (*i.e.*, Pearson coefficient minima) of RCP8.5-based data (last 30 years of the 21st century; 2071–2100) to baseline Control Run data (1971–2000) along the coastline by each model implementation.

The localized 30-year $COR_{min}(SLP_{min}$-$SSH_{max})$ for all RCM-forced MeCSS model implementations follows a rather similar and consistent pattern in terms of geographical distribution (Figs. 21–23; upper and mid graphs). The "highest" correlations (lowest $COR_{min}$) are observed in several parts along the northern Mediterranean coasts, namely the littoral zones of the Gulfs of Valencia and Lions, the Ligurian and northern Adriatic Seas ($COR_{min} = -0.50$ to $-0.65$). They are followed by lower values on the coastal zones of mid-latitude areas around Corsica, Sardinia, the mid-zonal Italian Peninsula and the Adriatic, and the northern Aegean Sea ($COR_{min} = -0.55$ to $-0.40$). Significant, yet lower, correlations can be found in Sicily, South Italy, Peloponnese, Crete, the southern Aegean archipelago, and Alboran Sea ($COR_{min} = -0.45$ to $-0.25$). This signifies the systematic influence of Mediterranean deep depression systems on the coastal storm surges of the Mediterranean basin in a progressive manner from its South to the North. The Gulfs of Gabes and Alexandretta show even lower correlations ($COR_{min} = -0.25$ to $-0.20$; even though they are locations of exceptionally high storm surge maxima, probably also influenced significantly by local wind patterns). However, they discern from the rest of the southern parts of the Mediterranean coastal zone ($COR_{min} = -0.15$ to 0.00), where the effect of deep depressions on sea level extremes seems minimal (especially for CMCC-driven MeCSS simulations). All the above refer to the Reference Period, nonetheless, also apply to the Future Period estimations, where differentiations between the southern and the northern parts is more pronounced (especially for CMCC-fed MeCSS runs). This could be attributed to the known projected northward shift of the main cyclonic centres and tracks of Medicanes or storms in general over the Mediterranean during the 21st century, based on climate change scenarios.

In the lower graphs of Figs. 21–23, the differences (Future-Reference) of $COR_{min}$ reveal that when they are negative (towards blue and purple colours) it implies an increase of the deep depressions' influence on the storm surges, while positive values entail a decrease of the deep depression events on the occurrence of storm surge maxima. Therefore, there is a very clear pattern of an estimated slight attenuation of the deep cyclones' effect on the episodic increases of coastal sea level in Sardinia, Corsica, the Ligurian and Adriatic Seas, and the entire Italian peninsula for all RCM-fed implementations towards the end of the 21st century. This is projected to be the case also for Alboran Sea, the Gulf of Valencia, the north-western African coasts, and the Ionian, Aegean, and Libyan Sea coasts, especially for the CMCC- and GUF-forced MeCSS simulations, respectively. On the other hand, a possible increase of the Mediterranean deep depressions' influence on the coastal storm surges might be the case for the Gulf of Lions the Ionian, Aegean and Levantine Sea basins, covering the north-central and north-eastern coasts of Africa (CMCC-forced MeCSS).

Similarly, for CNRM- and GUF-based Future Period runs, Alboran Sea, the Gulfs of Gabes and Alexandretta are estimated to be further increasingly influenced by the projected deep depressions patterns, while these kinds of cyclones are prone to further boost the storm surge maxima of the Aegean Sea for CNRM-based implementations towards the end of the 21st century. All the above refer to the RCP8.5 scenario during the Future Period 2071–2100 compared to the 20th century baseline levels of the Reference Period. Conclusively, the projected climate change scenarios, examined herein, allow us to investigate several differentiations in estimated future storminess patterns. Generally, a positive influence of deep depressions to storm surge maxima would probably refer to areas with mid-to-high $SSH_{max}$ (*e.g.*, Aegean, Ionian, Gulf of Lions or Valencia or Gabes, *etc.*), but not the highest throughout the basin (*e.g.*, Venice lagoon, Ligurian, Adriatic, *etc.*). In the latter coastal regions, however, intense local wind forcing mechanisms (*i.e.*, Scirocco) play a most significant role in the formation of high storm surges.

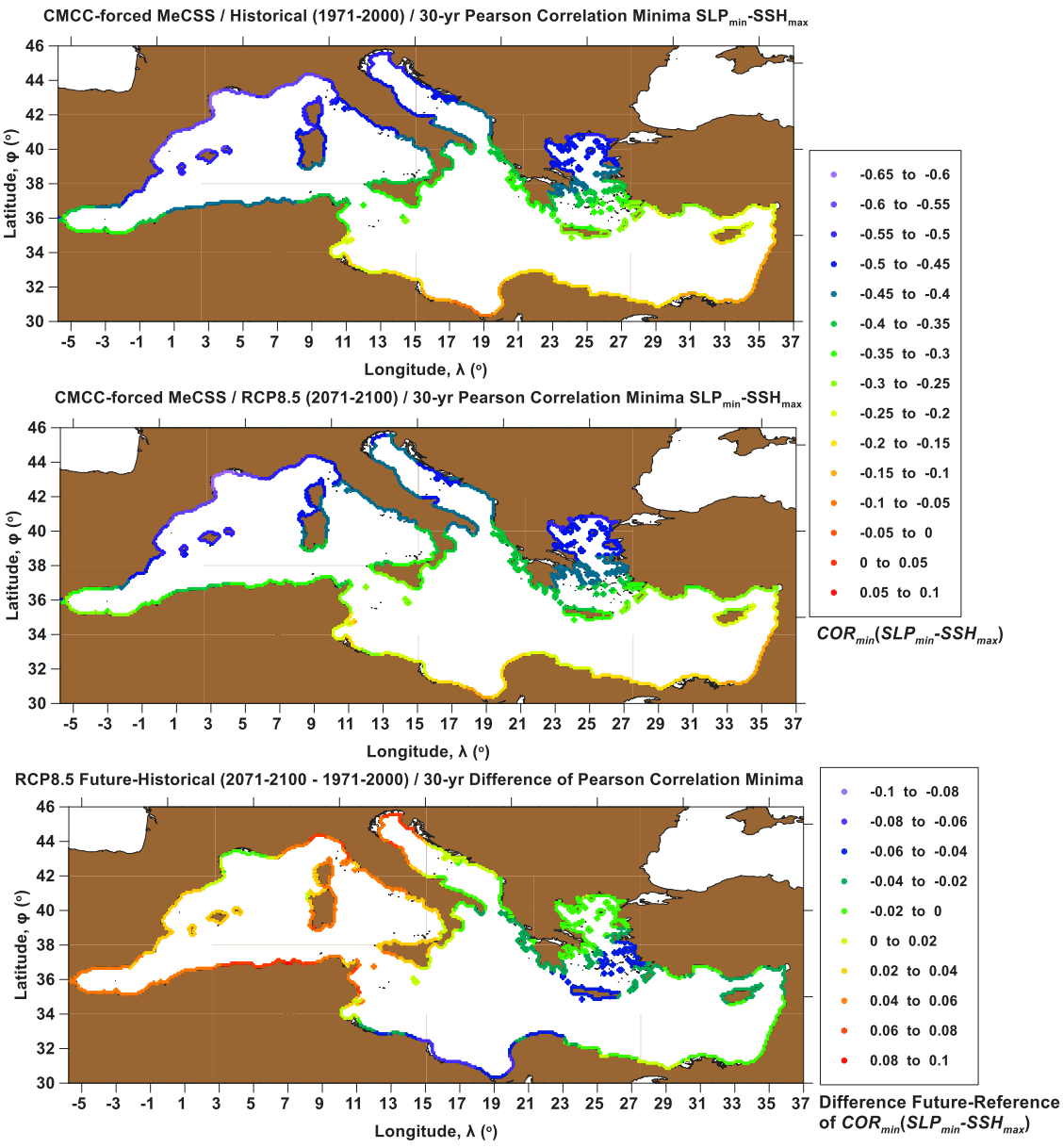


**Fig. 21.** Spatial distribution (along the Mediterranean coastline) of statistically significant ($p_{value}$ < 0.01 by Mann–Kendall test) Pearson correlation minima for SSH maxima (m) to the identified Deep Depression centres and its SLP values (hPa). Representation on the Mediterranean coastal cells during the Reference Period (1971–2000; top graph) and Future Period (2071–2100; mid graph) for the RCP8.5 scenario by the CMCC-forced MeCSS. Difference of Pearson correlation values between the Future - Reference Periods (lower graph).

## 6. Discussion

This study presents a systematic analysis of climatic simulations output about atmospheric patterns and barotropic ocean circulation in the Mediterranean basin. We follow an integrated approach of evaluating certain products (MED-44 SLP and winds) of the Med-CORDEX database and further feeding them as input to basin-scale storm surge modelling (MeCSS). A control run baseline for MeCSS model in a 30-year Reference Period is thoroughly validated against *in situ* sea level observations by tide-gauges. The results corroborate a projected storminess attenuation towards the end of the 21st century (under RCP4.5 and 8.5 scenarios), yet locally estimated increases or decreases of storm surge maxima around the Mediterranean coastal zone is pinpointed and thoroughly discussed (depending on RCM-forced MeCSS implementation). We conclusively propose a heuristic analysis for the quantification of the identified deep depressions (extreme low-pressure systems) effect on the coastal sea level elevation due to storm surges towards 2100. The signal of possible projected climate change effects is also provided in the form of comparisons by Future–Reference Period outputs.

An important issue, which has come up in our analysis, concerns the effects of climate and marine model resolutions on the produced results. This particularly refers to the reproduction of storm surges in the coastal zone, and therefore also to atmospheric data (e.g., wind fields in the open sea and coastal waters) resolution which influences the storm surge evolution.

According to Ferrarin et al. (2021), who analysed one of the most extreme flooding events in terms of physics in Venice, it is necessary to use a high-resolution model (1 km) in order to describe the local processes and the interaction with the local topography, as well as to reproduce the small-scale cyclonic vortices that develop in northern Adriatic Sea and affect the area of study. But these kinds of resolutions are impossible to achieve for the entire Mediterranean basin in terms of computational cost, especially for the amount of simulations we

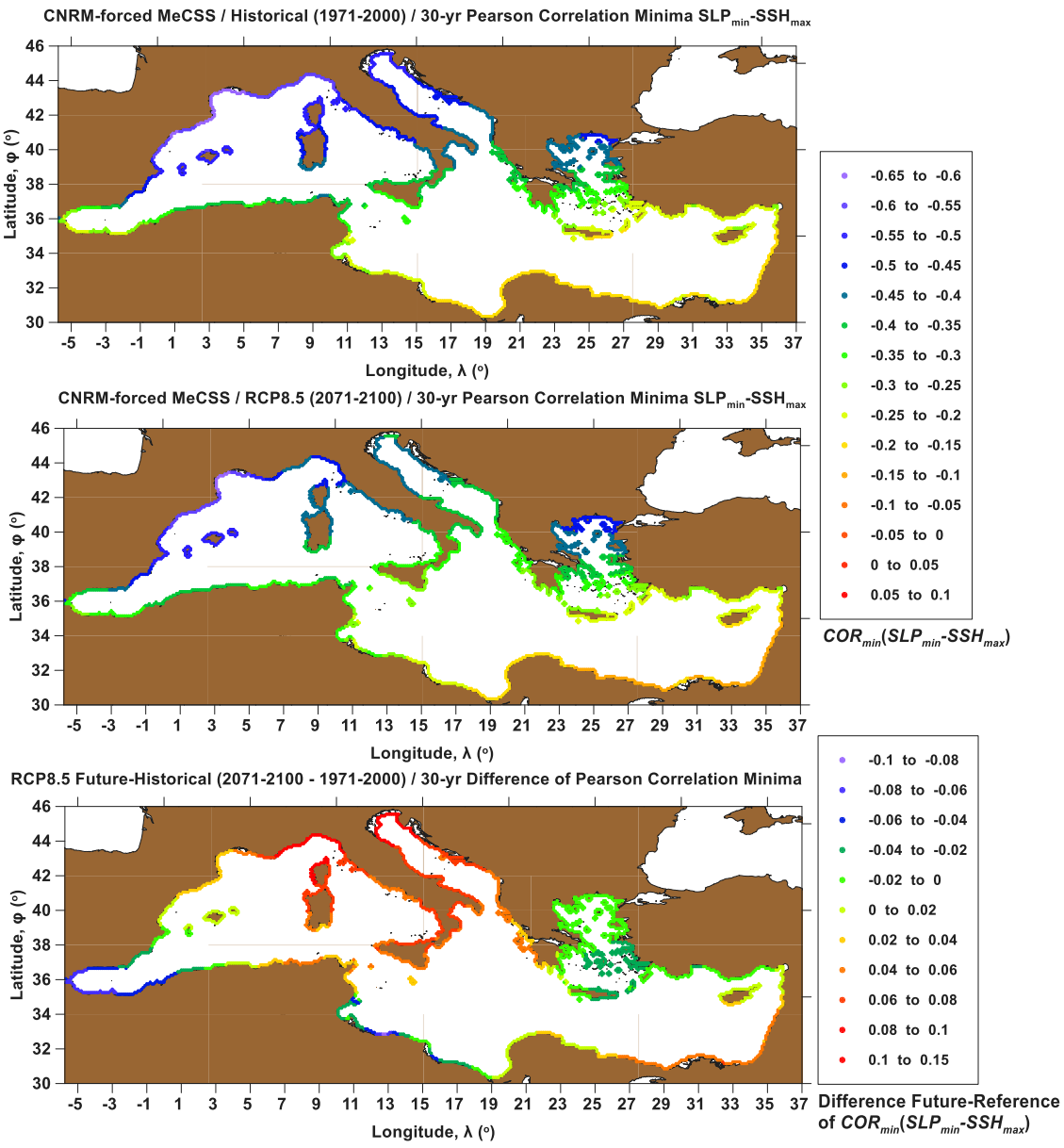


**Fig. 22.** Spatial distribution (along the Mediterranean coastline) of statistically significant ($p_{value}$ < 0.01 by Mann–Kendall test) Pearson correlation minima for SSH maxima (m) to the identified Deep Depression centres and its SLP values (hPa). Representation on the Mediterranean coastal cells during the Reference Period (1971–2000; top graph) and Future Period (2071–2100; mid graph) for the RCP8.5 scenario by the CNRM-forced MeCSS. Difference of Pearson correlation values between the Future - Reference Periods (lower graph).

implemented in our study, i.e., 15 sets of simulations by 3 RCMs × 2 RCPs × (2 Future Periods + 1 Reference Period).

Denamiel et al. (2021) discuss the balancing accuracy and efficiency of atmospheric models in the northern Adriatic sub-basin during the blowing of high Bora winds. They comment on the need for atmospheric model resolutions of O(100 m) especially in focused, fine-scale, process-oriented studies to achieve accurate representation of severe Bora rotor dynamics. Typical RCM resolutions of 10 km are not considered accurate enough to drive the marine coastal processes and a discussion is introduced about "kilometre-scale" atmospheric models in order to balance accuracy and efficiency in coupled atmosphere–ocean climate studies in the Adriatic. A divergence of results for both ERA5 reanalysis and WRF 15-km model output from super-high resolution weather modelling with WRF 1.5-km is apparent especially in terms of wind speeds. This is a crucial point and certainly sets new ground for climate studies in the coastal ocean, but such an approach is still applicable only in focused local case studies (e.g., northern Adriatic sub-basin) referring to confined areas of the coastal zone rather than the entire Mediterranean basin.

Moreover, according to Denamiel and Vilibić (2022) the next-generation climate modelling efforts should focus on (sub-)kilometre-scale simulations for extreme storm surges and their projections in the 21st century. As a proof-of-concept, they present long-term sea-level variations and distributions at the climate timeframe, yet again in the focused spatial scale of the Adriatic Sea's small lagoons and bays. The authors assert that this newly developed methodology could lead to more targeted local mitigation strategies for the storm surge hazard in regional studies.

Furthermore, the utilized CERA-20C data (most up-to-date reanalysis dataset during the study implementation in 2019; ERA5 dataset was not published yet) for the validation of the Med-CORDEX (MED-44) datasets have a lower resolution of 125 km compared to the latter (of 44 km downscaled to 10 km), therefore CERA-20C wind fields might not be representative for fine scale effects of winds especially in coastal

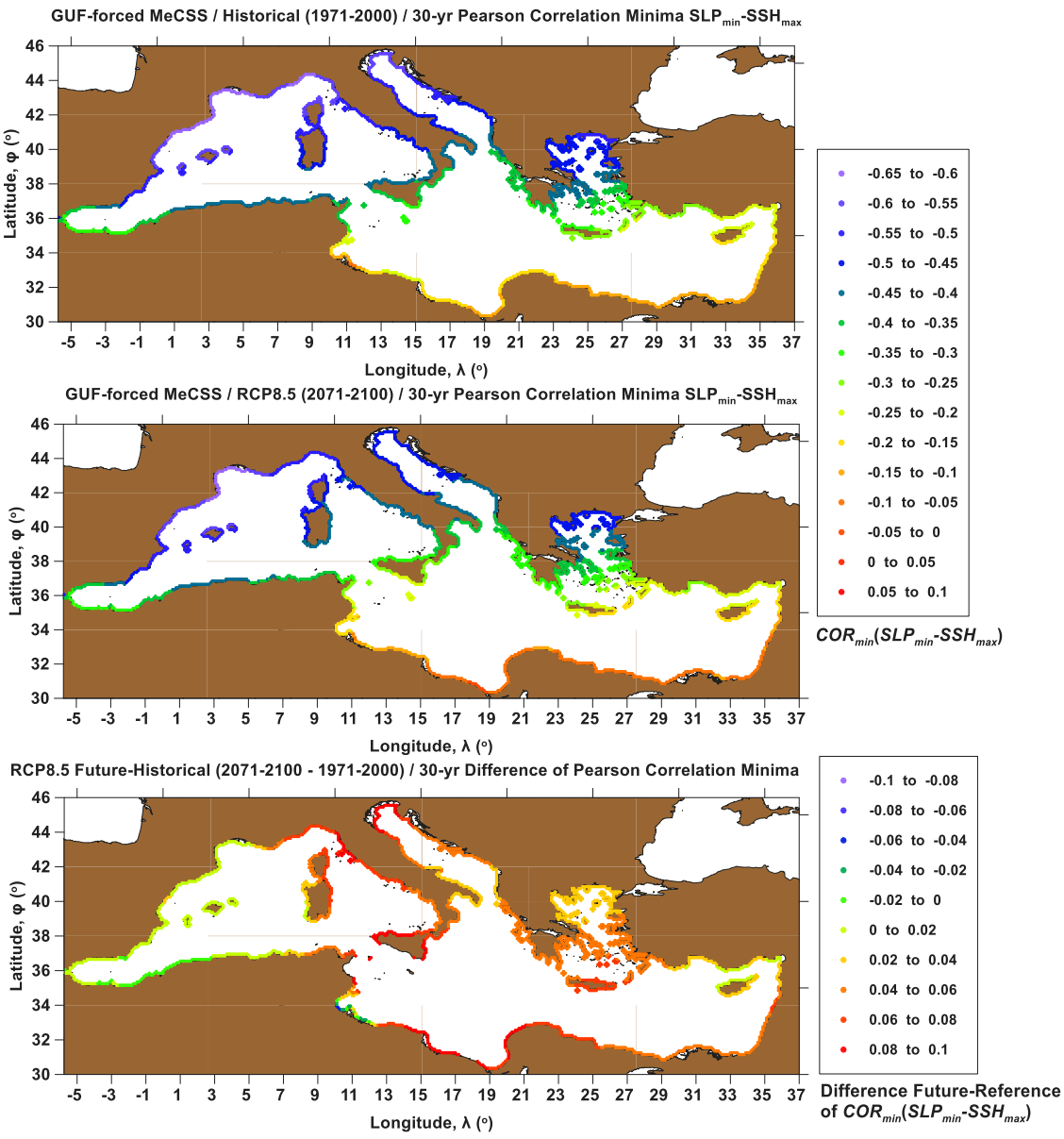


**Fig. 23.** Spatial distribution (along the Mediterranean coastline) of statistically significant ($p_{value}$ < 0.01 by Mann–Kendall test) Pearson correlation minima for SSH maxima (m) to the identified Deep Depression centres and its SLP values (hPa). Representation on the Mediterranean coastal cells during the Reference Period (1971–2000; top graph) and Future Period (2071–2100; mid graph) for the RCP8.5 scenario by the GUF-forced MeCSS. Difference of Pearson correlation values between the Future - Reference Periods (lower graph).

areas, where diverse topography of shorelines play an important role in atmospheric dynamics. However, the spatial resolution of CERA-20C dataset that was utilized was downscaled to 0.25° × 0.25° for easier comparisons. It is further noted that the CERA assimilation system has the ability to produce a more balanced and consistent Earth System climate reconstruction, as it takes into account the interactions between the atmosphere and the ocean.

Our study relies on mainly detecting the effects of SLP on the sea level elevation around the entire basin in a large synoptic-scale analysis. Therefore, SLP is considered to be the main driver for sea level elevation as it can be adequately simulated by the MED-44 RCMs feeding the 10-km resolution storm surge model. The effects of winds are of course important (especially in fine coastal scales) and still simulated in our model but in a rather cruder way than the effects of SLP, as wind fields are highly irregular more steeply changing in space and time. Nevertheless, our results focus on synoptic scale climatology of deep depressions (by SLP minima) on the coastal SSH. By the term "coastal" herein, we refer to a rather crude-scale representation of SSH on the continental shelf, and not the exact, fine-scale, sea level elevation on the coastline, which would certainly require a very detailed dynamic downscaling of model runs. This is still impossible to achieve in terms of computational cost in a systematic way for the entire Mediterranean coastal zone for a climatic analysis from 1971 to 2100 involving several combined cases RCMs and RCPs. Thus, we opted to check if the reasonably reproduced weather patterns (mainly SLP and winds) could be used as forcing drivers for large-scale maritime hydrodynamic simulations in the open sea of the Mediterranean basin, and not focus too much on fine scale topographic peculiarities and local coastal wind patterns. Certain local wind patterns could drive coastal waters to littoral run up in very diverse ways, but this is an issue for a future study, where we will focus on a lot finer scales for coastal inundation (also involving wave-induced sea levels) on selected areas of the Mediterranean coastal zone.

Our results on the detection of deep depressions (please refer to Figs. 6–8) can be also loosely compared to Reale et al. (2022) outputs (please refer to their Figs. 2–3). The patterns of spatial distribution of deep depressions (and the annual density of cyclone tracks) seem generically similar with a pronounced centre over the Ligurian Sea and

the southcentral Italian Peninsula including some cells expanding also to the central Adriatic Sea. Comparisons between the two works cannot be straightforward, as they refer to different timeframes (1971–2000 and 1981–2005, in ours and (Reale et al., 2022) analysis, respectively), while we compute the number of deep depressions in a 30-year period and Reale et al. (2022) present the spatial distribution of annual mean number of cyclone tracks in each 1.5° cell of the Mediterranean. However, similar patterns can be found for wind speed fields, too, given the applied comparison restrictions.

## 7. Conclusions

### *7.1. Conclusive remarks about atmospheric modelling aspects under the effects of climate change*

In the presented research, the analyses are based on three implemented RCMs, namely CMCC-CCLM, CNRM-ALADIN52, and GUF-CCLM-NEMO, for RCP4.5 and RCP8.5 scenarios of the 21st century. Atmospheric modelling datasets cover the Reference (1971–2000) and Future (2071–2100) Periods of climate projections. Thorough validation of the RCM outputs was conducted by comparisons of the (Control Run) Reference Period datasets against the most recent CERA-20C reanalysis data. No definite conclusion can be deduced concerning the skill score of the three models for all regions of the Mediterranean about the barometric systems, based on SLP and wind patterns; however, the CCLM model implementations of both the CMCC and GUF institutions seem to slightly dominate over the CNRM's ALADIN model runs. This is also the case for the detection of deep depressions over the Mediterranean, which is crucial for the simulation of storm surges and *SSH* variations due to climate change. In some cases, based on changing between seasonal and annual analyses and concerning warm or cold periods of the year, the CNRM-ALADIN52 model outputs are found to be superior to the rest of the model results. Therefore, all climatic input datasets were used for the forcing of the MeCSS model implementations, providing ensembles of results for a more robust representation of the future climate change impacts on Mediterranean coastal sea level elevations in the 21st century.

From the analysis of the future projections of the three examined models (CMCC, CNRM and GUF) under RCP4.5–8.5, for Sea Level Pressure (SLP), wind speed and extreme cyclones the following could be concluded:

• SLP is expected to increase on an annual basis during the last 30 years of the 21st century over the Mediterranean. This is probably associated to a northward shift of cyclonic systems also found by other researchers in the past under a different RCM/RCP scrutiny.

• Conversely to the other three seasons, in summer, the SLP values are expected, in general, to decrease with the most intense negative differences (future–present day) found over the sea rather than the continental areas.

• Regarding wind patterns, the areas with the stronger wind speeds remain the same in the Future as in the Reference Period.

• Both CMCC and GUF models estimate that winds will become stronger over the Aegean Sea (~2.5 m/s) meaning that this increase will affect Greece and especially the islands of the Aegean archipelago.

• Moreover, in summer, the Etesian winds are estimated to become even stronger in the future with larger positive differences over the area of the Aegean Sea.

• All three models estimate the occurrence of deep cyclones in the largest part of the Mediterranean region. In the cases of CMCC and GUF models, these cyclones are expected to have their centres mainly overland, while, according to CNRM model, they are estimated to occur almost evenly between continental and oversea areas.

• Even though deep depressions are bound to occur in the Future Period, their frequency is generally going to decrease towards the end of the 21st century.

### *7.2. Conclusive remarks about storm surge modelling aspects under the effects of climate change*

Several implementations of maritime hydrodynamic simulation for storm surges throughout the entire Mediterranean Sea basin were conducted. MeCSS model simulated the sea level variations and barotropic hydrodynamic circulation in offshore and coastal areas of the Mediterranean both at present and future climatic conditions (Reference and Future Periods,1971–2000 and 2071–2100) under RCP4.5 and 8.5 scenarios. The model takes into account the inverse barometer effect and the win drag on the sea surface providing reliable estimations of storm-induced Sea Surface Height (SSH) variations locally under the estimated effects of climate change on marine water bodies. MSL rise estimations in the Mediterranean under the Med-CORDEX initiative or other possible interactive effects on storm surge patterns at specific areas by *e.g.*, tides, seiches, meteotsunamis, wave-induced runup, *etc.*, were not considered in this study, as they were out of scope.

The calibration and simulation of the storm surge model was conducted for a decadal period around the Millennium, for which there were available *in situ* observations by the HNHS. For the simulation of the climate change impacts on storm-induced sea level in the coastal zone of Mediterranean, the modelling results of three RCMs (CMCC, CNRM and GUF), were used as forcing input to the MeCSS model. The following conclusions can be deduced:

Overall, the cumulative comparison of measured and simulated 10-year mean SSIs for the three MeCSS implementations reveals that there is a rather high correlation (*COR* > 0.79 reaching up to 0.89) with the lowest RMSEs of SSI and $SSH_{max}$ (<3 cm; being 13% of $SSI_{mean}$) referring to the GUF-forced MeCSS run. This is also backed up by the very high skill scores *WSS* > 0.80, rendering the GUF-forced MeCSS model setup the generally (yet not locally) most reliable performance of the MeCSS model for the east-central Mediterranean region.

Generally, the MeCSS model can reproduce the storm surge patterns for all the classes of SSH percentiles in an adequate way, and thus the statistical distributions of the modelled SSH data are considered to be reliable for further use by coastal engineers and scientists especially for coastal water resources management.

Moreover, the MeCSS model can also adequately reproduce the storm surge patterns for all the classes of statistical thresholds, which correspond to heuristically defined coherent, intense, and extreme events. It was also found to perform well in reproducing the probabilistic features of storm surge patterns in terms of the amount and occurrence frequency of surge events (*viz.* "local" maxima in the modelled SSH timeseries). However, a tendency is traced for the present MeCSS model implementations to underestimate small values of SSH and perform better for the estimation of large SSHs representative of intense and extreme storm surge events. Therefore, the reproduced probabilistic parametric features of the modelled SSH data are reliable for further coastal impact analysis.

In general, a plausible decrease of SSH maxima is estimated for the last 30 years of the 21st century, compared to those of the Reference Period. Moreover, a slight reduction of average storm-induced sea level ($SSH_{mean}$; MSL component attributed solely to the meteorological residual of sea level elevation) is also apparent towards the end of the 21st century. Extreme magnitudes of $SSH_{max}$ range between 0.35 and 0.50 m in the Mediterranean with higher values along parts of its northern coasts (Venice lagoon, Gulf of Lions, northern Adriatic and Aegean Seas, *etc.*) and the Gulf of Gabes in its southern part. Overall, the spatial distributions of surge level maxima are estimated to remain similar to those of the Reference Period throughout the entire Mediterranean coastal zone.

Differentiations between the two scenarios (RCP4.5–8.5) used are obvious, not so much related to the spatiotemporal distribution of $SSH_{max}$, which shows a very stable pattern, but more in terms of magnitudes of the extreme surge-induced sea levels. For these, a decrease of $SSH_{max}$ values that ranges from −30% to −2% can be observed

towards the end of the 21st century, especially for RCP8.5-driven MeCSS simulations.

The RCP-driven scenarios of MeCSS implementations estimate a general attenuation of storminess in the Mediterranean basin during the last third of the 21st century. Of course, this is a spatially averaged estimation, and for some specific coastal sites in Croatia, Spain Italy, and France, such as Rovinj, Bakar, Toulon, Trieste, Ajaccio, Genova, Marseilles, Naples, Venice, Cagliari, Ancona, Ibixa, and Barcelona, the $SSH_{max}$ is expected to increase from 1% to 22% towards the end of the 21st century.

Analogously similar or proportional changes are found for the CNRM-forced and the GUF-forced MeCSS simulated results, although with a more pronounced attenuation pattern for these cases and differentiations of the locations of positive/negative climate change signals.

### 7.3. Conclusive remarks about the correlation of deep depressions to storm surges under the effects of climate change

By heuristically correlating the occurrence of deep depressions to storm surge maxima on the coast, in a localized manner throughout the two 30-year periods of study for all RCM-forced MeCSS model implementations, it seems that the effect of deep cyclones on coastal sea levels follows a similar and consistent geographical pattern. The "highest" correlations of deep depression events to sea level highs (*i.e.*, lowest Pearson coefficients due to the inverse barometer effect) were observed in several parts along the northern Mediterranean coasts (Gulfs of Valencia and Lions, Ligurian and northern Adriatic Seas). They are followed by mid-latitude areas around Corsica, Sardinia, the mid-zonal Italian Peninsula and the Adriatic, and the northern Aegean Sea. The influence of deep depressions on storm surges was lower for Sicily, South Italy, Peloponnese, Crete, the southern Aegean archipelago, and Alboran Sea. A pattern of northward increase in the influence of Mediterranean deep depression systems on the coastal storm surges of the basin is obvious. The only exceptions in the generally unaffected southern Mediterranean littorals are the Gulfs of Gabes and Alexandretta. These apply to the Reference Period, however, seem to repeat for Future Period estimations, even with more pronounced differentiations between the southern and the northern parts (especially for the CMCC-based analysis). A projected northward shift of the main cyclonic centres and tracks of storms over the Mediterranean towards the end of the 21st century, is likely the reason for the latter.

All the following conclusions refer to the RCP8.5 scenario during the Future Period 2071–2100 compared to the 20th century baseline levels of the Reference Period. The climate change signal (difference of Future–Reference Period) of the deep cyclones' effect on the episodic increases of coastal sea level seems to have a very clear pattern of slight attenuation in certain regions. These refer to Sardinia, Corsica, the Ligurian and Adriatic Seas, and the entire Italian peninsula for all RCM-fed implementations towards the end of the 21st century. Conditionally, this is the case for the Gulf of Valencia, the north-western African coasts, the Alboran, Ionian, Aegean, and Libyan Sea coasts, under specific combinations of RCM/RCP forcings. On the other hand, a possible increase of the Mediterranean deep depressions' influence on the coastal storm surges might be the case for the Gulf of Lions, the Ionian, Aegean and Levantine Sea basins, covering the north-central and north-eastern coasts of Africa only under the CMCC-forced MeCSS outputs.

Based on CNRM- and GUF-based Future Period projections under the RCP8.5 scenario, Alboran Sea, the Gulfs of Gabes and Alexandretta are estimated to be further increasingly influenced by the projected deep depressions in the 21st century. The entire Aegean Sea's coasts are also prone to be influenced by deep cyclones under the CNRM-based projections towards the end of the 21st century. Conclusively, the projected climate change scenarios, examined herein, allow us to investigate several differentiations in estimated future storminess patterns. A general consensus is that a positive influence of deep depressions to storm surge maxima would probably refer to areas of mid-to-high $SSH_{max}$ (*e.g.*, Aegean, Ionian, Gulf of Lions or Valencia or Gabes, *etc.*), but not the highest throughout the basin (*e.g.*, Venice lagoon, Ligurian, Adriatic, *etc.*). In the latter coastal regions, however, intense local wind forcing mechanisms (*i.e.*, Scirocco) might play a most significant role in the formation of high storm surges.

### 7.4. Future steps

The results produced within this study can be used for investigations in specific locations of the Mediterranean basin within integrated hydrologic/hydrodynamic modelling under projected climate change conditions during the 21st century. Our next goals are to implement nonstationary Extreme Value Analysis of nearshore storm surges (Galiatsatou et al., 2019, 2021; Makris et al., 2018) in order to assess design water levels at the shoreline under the effects of projected climate change applied to the entire Mediterranean coastal zone, focusing on lowland littoral areas and river deltas. We further intend to focus on the entire Greek coastal zone and define vulnerability maps of extended coastal inundation (by CoastFLOOD model) due to storm surges on regions with protected low-elevation areas, exposed floodplains, engineered waterfronts, and port structures for the 21st century (Makris et al., 2020a,b; Skoulikaris et al., 2021; Androulidakis et al., 2022). These results may be used as output for a regional scale integrated coastal zone management projects.

## CRediT authorship contribution statement

**Christos V. Makris:** Conceptualization, Methodology, Software, Validation, Formal analysis, Investigation, Resources, Data curation, Writing – original draft, Writing – review & editing, Visualization, Supervision. **Konstantia Tolika:** Methodology, Software, Validation, Formal analysis, Investigation, Writing – original draft, Writing – review & editing, Visualization, Supervision. **Vasilis N. Baltikas:** Methodology, Software, Formal analysis, Investigation, Resources, Data curation, Visualization. **Kondylia Velikou:** Methodology, Software, Validation, Formal analysis, Investigation, Data curation, Writing – review & editing, Visualization. **Yannis N. Krestenitis:** Conceptualization, Investigation, Resources, Writing – review & editing, Supervision, Project administration, Funding acquisition.

## Declaration of competing interest

The authors declare that they have no known competing financial interests or personal relationships that could have appeared to influence the work reported in this paper.

## Data availability

Data will be made available on request.

## Acknowledgements

This research is part of the MEDAQCLIM project: *Integrated Quantitative Assessment of Climate Change Impacts on Mediterranean Coastal Water Resources and Socioeconomic Vulnerability Mapping*, which is financed by the National Action Plan: "European R&D Cooperation—Grant Act of Greek partners successfully participating in Joint Calls for Proposals of the European Networks ERA-NETS" and the "Competitiveness, Entrepreneurship & Innovation" Program.

## Appendix A

*A.1. The statistical measures used in the analysis refer to the following parameters*

The *SSI* (and $SSH_{max}$ etc. factors) for both simulated and observed timeseries of storm surge levels is calculated for each of the five stations, along with the corresponding Percent Error ($E$):

$$E(\%) = 100 \cdot \left(\overline{SSI_{\mathrm{mod}}} - \overline{SSI_{obs}}\right) \Big/ \left(\frac{\overline{SSI_{\mathrm{mod}}} + \overline{SSI_{obs}}}{2}\right) \quad (1)$$

where $SSI_{mod}$ and $SSI_{obs}$ are the mean *SSI* over the 10-years study period as derived from modelled and observed data, respectively. It is noted that $E$ is positive when the model overestimates the amplitude of the sea level against observed data. In order to provide more information about the significance of the error, the Error Index ($EI$) is also calculated according to the following relation:

$$EI = \left(\overline{SSI_{mod}} - \overline{SSI_{obs}}\right) \Big/ \sqrt{\left(\sigma^2_{SSI_{mod}} + \sigma^2_{SSI_{obs}}\right)/2} \quad (2)$$

where $\sigma$ is the mean standard deviation of *SSIs* corresponding to either the simulated (mod) or observed (obs) timeseries for each station. The aforementioned parameters refer to the entire timeseries of *SSH* and respective calculated *SSI* parameters in each examined station. For further general evaluation of the MeCSS model performance the root-mean-square error (*RMSE*) of 10-year average values of *SSI* between modelled and observed values in each of the five stations is also provided as:

$$RMSE = \sqrt{\frac{\sum_{i=1}^{5}\left(SSI_{mod,i} - SSI_{obs,i}\right)^2}{5}} \quad (3)$$

The percentage index of the ratio $RMSE/SSI_{mean}$ ($SSI_{mean}$ corresponds to the average *SSI* value of all model results and observations) is also given, followed by the classic Pearson product-moment correlation coefficient $COR(x)$, viz. the covariance of the modelled and observed *SSI* variables divided by the product of their standard deviations:

$$COR\left(SSI_i\right) = \left(\frac{\sum_{i=1,5}\left(SSI_{\mathrm{mod}} - \overline{SSI_{\mathrm{mod}}}\right)\cdot\left(SSI_{obs} - \overline{SSI_{obs}}\right)}{\sum_{i=1,5}\left(SSI_{\mathrm{mod}} - \overline{SSI_{\mathrm{mod}}}\right)^2 \cdot \sum_{i=1,5}\left(SSI_{obs} - \overline{SSI_{obs}}\right)^2}\right) \quad (4)$$

The Pearson coefficient ($\leq$1; 1 being the full agreement between modelled and observed *SSIs*) measures the strength of linear dependence between experimental and numerical data but does not directly compare their actual values. Therefore, the combination with the *RMSE* provides a clearer insight on the MeCSS model performance skill.

Moreover, the Willmott Skill Score (*WSS*) or Index of Agreement (Willmott et al., 2012) is also calculated for *SSI* (and other SSH magnitudes) as:

$$WSS_{SSI} = 1 - \frac{\sum_{i=1}^{5}\left|SSI_{\mathrm{mod}} - SSI_{obs}\right|^2}{\sum_{i=1}^{5}\left(\left|SSI_{\mathrm{mod}} - \overline{SSI_{\mathrm{mod}}}\right| + \left|SSI_{obs} - \overline{SSI_{obs}}\right|\right)^2} \quad (5)$$

The higher the *WSS* (with $\leq$1 as a limit), the better match is reached between simulated values of *SSI* and observations form tide gauges, while *WSS* values close to 0 indicate disagreement between the two samples.

The Hit-Rate-of-Percentiles (*HRP*) index (Schoetter et al., 2012; Makris et al., 2016) is also used as a model evaluation metric. Namely, for the *HRP* index, one computes the absolute differences between the sorted (from 1st to 99th) percentiles of simulated and observed values (herein of *SSH*). Then the *HRP* index is defined as the sum of the categorical fractions, i.e., the differences compared to an allowed deviation (herein it is taken as the average of standard deviations of all modelled and observed *SSH* timeseries, $\sigma_{SSH}$). In the analysis of Schoetter et al. (2012), if the *HRP* index (with range between 0 and 1) is greater than 0.95, then the model efficiently represents the regarded observation timeseries and the simulated dataset under examination does not need to be corrected for bias. The *HRP* index is independent of the variable under evaluation.

## Appendix B. Supplementary data

Supplementary material related to this article can be found online at https://doi.org/10.1016/j.ocemod.2022.102149.

## References


Adloff, F., Jordà, G., Somot, S., Sevault, F., Arsouze, T., Meyssignac, B., Li, L., Planton, S., 2018. Improving sea level simulation in Mediterranean regional climate models. Clim. Dynam. 51 (3), 1167–1178.

Adloff, F., Somot, S., Sevault, F., Jordà, G., Aznar, R., Deque, M., Herrmann, M., Marcos, M., Dubois, C., Padorno, E., Alvarez-Fanjul, E., Gomis, D., 2015. Mediterranean sea response to climate change in an ensemble of twenty first century scenarios. Clim. Dynam. 45, 2775–2802.

Alpert, P., Neeman, B.U., Shay-EL, Y., 1990. Climatological analysis of Mediterranean cyclones using EMCWF data. Tellus 42A, 65–77.

Anagnostopoulou, C., Zanis, P., Katragkou, E., Tegoulias, I., Tolika, K., 2014. Recent past and future patterns of the Etesian winds based on regional scale climate model simulations. Clim. Dynam. 42, 1819–1836.

Androulidakis, Y., Kombiadou, K., Makris, C., Baltikas, V., Krestenitis, Y., 2015. Storm surges in the Mediterranean Sea: variability and trends under future climatic conditions. Dyn. Atmos. Oceans 71, 56–82.

Androulidakis, Y., Makris, C., Mallios, Z., Pytharoulis, I., Baltikas, V., Krestenitis, Y., 2022. Storm surges during IANOS Medicane. In: Natural Hazards. Springer, http://dx.doi.org/10.21203/rs.3.rs-1781884/v1.

Belušić, A., Prtenjak, M.T., Güttler, I., Ban, N., Leutwyler, D., Schär, C., 2018. Near-surface wind variability over the broader Adriatic region: insights from an ensemble of regional climate models. Clim. Dynam. 50 (11), 4455–4480.

Boyes, S., Elliott, M., 2019. European challenges to coastal management from storm surges: Problem-structuring framework and actors implicated in responses. In: Facing Hydrometeorological Extreme Events: A Governance Issue. pp. 339–361.

Bubnová, R., Hello, G., Bénard, P., Geleyn, J.F., 1995. Integration of the fully elastic equations cast in the hydrostatic pressure terrain-following coordinate in the framework of the ARPEGE/Aladin NWP system. Mon. Weather Rev. 123 (2), 515–535.

Calafat, F.M., Avgoustoglou, E., Jorda, G., Flocas, H., Zodiatis, G., Tsimplis, M.N., Kouroutzoglou, J., 2014. The ability of a barotropic model to simulate sea level extremes of meteorological origin in the Mediterranean Sea, including those caused by explosive cyclones. J. Geophys. Res.: Oceans 119, 7840–7853. http://dx.doi.org/10.1002/2014JC010360.

Calafat, F.M., Wahl, T., Tadesse, M.G., Sparrow, S.N., 2022. Trends in Europe storm surge extremes match the rate of sea-level rise. Nature 603, 841–845. http://dx.doi.org/10.1038/s41586-022-04426-5.

Campins, J., Genovés, A., Picornell, M.A., Jansà, A., 2011. Climatology of Mediterranean cyclones using the ERA-40 dataset. Int. J. Climatol. 31, 1596–1614. http://dx.doi.org/10.1002/joc.2183.

Carillo, A., Sannino, G., Artale, V., Ruti, P.M., Calmanti, S., Dell'Aquila, A., 2012. Steric sea level rise over the Mediterranean Sea: present climate and scenario simulations. Clim. Dynam. 39 (9–10), 2167–2184.

Cavicchia, L., von Storch, H., Gualdi, S., 2014. Mediterranean tropical-like cyclones in present and future climate. J. Clim. 27 (19), 7493–7501.

Ciavola, P., Ferreira, O., Haerens, P., Van Koningsveld, M., Ar-maroli, C., 2011. Storm impacts along European coastlines. Part 2: lessons learned from the MICORE project. Environ. Sci. Policy 14, 924—933. http://dx.doi.org/10.1016/j.envsci.2011.05.009.

Cid, A., Castanedo, S., Abascal, A.J., Menéndez, M., Medina, R., 2014. A high resolution hindcast of the meteorological sea level component for Southern Europe: the GOS dataset. Clim. Dynam. 43 (7), 2167–2184.

Cid, A., Menéndez, M., Castanedo, S., Abascal, A.J., Méndez, F.J., Medina, R., 2016. Long-term changes in the frequency, intensity and duration of extreme storm surge events in southern Europe. Clim. Dynam. 46 (5), 1503–1516.

Conte, D., Lionello, P., 2013. Characteristics of large positive and negative surges in the Mediterranean Sea and their attenuation in future climate scenarios. Glob. Planet. Change 111, 159–173.

Cramer, W., Guiot, J., Fader, M., Garrabou, J., Gattuso, J.-P., Iglesias, A., Lange, M.A., Lionello, P., Llasat, M.C., Paz, S., Peñuelas, J., Snoussi, M., Toreti, A., Tsimplis, M.N., Xoplaki, E., 2018. Climate change and interconnected risks to sustainable development in the Mediterranean. Nature Clim. Change 8 (11), 972–980.

De Vries, H., Breton, M., de Mulder, T., Krestenitis, Y., Proctor, R., Ruddick, K., et al., 1995. A comparison of 2D storm surge models applied to three shallow European seas. Environ. Softw. 10 (1), 23–42.

Denamiel, C., Tojčić, I., Vilibić, I., 2021. Balancing accuracy and efficiency of atmospheric models in the northern Adriatic during severe bora events. J. Geophys. Res.: Atmos. 126, e2020JD033516.

Denamiel, C., Vilibić, I., 2022. Next-generation (sub-) kilometre-scale climate modelling for extreme storm-surge hazard projections. Nature Commun. http://dx.doi.org/10.21203/rs.3.rs-1532623/v1.

Enríquez, A.R., Wahl, T., Marcos, M., Haigh, I.D., 2020. Spatial footprints of storm surges along the global coastlines. J. Geophys. Res.: Oceans 125 (9), e2020JC016367.

Fang, J., Sun, S., Shi, P., Wang, J.A., 2014. Assessment and mapping of potential storm surge impacts on global population and economy. Int. J. Disaster Risk Sci. 5 (4), 323–331.

Ferrarin, C., Bajo, M., Benetazzo, A., Cavaleri, L., Chiggiato, J., Davison, S., Davolio, S., Lionello, P., Orlić, M., Umgiesser, G., 2021. Local and large-scale controls of the exceptional Venice floods of 2019. Prog. Oceanogr. 197, 102628.

Flaounas, E., Davolio, S., Raveh-Rubin, S., Pantillon, F., Miglietta, M.M., Gaertner, M.A., Hatzaki, M., Homar, V., Khodayar, S., Korres, G., Kotroni, V., 2021. Mediterranean cyclones: Current knowledge and open questions on dynamics, prediction, climatology and impacts. Weather Clim. Dyn. Discuss. 1–68.

Flaounas, E., Kelemen, F.D., Wernli, H., Gaertner, M.A., Reale, M., Sanchez-Gomez, E., Lionello, P., Calmanti, S., Podrascanin, Z., Somot, S., Akhtar, N., 2018. Assessment of an ensemble of ocean–atmosphere coupled and uncoupled regional climate models to reproduce the climatology of Mediterranean cyclones. Clim. Dynam. 51 (3), 1023–1040.

Flocas, A.A., 1988. Frontal depressions over the Mediterranean Sea and central southern Europe. Méditerranée 4, 43–52.

Flocas, H.A., Karacostas, T.S., 1996. Cyclogenesis over the Aegean Sea: Identifications and synoptic categories. Meteorol. Appl. 3, 53–61.

Fortelli, A., Fedele, A., De Natale, G., Matano, F., Sacchi, M., Troise, C., Somma, R., 2021. Analysis of sea storm events in the mediterranean sea: The case study of 28 2020 sea storm in the Gulf of Naples, Italy. Appl. Sci. 11, 11460.

Gaertner, M.Á., González-Alemán, J.J., Romera, R., Domínguez, M., Gil, V., Sánchez, E., Gallardo, C., Miglietta, M.M., Walsh, K.J., Sein, D.V., Somot, S., 2018. Simulation of medicanes over the mediterranean sea in a regional climate model ensemble: impact of ocean–atmosphere coupling and increased resolution. Clim. Dynam. 51 (3), 1041–1057.

Galiatsatou, P., Makris, C., Krestenitis, Y., Prinos, P., 2021. Nonstationary extreme value analysis of nearshore sea-state parameters under the effects of climate change: Application to the Greek coastal zone and port structures. J. Mar. Sci. Eng. 9 (8), 817. http://dx.doi.org/10.3390/jmse9080817.

Galiatsatou, P., Makris, C., Prinos, P., Kokkinos, D., 2019. Nonstationary joint probability analysis of extreme marine variables to assess design water levels at the shoreline in a changing climate. Nat. Hazards 98 (3), 1051–1089. http://dx.doi.org/10.1007/s11069-019-03645-w.

Garcies, L., Homar, V., 2011. Verification of objective sensitivity climatologies of Mediterranean intense cyclones: test against human judgement. Q. J. R. Meteorol. Soc. 137, 1467–1481.

Giorgi, F., 2006. Climate change hot-spots. Geophys. Res. Lett. 33 (8), L08, 707.

Giorgi, F., Lionello, P., 2008. Climate change projections for the Mediterranean region. Glob. Planet. Change 63 (2–3), 90–104.

Gomis, D., Ruiz, S., Sotillo, M.G., Álvarez-Fanjul, E., Terradas, J., 2008. Low frequency Mediterranean sea level variability: the contribution of atmospheric pressure and wind. Glob. Planet. Change 63, 215–229.

Gualdi, S., Somot, S., Li, L., Artale, V., Adani, M., Bellucci, A., Braun, A., Calmanti, S., Carillo, A., Dell'Aquila, A., Deque, M., Dubois, C., Elizalde, A., Harzallah, A., Jacob, D., et al., 2013. The CIRCE simulations: Regional climate change projections with realistic representation of the Mediterranean Sea. Bull. Am. Meteorol. Soc. 94 (1), 65–81.

Hallegatte, S., Green, C., Nicholls, R.J., Corfee-Morlot, J., 2013. Future flood losses in major coastal cities. Nature Clim. Change 3 (9), 802–806.

Hochman, A., Marra, F., Messori, G., Pinto, J.G., Raveh-Rubin, S., Yosef, Y., Zittis, G., 2021. ESD reviews: extreme weather and societal impacts in the eastern Mediterranean. Earth Syst. Dyn. Discuss. 1–53.

IPCC, 2014. In: Core Writing Team, Pachauri, R.K., Meyer, L.A. (Eds.), Climate Change 2014: Synthesis Report. Contribution of Working Groups I, II and III to the Fifth Assessment Report of the Intergovernmental Panel on Climate Change. IPCC, Geneva, Switzerland, p. 151.

Jordà, G., Gomis, D., Álvarez-Fanjul, E., Somot, S., 2012. Atmospheric contribution to mediterranean and nearby Atlantic sea level variability under different climate change scenarios. Glob. Planet. Change 80–81, 198–214.

Krestenitis, Y., Androulidakis, Y., Kombiadou, K., Makris, C., Baltikas, V., 2014. Modeling storm surges in the mediterranean sea under the A1B climate scenario. In: Proceedings of 12th International Conference on Meteorology, Climatology and Atmospheric Physics (COMECAP), Heraklion (Crete), Greece, 28-31 May 2014. pp. 91–95, Part of ISBN: 978-960-524-430-9.

Krestenitis, Y.N., Androulidakis, Y.S., Kontos, Y.N., Georgakopoulos, G., 2011. Coastal inundation in the north-eastern Mediterranean coastal zone due to storm surge events. J. Coast. Conserv. 15 (3), 353–368.

Krestenitis, Y., Kombiadou, K., Androulidakis, Y., Makris, C., Baltikas, V., Skoulikaris, C., Kontos, Y., Kalantzi, G., 2015. Operational oceanographic platform in Thermaikos Gulf (Greece): Forecasting and emergency alert system for public use. In: Proceedings of 36th International Association of Hydraulic Research (IAHR) World Congress, the Hague, the Netherlands, 28 June – 3 July, 2015.

Krestenitis, Y., Pytharoulis, I., Karacostas, T., Androulidakis, Y., Makris, C., Kombiadou, K., Tegoulias, I., Baltikas, V., Kotsopoulos, S., Kartsios, S., 2017. Severe weather events and sea level variability over the Mediterranean Sea: the WaveForUs operational platform. In: Karacostas, T., Bais, A., Nastos, P.T. (Eds.), Perspectives of Atmospheric Sciences. In: Springer Atmospheric Sciences, Pt.1: Meteorology, pp. 63–68. http://dx.doi.org/10.1007/978-3-319-35095-0_9.

Lagouvardos, K., Karagiannidis, A., Dafis, S., Kalimeris, A., Kotroni, V., 2021. Ianos - A hurricane in the Mediterranean. Bull. Am. Meteorol. Soc. 1–31.

Laloyaux, P., Balmaseda, M., Dee, D., Mogensen, K., Janssen, P., 2016. A coupled data assimilation system for climate reanalysis. Q. J. R. Meteorol. Soc. 142 (694), 65–78.

Laloyaux, P., de Boisseson, E., Balmaseda, M., Bidlot, J.R., Broennimann, S., Buizza, R., Dalhgren, P., Dee, D., Haimberger, L., Hersbach, H., Kosaka, Y., 2018. CERA-20C: A coupled reanalysis of the twentieth century. J. Adv. Modelling Earth Syst. 10 (5), 1172–1195.

Li, L., Casado, A., Dell'Aquila, A., Dubois, C., Elizalde, A., L'Hévéder, B., Lionello, P., Sevault, F., Somot, S., Ruti, P., Zampieri, M., 2011. Modelling of the Mediterranean climate system (chapter 7). In: Lionello, P. (Ed.), Mediterranean Climate Variability. Elsevier B.V., Amsterdam, pp. 419–448.

Lionello, P., Abrantes, F., Gacic, M., Planton, S., Trigo, R., Ulbrich, U., 2014. The climate of the Mediterranean region: research progress and climate change impacts. Reg. Environ. Change 14 (5), 1679–1684.

Lionello, P., Barriopedro, D., Ferrarin, C., Nicholls, R.J., Orlić, M., Raicich, F., Reale, M., Umgiesser, G., Vousdoukas, M., Zanchettin, D., 2021. Extreme floods of Venice: characteristics, dynamics, past and future evolution. Nat. Hazards Earth Syst. Sci. 21 (8), 2705–2731.

Lionello, P., Bhend, J., Buzzi, A., Della-Marta, P.M., Krichak, S.O., Jansa, A., Maheras, P., Sanna, A., Trigo, I.F., Trigo, R., 2006b. Cyclones in the Mediterranean region: climatology and effects on the environment. Dev. Earth Environ. Sci. 4, 325–372.

Lionello, P., Boldrin, U., Giorgi, F., 2008. Future changes in cyclone climatology over Europe as inferred from a regional climate simulation. Clim. Dynam. 30 (6), 657–671.

Lionello, P., Cavaleri, L., Nissen, K.M., Pino, C., Raicich, F., Ulbrich, U., 2012. Severe marine storms in the Northern Adriatic: Characteristics and trends. Phys. Chem. Earth Parts A/B/C 40, 93–105.

Lionello, P., Conte, D., Reale, M., 2019. The effect of cyclones crossing the Mediterranean region on sea level anomalies on the Mediterranean Sea coast. Nat. Hazards Earth Syst. Sci. 19 (7), 1541–1564.

Lionello, P., Dalan, F., Elvini, E., 2002. Cyclones in the Mediterranean region: the present and the doubled $CO_2$ climate scenarios. Clim. Res. 22, 147–159. http://dx.doi.org/10.3354/cr022147.

Lionello, P., Malanotte-Rizzoli, P., Boscolo, R., 2006a. Mediterranean Climate Variability. Elsevier.

Lionello, P., Trigo, I.F., Gil, V., Liberato, M.L., Nissen, K.M., Pinto, J.G., Raible, C.C., Reale, M., Tanzarella, A., Trigo, R.M., Ulbrich, S., 2016. Objective climatology of cyclones in the Mediterranean region: a consensus view among methods with different system identification and tracking criteria. Tellus A 68 (1), 29391.

Madec, G., Bourdallé-Badie, R., Bouttier, P.A., Bricaud, C., Bruciaferri, D., Calvert, D., Chanut, J., Clementi, E., Coward, A., Delrosso, D., Ethé, C., 2017. NEMO ocean engine. Notes Pôle Modél. Inst. Pierre-Simon Laplace (IPSL) (ISSN: 1288-1619) (27), http://dx.doi.org/10.5281/zenodo.3248739.

Maheras, P., 1983. Les types de temps depressionnaires perturbés au-dessus de la mer Egée. Riv. Meteorol. Aeronaut. 43, 13–22.

Maheras, P., Flocas, H., Patrikas, I., Anagnostopoulou, C., 2001. A 40-year objective climatology of surface cyclones in the Mediterranean region: spatial and temporal distribution. Int. J. Climatol. 21, 109–130.

Makris, C., Androulidakis, Y., Baltikas, V., Kontos, Y., Karambas, T., Krestenitis, Y., 2019. HiReSS: Storm surge simulation model for the operational forecasting of sea level elevation and currents in marine areas with harbor works. In: Proceedings of 1st International Scientific Conference on Design and Management of Port Coastal and Offshore Works (DMPCO), Athens, Greece, 8-11 May 2019, Vol. 1. pp. 11–15.

Makris, C., Androulidakis, Y., Karambas, T., Papadimitriou, A., Metallinos, A., Kontos, Y., Baltikas, V., Chondros, M., Krestenitis, Y., Tsoukala, V., Memos, C., 2021. Integrated modelling of sea-state forecasts for safe navigation and operational management in ports: Application in the Mediterranean Sea. Appl. Math. Model. 89 (2), 1206–1234. http://dx.doi.org/10.1016/j.apm.2020.08.015.

Makris, C.V., Androulidakis, Y.S., Krestenitis, Y.N., Kombiadou, K.D., Baltikas, V.N., 2015. Numerical modelling of storm surges in the Mediterranean Sea under climate change. In: Proceedings of 36th International Association of Hydraulic Research (IAHR) World Congress. The Hague, The Netherlands, 28 June – 3 July, 2015.

Makris, C., Baltikas, V., Androulidakis, Y., Krestenitis, Y., 2020b. Coastal inundation due to storm surges on a Mediterranean Deltaic Area under the effects of climate change. In: Proceedings of 7th International Conference on Civil Protection & New Technologies, SAFE GREECE 2020. Part of ISSN 2654-1823.

Makris, C., Baltikas, V., Tolika, K., Velikou, K., Skoulikaris, Ch., Krestenitis, Y., 2020a. Climate change impacts on the storm surges of Mediterranean Coastal Areas. In: Proceedings of 6th IAHR Europe Congress 2020, Transferred as Online Event on 15-18 February 2021, Warsaw, Poland. pp. 465–466, Part of ISBN 978-83-66847-01-9.

Makris, C., Galiatsatou, P., Androulidakis, Y., Kombiadou, K., Baltikas, V., Krestenitis, Y., Prinos, P., 2018. Climate change impacts on the coastal sea level extremes of the east-central Mediterranean Sea. In: Proceedings of XIV PRE Conference, in Chapter: Climate Change Impacts and Adaptation Measures, Thessaloniki, Greece, 3-6 July 2018. pp. 695–704, Part of ISBN:978-960-99922-4-4.

Makris, C., Galiatsatou, P., Tolika, K., Anagnostopoulou, C., Kombiadou, K., Prinos, P., Velikou, K., Kapelonis, Z., Tragou, E., Androulidakis, Y., Athanassoulis, G., Vagenas, C., Tegoulias, I., Baltikas, V., Krestenitis, Y., Gerostathis, T., Belibassakis, K., Rusu, E., 2016. Climate change effects on the marine characteristics of the aegean and the ionian seas. Ocean Dyn. 66 (12), 1603–1635. http://dx.doi.org/10.1007/s10236-016-1008-1.

Marcos, M., Jordà, G., Gomis, D., Pérez, B., 2011. Changes in storm surges in southern Europe from a regional model under climate change scenarios. Glob. Planet. Change 77 (3–4), 116–128.

Marcos, M., Tsimplis, M.N., Shaw, A.G., 2009. Sea level extremes in southern Europe. J. Geophys. Res.: Oceans (1978–2012) 114 (C1).

Martzikos, N.T., Prinos, P.E., Memos, C.D., Tsoukala, V.K., 2021. Statistical analysis of Mediterranean coastal storms. Oceanologia 63 (1), 133–148.

McInnes, K.L., Macadam, I., Hubbert, G.D., O'Grady, J.G., 2009. A modelling approach for estimating the frequency of sea level extremes and the impact of climate change in southeast Australia. Nat. Hazards 51 (1), 115–137.

Mel, R.A., Feudo, T.Lo., Miceli, M., Sinopoli, S., Maiolo, M., 2022. A coupled modelling system to assess the effect of Mediterranean storms under climate change. Nat. Hazards Earth Syst. Sci. Discuss. http://dx.doi.org/10.5194/nhess-2022-67, [preprint].

Međugorac, I., Orlic, M., Janekovic, I., Pasaric, Z., Pasaric, M., 2018. Adriatic storm surges and related cross-basin sea-level slope. J. Mar. Syst. 181, 79–90.

Međugorac, I., Pasarić, M., Güttler, I., 2021. Will the wind associated with the Adriatic storm surges change in future climate? Theor. Appl. Climatol. 143 (1), 1–18.

Moss, R.H., Babiker, M., Brinkman, S., Calvo, E., Carter, T., Edmonds, J.A., Elgizouli, I., Emori, S., Lin, E., Hibbard, K., Jones, R., 2008. Towards New Scenarios for Analysis of Emissions, Climate Change, Impacts, and Response Strategies (No. PNNL-SA-63186). Pacific Northwest National Lab. (PNNL), Richland, WA (United States).

Moss, R.H., Edmonds, J.A., Hibbard, K.A., Manning, M.R., Rose, S.K., Van Vuuren, D.P., Carter, T.R., Emori, S., Kainuma, M., Kram, T., Meehl, G.A., 2010. The next generation of scenarios for climate change research and assessment. Nature 463 (7282), 747–756.

Mosso, C., Mestres, M., Sierra, J.P., Sanchez-Arcilla, A., Goodess, C., 2009. Waves and surges in the Valencia Gulf. Variability rather than climate change. J. Coast. Res. SI56, 243–247.

Nicholls, R.J., 2006. Storm surges in coastal areas. Natural disaster hotspots: Case studies. Disaster Risk Manag. 6, 79–108.

Nicholls, R.J., 2010. Impacts of and responses to sea-level rise. In: Church, J.A., et al. (Eds.), Understanding Sea-Level Rise and Variability. Wiley-Blackwell, Chichester, U. K, pp. 17–51.

Nicholls, R.J., Hoozemans, F.M.J., 1996. The Mediterranean: vulnerability to coastal implications of climate change. Ocean Coast. Manag. 31 (2–3), 105–132.

Nissen, K.M., Leckebusch, G.C., Pinto, J.G., Renggli, D., Ulbrich, S., Ulbrich, U., 2010. Cyclones causing wind storms in the Mediterranean: characteristics, trends and links to largescale patterns. Nat. Hazards Earth Syst. Sci. 10, 1379–1391. http://dx.doi.org/10.5194/nhess-10-1379-2010.

Obermann, A., Bastin, S., Belamari, S., Conte, D., Gaertner, M.A., Li, L., Ahrens, B., 2018. Mistral and Tramontane wind speed and wind direction patterns in regional climate simulations. Clim. Dyn. 51 (3), 1059–1076.

Pawlowicz, R., Beardsley, B., Lentz, S., 2002. Classical tidal harmonic analysis including error estimates in MATLAB using T-TIDE. Comput. Geosci. 28, 929–937.

Radinovic, D., 1987. Mediterranean Cyclones and their Influence on the Weather and Climate. Programme on Short and Medium Range Weather Prediction Research (PSMP), W.M.O. Sofia, 24.

Radnóti, G., Ajjaji, R., Bubnová, R., Caian, M., Cordoneanu, E., Von Der Emde, K., Gril, J.D., Hoffman, J., Horanyi, A., Issara, S., Ivanovici, V., 1995. The spectral limited area model ARPEGE/ALADIN. PWPR Rep. Ser. 7, 111–117.

Reale, M., Cabos Narvaez, W.D., Cavicchia, L., Conte, D., Coppola, E., Flaounas, E., Giorgi, F., Gualdi, S., Hochman, A., Li, L., Lionello, P., 2022. Future projections of mediterranean cyclone characteristics using the Med-CORDEX ensemble of coupled regional climate system models. Clim. Dynam. 1–24 (58), 2501–2524.

Reale, M., Lionello, P., 2013. Synoptic climatology of winter intense precipitation events along the Mediterranean coasts. Nat. Hazards Earth Syst. Sci. 13 (7), 1707–1722.

Rousi, 2014. Estimation of Future Climate Change in the Mediterranean using Regional Climate Models (Ph.D. thesis). School of Geology, Aristotle University of Thessaloniki, Greece, http://dx.doi.org/10.12681/eadd/35162.

Ruti, P.M., Somot, S., Giorgi, F., Dubois, C., Flaounas, E., Obermann, A., Dell'Aquila, A., Pisacane, G., Harzallah, A., Lombardi, E., Ahrens, B., 2016. MED-CORDEX initiative for Mediterranean climate studies. Bull. Am. Meteorol. Soc. 97 (7), 1187–1208.

Sánchez-Arcilla, A., Jiménez, J.A., Valdemoro, H.I., Gracia, V., 2008. Implications of climatic change on Spanish Mediterranean low-lying coasts: the Ebro delta case. J. Coast. Res. 24 (2), 306–316.

Sanchez-Gomez, E., Somot, S., 2018. Impact of the internal variability on the cyclone tracks simulated by a regional climate model over the Med-CORDEX domain. Clim. Dynam. 51 (3), 1005–1021.

Satta, A., Puddu, M., Venturini, S., Giupponi, C., 2017. Assessment of coastal risks to climate change related impacts at the regional scale: The case of the Mediterranean region. Int. J. Disaster Risk Reduct. 24, 284–296.

Schoetter, R., Hoffmman, P., Rechid, D., Schlunzen, K.H., 2012. Evaluation and bias correction of reginal climate model results using model evaluation measures. J. Appl. Meteorol. Climatol. 51, 1670–1684.

Šepić, J., Vilibić, I., Jordà, G., Marcos, M., 2012. Mediterranean sea level forced by atmospheric pressure and wind: Variability of the present climate and future projections for several period bands. Glob. Planet. Change 86, 20–30.

Šepić, J., Vilibic, I., Lafon, A., Macheboeuf, L., Ivanovic, Z., 2015. High-frequency sea level oscillations in the mediterranean and their connection to synoptic patterns. Prog. Oceanogr. 137, 284–298.

Sevault, F., Somot, S., Alias, A., Dubois, C., Lebeaupin-Brossier, C., Nabat, P., Adloff, F., Déqué, M., Decharme, B., 2014. A fully coupled mediterranean regional climate system model: design and evaluation of the ocean component for the 1980–2012 period. Tellus A 66 (1), 23967.

Skoulikaris, Ch., Makris, Ch., Katirtzidou, M., Baltikas, V., Krestenitis, Y., 2021. Assessing the vulnerability of a deltaic environment due to climate change impact on surface and coastal waters: the case of Nestos River (Greece). Environ. Model. Assess. 26, 459–486. http://dx.doi.org/10.1007/s10666-020-09746-2.

Snoussi, M., Ouchani, T., Niazi, S., 2008. Vulnerability assessment of the impact of sea-level rise and flooding on theMoroccan coast: the case of theMediterranean eastern zone. Estuar. Coast. Shelf Sci. 77, 206–213.

Somot, S., Ruti, P., Ahrens, B., Coppola, E., Jordà, G., Sannino, G., Solmon, F., 2018. Editorial for the Med-CORDEX special issue. Clim. Dynam. 51 (3), 771–777.

Somot, S., Sevault, F., Déqué, M., Crépon, M., 2008. 21St century climate change scenario for the Mediterranean using a coupled atmosphere–ocean regional climate model. Glob. Planet. Change 63 (2–3), 112–126.

Spiridonov, V., Déqué, M., Somot, S., 2005. ALADIN-CLIMATE: from the origins to present date. ALADIN Newsl. 29, 89–92.

Thorncroft, C.D., Flocas, H.A., 1997. A case study of saharan cyclogenesis. Mon. Weather Rev. 125, 1147–1165.

Tolika, K., Makris, Ch., Baltikas, V., Velikou, K., Krestenitis, Y., 2021. On the assessment of RCMs in simulating deep cyclones over the Mediterranean region: Impacts on the storm surges of coastal areas. In: Proceedings of 15th International Conference on Meteorology, Climatology and Atmospheric Physics (COMECAP), 26-29 September 2021. Ioannina, Greece.

Toomey, T., Amores, A., Marcos, M., Orfila, A., Romero, R., 2022. Coastal hazards of tropical-like cyclones over the Mediterranean Sea. J. Geophys. Res.: Oceans e2021JC017964.

Trigo, I.F., Bigg, G.R., Davis, T.D., 2002a. Climatology of cyclogenesis mechanisms in the Mediterranean. Mon. Weather Rev. 130, 549–569.

Trigo, I.F., Davies, T.D., Bigg, G.R., 1999. Objective climatology of cyclones in the Mediterranean region. J. Clim. 12, 1685–1696.

Trigo, R.M., Osborn, J.T., Corte-Real, M.J., 2002b. The North Atlantic Oscillation influence on Europe: climate impacts and associated physical mechanisms. Clim. Res. 20, 9–17.

Tsimplis, M.N., Shaw, A.G.P., 2010. Seasonal sea level extremes in the Mediterranean Sea and at the Atlantic European coasts. Nat. Hazard. Earth Syst. Sci. 10 (7), 1457–1475.

Ullmann, A., Moron, V., 2008. Weather regimes and sea surge variations over the Gulf of Lions (French Mediterranean coast) during the 20th century. Int. J. Climatol. 28, 159–171. http://dx.doi.org/10.1002/joc.1527.

Van Vuuren, D.P., Edmonds, J., Kainuma, M., Riahi, K., Thomson, A., Hibbard, K., Hurtt, G.C., Kram, T., Krey, V., Lamarque, J.F., Masui, T., 2011. The representative concentration pathways: an overview. Clim. Change 109 (1), 5–31.

Velikou, K., Tolika, K., Anagnostopoulou, C. others, 2019. Sensitivity analysis of RegCM4 model: present time simulations over the mediterranean. Theor. Appl. Climatol. 136, 1185–1208. http://dx.doi.org/10.1007/s00704-018-2547-9.

Von Storch, H., Woth, K., 2008. Storm surges: perspectives and options. Sustain. Sci. 3 (1), 33–43.

Vousdoukas, M.I., Mentaschi, L., Voukouvalas, E., Verlaan, M., Jevrejeva, S., Jackson, L.P., Feyen, L., 2018. Global probabilistic projections of extreme sea levels show intensification of coastal flood hazard. Nature Commun. 9 (1), http://dx.doi.org/10.1038/s41467-018-04692-w, 2360–2312.

Vousdoukas, M.I., Voukouvalas, E., Annunziato, A., Giardino, A., Feyen, L., 2016. Projections of extreme storm surge levels along Europe. Clim. Dynam. 47, 3171–3190.

Wahl, T., Chambers, D.P., 2016. Climate controls multidecadal variability in US extreme sea level records. J. Geophys. Res.: Oceans 121, 1274–1290. http://dx.doi.org/10.1002/2015JC011057.

Wahl, T., Haigh, I.D., Nicholls, R.J., Arns, A., Dangendorf, S., Hinkel, J., Slangen, A.B.A., 2017. Understanding extreme sea levels for broad-scale coastal impact and adaptation analysis. Nature Commun. 8 (1), 16075. http://dx.doi.org/10.1038/ncomms16075.

Wahl, T., Mudersbach, C., Jensen, J., 2012. Assessing the hydrodynamic boundary conditions for risk analyses in coastal areas: A multivariate statistical approach based on copula functions. Nat. Hazards Earth Syst. Sci. 12, 495–510.

Willmott, C.J., Robeson, S.M., Matsuura, K., 2012. Short communication: A refined index of model performance. Int. J. Climatol. 32, 2088–2094.